STUDY OF REACTIONS OF CARBON DIOXIDE AND SULFUR

CONTAINING COMPOUNDS WITH ETHANOLAMINES

By

MAHMUD AZIZUR RAHMAN

Bachelor of Science in Engineering
University of Engineering & Technology
Dacca, Bangladesh
1976

Master of Science
Oklahoma State University
Stillwater, Oklahoma
1978

Submitted to the Faculty of the Graduate College
of the Oklahoma State University
in partial fulfillment of the requirements
for the Degree of
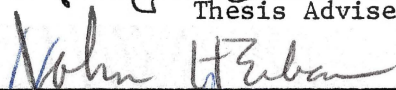DOCTOR OF PHILOSOPHY
May, 1984

STUDY OF REACTIONS OF CARBON DIOXIDE AND SULFUR
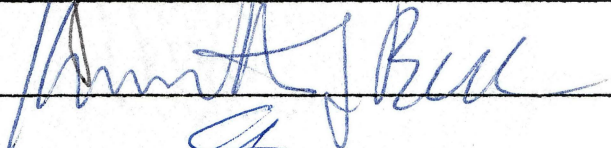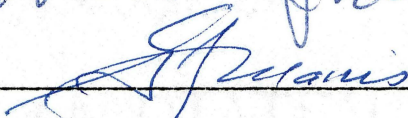
CONTAINING COMPOUNDS WITH ETHANOLAMINES

Thesis Approved:
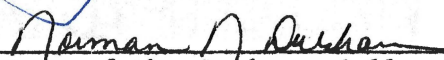
_____
Thesis Adviser

_____

_____

_____

_____
Dean of the Graduate College

PREFACE

This study is concerned with the reactions of acidic gases with various alkanolamines. The acidic gases considered were hydrogen sulfide, carbon dioxide, carbonyl sulfide, and methyl mercaptan. Amines investigated were monoethanolamine, diethanolamine, diglycolamine, diisopropanolamine, methyldiethanolamine, and dimethylethanolamine. The first part of this work was to identify the products formed during reaction between acid-gases and amines using nuclear magnetic resonance spectroscopy. The second part was to quantitatively determine the best solvent for each acid-gas by obtaining reaction rates and solubility parameters. Extension of this work appears promising and I expect that continuations of this study will be successful.

Finally, I would like to express my gratitude to my parents, brothers, and sister for their understanding and encourgement during the period of my graduate study.

TABLE OF CONTENTS

LIST OF TABLES

LIST OF FIGURES

x

NOMENCLATURE

(Amine), (AM)	amine concentration, gm. mol/lit
D_A	diffusivity of acid-gas in amine, cm/sec
k_{AM}, k_D	rate constant for amine
k_L	mass transfer coefficient, cm/sec
n	moles
r_m	rate of reaction of CO_2
r_c	rate of reaction of COS
R	rate of acid-gas conversion per unit area, mol/cm^2-sec
R_G	universal gas constant, 10.73 psia ft^3/lb.mol.R
S	solubility, gm.mol/atm-cm^3
t	time, sec
T	temperature
V	volume occupied by acidic gas, ml
V_G	molecular volume of solute at normal boiling point, cm^3/gm-mole
x	association factor
Z	compressibility factor
$\alpha, \beta, \gamma, \delta$	position relative to nitrogen atom
μ	viscosity of amine, cP

CHAPTER I

INTRODUCTION

The removal of carbon dioxide, carbonyl sulfide, hydrogen sulfide, and methyl mercaptan from gaseous mixtures is an important industrial operation in the natural gas and petroleum gas processing industry. Removal of these acidic gases is necessary to prevent corrosion in metals and also eliminate potentially hazardous impact on the environment.

In principle many methods could be employed for the removal of acidic gases, but economic considerations dictate using liquid absorption techniques. An economic reactive solvent would have an appreciable chemical reactivity with one or all the acidic gases and would not react irreversibly with the acidic gases and be easily regenerable. Of the many types of solvents available, the alkanolamines are most frequently used for gas purification. The alkanolamines which are of commercial interest and considered in this study are monoethanolamine (MEA), β,β'-hydroxy-aminoethyl ether (Diglycolamine, DGA), diethanolamine (DEA), diisopropanolamine (DIPA), methyldiethanolamine (MDEA), and dimethylethanolamine (DMEA). The chemical structure of the amines is presented in Figure 1. Aqueous solutions of MEA, DGA, and DEA are in industrial use for removal of hydrogen sulfide and carbon dioxide (1, 2, 3). Much interest has recently been shown in using tertiary amines like MDEA as selective solvents for hydrogen sulfide (H_2S) in the presence of carbon dioxide (CO_2). Methyl mercaptan (CH_3SH) is not known to be reactive with alkanolamines and its

1
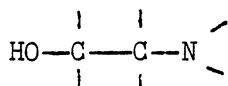
PRIMARY AMINES
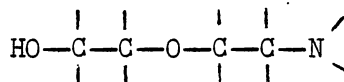
Monoethanolamine   β,β'-hydroxy-aminoethyl ether

SECONDARY AMINES
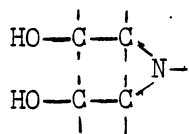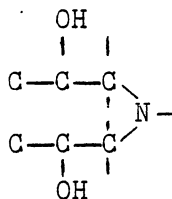
Diethanolamine   Diisopropanolamine

TERTIARY AMINES
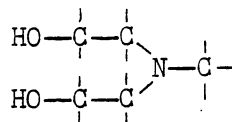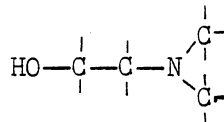
Methyldiethanolamine   Dimethylethanolamine

Figure 1. Molecular Structure of Amines

removal through amines is limited to its physical solubility only (1).
Carbonyl sulfide (COS) undergoes chemical transformation in the presence
of amines; with MEA the reaction is irreversible, that is, the product de-
composes to diethanolurea instead of regenerating MEA in the regenerator.
DGA has been reported to be an efficient solvent of COS and is regenerable.
(4, 5, 6).

Although the reaction of CO_2 with amines has been extensively stud-
ied, the kinetics of the reaction and the relevant products have not been
conclusively determined and the reaction mechanism is still a matter of
speculation. Literature data on H_2S and COS reactions with amines is less
abundant than in the case of CO_2 reactions, thus leading to still greater
uncertainty. Alkanolamines have never been a serious candidate for remov-
al of high concentrations of methyl mercaptan because of the much lower
acidity of the methyl mercaptan molecule in comparison to the hydrogen
sulfide molecule. Some literature data exist on methyl mercaptan reac-
tions with aqueous sodium hydroxide (7).

The objective of this study is to ascertain the reaction products of
the amine-acidic gas systems specified in Table I. The reaction vessel
is a stirred Claisen distilling flask and the reaction is monitored by re-
cording pressure and temperature of the reaction system over a period of
time. The reaction products are analyzed by means of nuclear magnetic
resonance spectroscopy to gain an understanding of the reactions between
the various amines and the acidic gases.

TABLE I

AMINE-ACIDIC GAS SYSTEMS

Amine					
Primary		Secondary		Tertiary	
MEA	DGA	DEA	DIPA	MDEA	DMEA
----	H_2S	----	H_2S	H_2S	H_2S
----	CO_2	----	CO_2	CO_2	CO_2
COS	COS	COS	COS	COS	COS
CH_3SH	CH_3SH	CH_3SH	CH_3SH	CH_3SH	CH_3SH

CHAPTER II

LITERATURE SURVEY

The chemistry of the reactions between carbon dioxide, carbonyl sul-
fide, hydrogen sulfide and methyl mercaptan, and amines and their aqueous
solutions is presented in this chapter.

The molecular structure of alkanolamines merits investigation before
specific reactions are studied in detail. The classification of molecular
structure of amines in Figure 1 is based on the degree of substitution of
hydrogen atoms bonded to the nitrogen atom. The replacement of one of the
hydrogen atoms of an ammonia molecule by an organic radical yields a pri-
mary amine like monoethanolamine and β,β'-hydroxy-aminoethyl ether; sub-
stitution of two hydrogen atoms gives a secondary amine such as diethano-
lamine and diisopropanolamine; triple substitution synthesizes tertiary
amines like methyldiethanolamine and dimethylethanolamine. The hydrogen
atoms on a partially substituted amine (primary and secondary), termed as
"labile hydrogen," determine the mechanism through which reactions proceed
with the acidic gases (8). The reactions can roughly be classified into
two groups: (a) acid-base proton transfer type, and (b) salt or carbamate
formation (thiocarbamate in case of COS) and subsequent acid-base proton
transfer between the ions (3, 10). The reactions of each of the acidic
gases with the amines under consideration are discussed briefly in the
following sections of this chapter.

Chemical Reactions of Hydrogen Sulfide With Amines

When a gas stream containing H_2S comes in contact with an amine, or for that matter any alkaline solution, it dissociates into an HS^- ion through a proton transfer reaction, which may be considered to be instantaneous as compared to the rate of diffusional processes (1, 2, 9).

$$H_2S + (Amine) \longrightarrow (Amine)^+ + HS^- \tag{2.1}$$
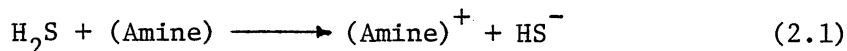
The HS^- ion does not generally dissociate into the $S^=$ ion except in very strong hydroxide solutions (9).

Chemical Reactions of Carbon Dioxide With Amines

The carbon dioxide reactions with amines may proceed through a simple acid-base complex or a carbamate salt depending on availability of labile hydrogen atoms. The primary and secondary amines generally undergo a carbamate formation reaction. In this reaction mechanism, a single carbon dioxide molecule interacts with two amine molecules to form a combination of an acid-base complex and a carbamate structure.

$$CO_2 + 2(Amine) \longrightarrow (Amine)^+ + (Amine-C\overset{\nearrow O}{\underset{\searrow O_-}{}}) \tag{2.2}$$
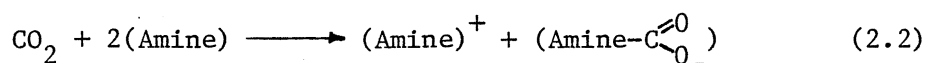
The kinetic rate of the CO_2 reaction through the carbamate type option is much more rapid relative to the simple acid-base interaction (8, 9).

In Equation (2.2), the carbamate ion forms an acid-base complex with the protonated amine. The reaction may be broken into two steps:

$$CO_2 + R_2NH \longrightarrow R_2NCOOH \tag{2.3}$$

$$R_2NCOOH + R_2NH \longrightarrow R_2NCOO^- + R_2NH_2^+ \tag{2.4}$$
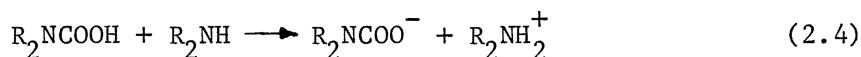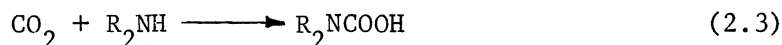
The reaction in Equation (2.3) is bimolecular, second order and rate determining, while the second step (Equation [2.4]) is assumed to occur instantaneously (11, 12).

The other type of CO_2 reaction leads to bicarbonate formation and occurs in aqueous solution (9).

$$CO_2 + H_2O \longrightarrow H_2CO_3 \qquad (2.5)$$

$$H_2CO_3 \longrightarrow H^+ + HCO_3^- \qquad (2.6)$$

$$HCO_3^- \longrightarrow H^+ + CO_3^= \qquad (2.7)$$

$$H^+ + (Amine) \longrightarrow (Amine)^+ \qquad (2.8)$$
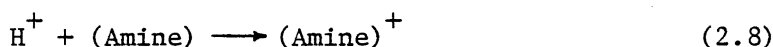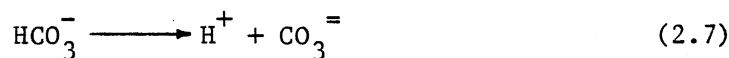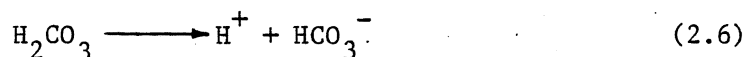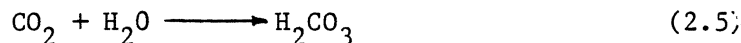
The first step in this reaction is the hydrolysis of CO_2 because of its acidic nature yielding carbonic acid. Subsequent dissociation of the H_2CO_3 molecule forms the bicarbonate (HCO_3^-) ion and a proton (H^+). The proton interacts with the amine to yield (Amine)$^+$. The overall kinetics of the bicarbonate formation reaction are slow because the carbonic acid formation step is kinetically slow (Equation [2.5]) and, as a consequence, is of little importance for primary and secondary amines (8, 9).

Amines have an additional functional group, i.e., -OH which may react with CO_2 as follows:

$$-OH + CO_2 \longrightarrow -OCOOH \qquad (2.9)$$

The substituted carbonic acid product (β-aminoethyl carbonic acid) is formed only in basic solutions of pH greater than 11; since the pH of even a slightly carbonated amine solution is less than 10, the formation of β-aminoethyl carbonate may be neglected (9). Thus the $-CH_2CH_2OH$ group may be considered to be an inert as far as reaction kinetics is considered.

For primary and secondary amines the carbamate option enables fast interaction with CO_2 compared to the tertiary amines which may react to form only the bicarbonates. As a result, tertiary amines are not employed for CO_2 removal. This fact, on the other hand, makes a tertiary amine an attractive solvent for mixtures of H_2S and CO_2 or COS impurities in a gas stream. The removal of H_2S is much faster than CO_2, enabling significant chemical selectivity toward H_2S under normal contactor operating conditions. The general belief that CO_2 encounters more steric hindrance or blockage of reactive sites than H_2S is unfounded because the critical diameter of a CO_2 molecule is less than that of H_2S (2). Thus, the probable cause of H_2S selectivity is not yet fully understood.

Batt (13) has shown that, for pure MEA, water is not essential for carbamate formation. The CO_2 reactions with MEA and DEA have been extensively investigated under various experimental conditions. A brief review of the kinetic information on amine reactions with CO_2 is presented as follows.

Hikita et al. (11) studied the kinetics of reactions of CO_2 with MEA and DEA solutions using a rapid mixing thermal method. The concentration of MEA and DEA was varied up to 0.177M and 0.719M over a temperature range of 5.6 to 40.3 C. The kinetic rate was found to be first order with respect to CO_2 and MEA, respectively. For the DEA system, the kinetic rate was of second order with respect to DEA.

Danckwerts and Sharma (3) presented the rate expression for primary and secondary amines as:

$$\text{Rate of reaction of } CO_2 \text{ (g mol} \cdot \text{lit}^{-1} \cdot \text{s}^{-1}) = k_{AM}(AM)(CO_2) \qquad (2.10)$$

where k_{AM} is the second order rate constant for the amine, and (AM) is

the concentration of amine (g mol.lit^{-1}). The rate constants for DIPA, MEA, and DEA at 25 C are reported to be 400, 7600, and 1500 lit·g mol^{-1}·s^{-1}, respectively (3, 12, 14, 15).

The only tertiary amine on which kinetic data are readily available is triethanolamine (11, 15, 16). Hikita (11) proposed a direct interaction between one mole of CO_2 and a mole of triethanolamine of the form:

$$CO_2 + (HOC_2H_4)_3N \longrightarrow (HOC_2H_4)_2NC_2H_4OCOOH \qquad (2.11)$$
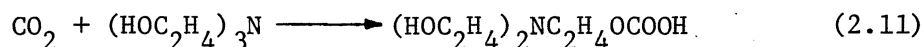
From the experimental data, they obtained a second order kinetic rate constant of 50 M.sec^{-1} at 25 C. The concentration of CO_2 was varied from 0.0052 to 0.0078 M, and the concentration of triethanolamine (TEA) was varied up to 1.06 M at a temperature range of 10-40 C.

Sada et al. (17) determined that one mole of CO_2 reacted with two moles of TEA and proposed a reaction scheme:

$$(HOC_2H_4)_3N + H_2O \longrightarrow (HOC_2H_4)_3NH^+ + OH^- \qquad (2.12)$$

$$CO_2 + 2OH^- \longrightarrow CO_3^= + H_2O \qquad (2.13)$$

The overall reaction is

$$CO_2 + 2 (HOC_2H_4)_3N + H_2O \longrightarrow 2 (HOC_2H_4)_3NH^+ + CO_3^= \qquad (2.14)$$
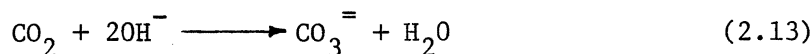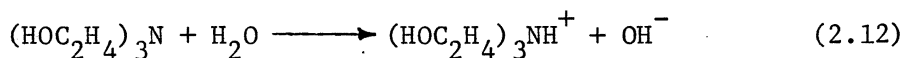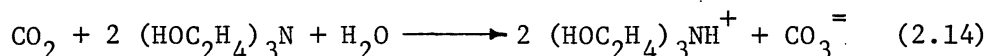
The experiment was carried out using a wetted wall column with the maximum concentrations of TEA and CO_2 being 1.596 and 0.0000309 M, respectively, at 25 C. The reaction rate constant (second order) was 16.8 M.sec^{-1} at 25 C.

Chemical Reactions of Carbonyl Sulfide With Amines

The removal of carbonyl sulfide from mixtures of gases by reactive

liquid solvents is an important industrial operation. The relevant reactions with a primary amine are

$$RNH_2 + COS \longrightarrow RNHCOS^- + H^+ \qquad (2.15)$$

$$RNH_2 + H^+ \longrightarrow RNH_3^+ \qquad (2.16)$$
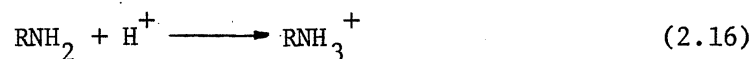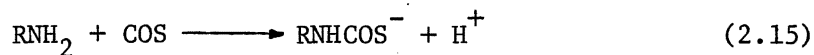
where R is generally an alkanolamine radical. This reaction, as in the case of CO_2, will also occur with a secondary amine to yield a thiocarbamate. The similarity in reactions of CO_2 and COS with an amine stems from the fact that both CO_2 and COS have equivalent electronic structure and as a result the rates of reaction of both the gases with an amine are comparable (3, 18, 19).

Although the rates of reaction of COS and CO_2 are similar in MEA, the reaction products in the case of COS are not regenerable as in the case of CO_2. The reactions of MEA with COS progress as follows (3, 20):

$$HOCH_2CH_2NH_2 + O=C=S \longrightarrow HOCH_2CH_2NH\overset{\text{O}}{\underset{\text{||}}{C}}-SH \qquad (2.17)$$

$$HOCH_2CH_2NH\overset{\text{O}}{\underset{\text{||}}{C}}-SH + H_2O \longrightarrow HOCH_2CH_2NH_2 + CO_2 + H_2S \qquad (2.18)$$

$$HOCH_2CH_2NH\overset{\text{O}}{\underset{\text{||}}{C}}-SH \xrightarrow{\text{heat}} \underset{O \quad NH}{H_2C \quad CH_2} + H_2S \qquad (2.19)$$

$$HOCH_2CH_2NH\overset{\text{O}}{\underset{\text{||}}{C}}-SH + H_2NCH_2CH_2OH \longrightarrow \underset{HOCH_2CH_2NH}{\overset{HOCH_2CH_2NH}{\diagdown}} C=O + H_2S$$

$$(2.20)$$

$$\begin{array}{l} \text{HOCH}_2\text{CH}_2\text{NH} \\ \hspace{3.5em} \diagdown \\ \hspace{4.5em}\text{C=O} \xrightarrow{\text{heat}} \\ \hspace{3.5em} \diagup \\ \text{HOCH}_2\text{CH}_2\text{NH} \end{array}$$

(2.21)

(structure: N(2-hydroxyethyl) imidazolidone) $+ \ H_2O$

(2.22)

(structure: oxazolidone $+ \ HOCH_2CH_2NH \longrightarrow$ N(2-hydroxyethyl) imidazolidone $+ \ H_2O$)

In Equation (2.17), MEA reacts reversibly with COS to form the thiocarbamate. Addition of water and heat may regenerate the amine (Equation [2.18]), but it may also lead to the synthesis of 2-oxazolidone as indicated in Equation (2.19). The thiocarbamate may react with MEA to form diethanolurea as presented in Equation (2.20). The diethanolurea cyclization reaction occurs on heating (Equation [2.21]) to yield N(2-hydroxyethyl) imidazolidone. This product can also be synthesized with the reaction of oxazolidone with MEA as indicated in Equation (2.22). In industrial operations, the loss of MEA may range from 10% to 100% depending on contactor conditions and strength of the amine solution (1, 3, 5, 6, 20).

DEA is not a very effective solvent for COS leading to large contactor sizes (1, 20). The performance of DIPA is generally comparable with DEA (3). However, Shell International has patented the ADIP process and the Sulfinol process, both of which employ DIPA as the reactive solvent (1, 21, 22). In the Sulfinol process, DIPA is used in conjunction with a physical organic solvent (Sulfolane, tetrahydrothiophene dioxide) and has proven very effective for COS and CH_3SH (1). The ADIP process solvent is 30-40% aqueous DIPA and requires fairly long residence times. It has

been very efficient for sweetening of refinery gases and liquids contain-ing H_2S and CO_2, as well as COS. No wastage of amine occurs through side reactions as in the case of MEA. Furthermore, low regeneration steam re-quirements and the non-corrosive nature of DIPA solutions make it a very attractive option for COS scrubbing.

Danckwerts and Sharma (3) indicate that 2-methyl aminoethanol (MAE), 2-ethyl aminoethanol (EAE), and 2,6-dimethyl morpholine (DMM) are capable of increasing the COS conversion fivefold over MEA, DEA, or DIPA.

The rate constants k_{AM} (defined as in the case of CO_2) for the reac-tions of COS with MEA, DEA, and DIPA are 16, 11, and 6 lit. g mol^{-1}, re-spectively (3, 18, 19). The rate of reaction of COS with any amine is reported to be slightly slower than with CO_2 (18, 19).

Absorption of Methyl Mercaptan in Amines

The removal of methyl mercaptan by amines is limited to its physical solubility (1). The difficulty of ionizing the mercaptan atom in weak bases like amines inhibits any chemical interaction. However, some kine-tic data are available for reactions with aqueous hydroxide solutions (7). The reaction is instantaneous with a forward rate constant in the order of 10^5 lit. g $moles^{-1} \cdot sec^{-1}$.

Experimental Techniques for Fast
Reaction Kinetic Studies

There are many experimental methods available to study fast reaction kinetics. Some of the commonly employed methods are:

1. Thermal continuous flow method (16).

2. Laminar liquid jet method (21).

3. Wetted-wall column method (21).

4. Shock tube method (16).

5. Membrane method (16).

6. Nuclear magnetic resonance spectroscopy (22).

7. Electron spin resonance spectroscopy (23).

8. Visible, ultra-violet and infrared absorption spectroscopy (22).

9. Stirred vessel reactor (21).

CHAPTER III

EXPERIMENTAL METHOD

The experimental setup is described in this chapter. The procedure
of equipment operation and sample loading for nuclear magnetic resonance
spectroscopy (NMR) analysis is also presented.

Apparatus

The experimental apparatus is shown in Figure 2. The reaction ves-
sel was a Claisen distillation flask. The volume of the reaction flask
was 552.5 ml. This volume was determined with the thermometer, glass
burette, and the supply lines inserted as in Figure 2 (see Appendix A).
Uncertainty in liquid amine volume measurements was less than 0.025 ml.
with the high precision burette which was 10 ml. in capacity and had a
capillary nozzle outlet. The temperature of the gas was measured at a
point just above the liquid-gas interface. A mercury thermometer with a
range of -4 F to 220 F was used to measure the gas temperature as the re-
action progressed. The piping consisted of 1/8 in. O.D. stainless steel,
except for the line to the vacuum pump which was 1/4 in. I.D. rubber tub-
ing of 1/4 in. thickness.

Materials

MEA and MDEA were obtained from Alfa Products and were of 96% and
97% purity, respectively. Aldrich Chemical Company provided DMEA of 99%

To air pressure
source

Numbers refer to in-line control valves
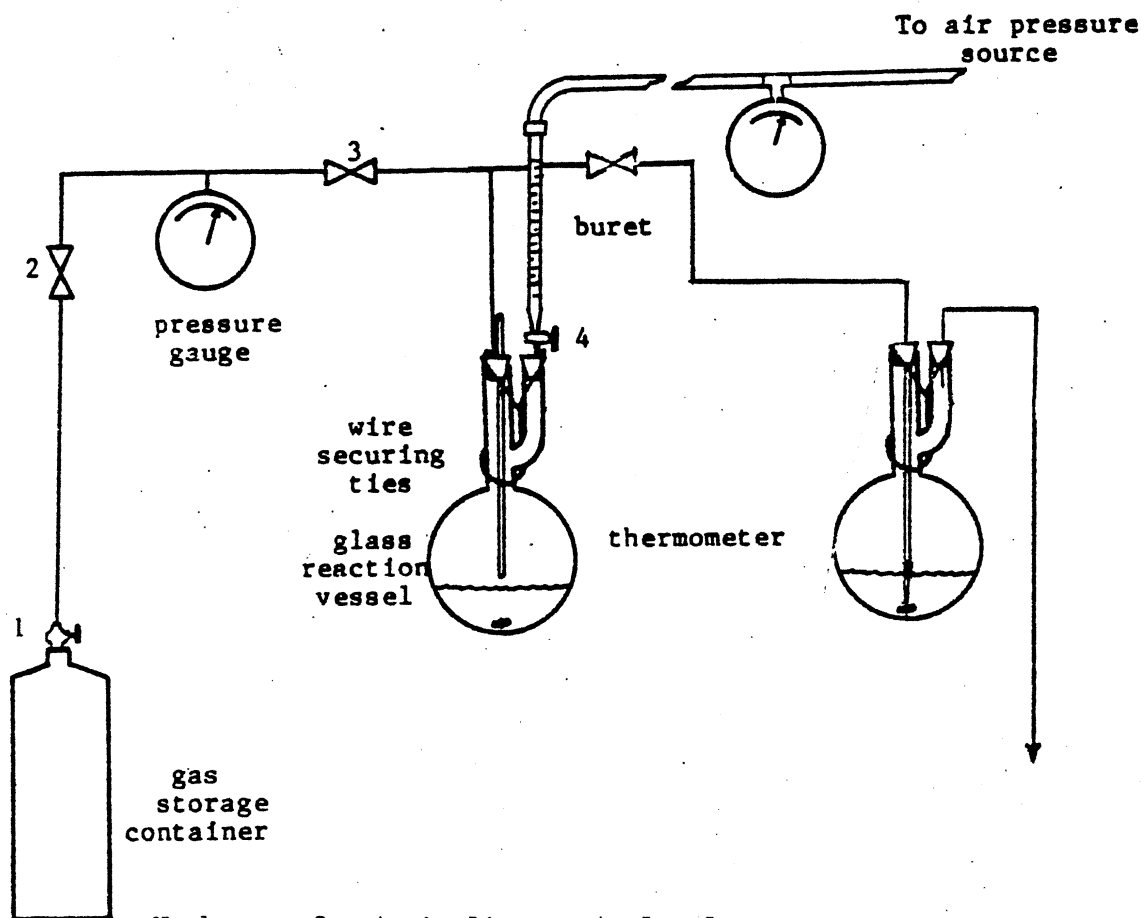
Figure 2. Experimental Apparatus

purity. Reagent grade DEA, assayed to be 99.8% pure, was obtained from Baker Chemical Company. ICN Pharmaceuticals supplied technical grade DIPA and DGA, both of about 95% purity.

Carbon dioxide and hydrogen sulfide gases were supplied by Linde and were of 99.5% purity. Carbonyl sulfide (97.5%) and methyl mercaptan (99.5%) gas cylinders were obtained from Matheson Corporation.

Wilmad Glass Company supplied the reagents and sample tubes for NMR spectroscopic analysis and their purities are as follows: deuterium oxide (heavy water) had a purity of 99.98%; the other solvent employed was deutero-chloroform (99.8%). Calibration of the NMR spectrum scale was performed using tetramethylsilane (TMS) of 99.9% NMR grade and its deuterated form was also of 99.9% NMR grade.

The surface area of the gas-liquid interface was measured using india ink as the reference fluid. The measurements were carried out for different fluid volumes and are presented in Appendix A.

Experimental Procedure

The reaction vessel is evacuated to 28 in. Hg. of vacuum. The acidic gas line valves No. 2 and No. 3 are regulated to allow entry of gas into the flask until the flask pressure reaches ambient pressure. Liquid alkanolamine is charged to the burette and its open end is connected to the air source. The acidic gas control valve is regulated so that the flask pressure is about 20 psig. Expansion of gas takes place in the flask and it is allowed to attain an equilibrium temperature. The air pressure on the burette is increased to 35 psig and the burette stopcock is opened to allow the amine to flow into the flask in an amount equivalent to one-to-one chemical transformation with the acidic gas. A rapid charge of liquid

amine into the reaction flask is ensured by the higher pressure in the
air line. The reaction flask is agitated so that the gas-liquid inter-
face does not remain stagnant. Temperature and pressure levels within
the reaction flask are recorded at one-minute intervals during the first
five minutes and then at five-minute intervals. At the end of an experi-
mental run, the gas residue is passed through a caustic wash before being
vented.

The results are tabulated in Appendix B. A sample calculation for
the amounts of acidic gas and liquid amine is presented in Appendix C.

The preparation of sample for NMR analysis is done as follows. Be-
cause of high viscosity, the amines require substantial dilution in NMR
solvents (D_2O or $DCCl_3$) to obtain sharp resolution in the proton NMR spec-
trum. The product conversion is generally low for most amines (5-15%);
therefore, a 12 mm. diameter sample tube is used instead of the regular
5 mm. tube. The reaction product sample is poured into a sample tube
and the NMR solvent is added to it. The viscosity of the NMR sample is
required to be of a magnitude similar to the viscosity of water for sharp
spectrum resolution; hence the ratio of product sample to NMR solvent is
kept around 1:6. Total volume of a sample within an NMR tube is about 4
ml. This enables relatively rapid scans during ^{13}C NMR analysis without
using an excessive amount of solvent or product sample. The amount of
TMS/deuterated TMS added to the sample is about 1% of the test sample.

CHAPTER IV

THEORETICAL DEVELOPMENT

A brief discussion on the reaction kinetics and the transport equations employed is presented. The direct solutions of the transport equations analytically do not lead to useful interpretation of the experimental data; hence limiting cases for the solutions are discussed.

Carbon Dioxide in Amine Solutions

The chemical reactions of CO_2 in primary or secondary amines yield the amine salt of the carbamic acid:

$$CO_2 + 2\ RR'NH \longrightarrow RR'NCOO^- + RR'NH_2^+ \qquad (4.1)$$
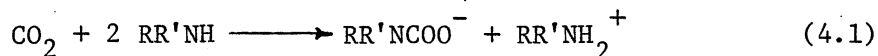
where

$\quad R = CH_2CH_2OH;$ and

$\quad R' = CH_2CH_2OH$ for DEA or H for MEA.

Absence of water eliminates reactions (2.5) to (2.8) from consideration. The rate of reaction r_M (g mol·lit^{-1}·sec^{-1}) of CO_2 may be expressed as (3, 11):

$$r_M = k_{AM} \cdot (Amine)(CO_2) \qquad (4.2)$$

where k_{AM} is the second-order rate constant for the amine (lit·g mol^{-1}· sec^{-1}), and (Amine) and (CO_2) are the concentration of amine and CO_2, respectively (g mol·lit^{-1}). The contributions of reactions with water and with the OH$^-$ ion to the overall rate of reaction need not be considered,

18

as the reaction occurs devoid of water. The presence of water would necessitate inclusion of rate constants of Equation (2.5) to the overall second-order rate constant. Equation (4.2) is valid for primary amines such as MEA and DGA.

Hikita et al. (11), using a rapid-mixing thermal method, showed that the reaction between CO_2 and DEA is of second-order with respect to the amine. Then Equation (4.2) is valid for DEA and DIPA if k_{AM} is made a function of amine concentration:

$$k_{AM} = k_D \text{ (Amine)} \tag{4.3}$$

where k_D is the forward rate constant of DEA and DIPA reactions with CO_2.

The reaction kinetics for the tertiary amine reaction with CO_2 are first order with respect to the amine (11). Thus Equation (4.2) is used for the sake of consistency, although Equation (4.1) is not valid for a tertiary amine.

Carbonyl Sulfide Reactions With Amines

Carbonyl sulfide reacts with an amine in a similar manner as carbon dioxide. The rate of reaction r_C (g mol·lit^{-1}·sec^{-1}) of COS may be written for primary amines as

$$r_C = k_{AM} \text{ (Amine)(COS)} \tag{4.4}$$

This is true for the reaction

$$COS + 2RNH_2 \longrightarrow RNHCOS^- + RNH_3^+ \tag{4.5}$$
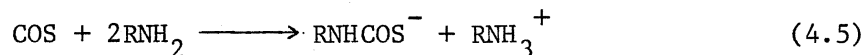
where R is an alkanol or an ether group, and k_{AM} is the forward reaction rate constant of the amine.

In the case of secondary amines, the rate may be also expressed as in Equation (4.4), where k_{AM} is represented as follows:

$$k_{AM} = k_E \text{ (Amine)}$$

where k_E is the forward rate constant of DEA and DIPA reactions with COS.

The reaction between a tertiary amine and COS is of the form of a weak Lewis Acid-Base interaction. The reaction order, as in the case of CO_2, is two overall and one with respect to the amine. Equation (4.4) is a representation of the reaction kinetics.

Reactions involving H_2S and an amine are generally instantaneous. Hence there is more interest in the determination of gas and liquid phase mass transfer coefficients. Also, the reversibility of reactions between H_2S and an amine cannot be ignored, so a knowledge of equilibrium constants is essential for accurate determination of liquid mass transfer coefficients.

Formulation of Transport Equations

In the experimental method described in Chapter III, the reaction rate of the acidic gases within the first minute was generally slow or moderate and stirring the reaction flask ensured that amine depletion at the gas-liquid interface was a minimum, that is, the concentration of amine at the surface was uniform. Under these conditions, the rate of CO_2 and COS consumed per unit area, R, is given by

$$R = P \cdot S \sqrt{D_A \cdot k_{AM} \cdot \text{(AM)}} \qquad (4.6)$$

where P is the pressure exerted by the acidic gas, S is its solubility, (AM) is the amine concentration, and k_{AM} is the rate coefficient (as

defined in Equation [4.2]) which is a function of (AM) for secondary amines.

Now,

$$R = (1/A) \, dn/dt \tag{4.7}$$

where A is the gas-liquid interfacial area, n is the amount of acidic gas consumed, and t is the time elapsed.

Substitution of Equation (4.7) into Equation (4.6) yields the following expression for the transient acidic gas conversion:

$$k_{AM} \, (AM) = (1/D_A) V^2/(Z \cdot S \cdot R_G \cdot T \cdot A)^2 \, (-d \, \ln P/dt)^2 \tag{4.8}$$

where Z is the compressibility factor, T is the absolute temperature in K, V is the volume occupied by the acidic gas in ml., and R_G is the gas constant.

In the case of methyl mercaptan, a non-reacting gas, a similar expression can be obtained for k_L, the mass transfer coefficient, and S, the solubility:

$$k_L = V/(Z \cdot A \cdot R_G \cdot T)(-d \, \ln P/dt) \tag{4.9}$$

Application of Equations (4.8) and (4.9) requires accurate knowledge of D_A and the solubility S.

The diffusivity is estimated from the Wilke and Chang correlation (21):

$$D = 7.4 \times 10^{-8} T \cdot x^{1/2} \cdot M^{1/2}/(\mu \cdot V_G^{0.6}) \tag{4.10}$$

where M is the molecular weight of solvent, T is the temperature in K, μ is the viscosity of solvent in cP, V_G is the molecular volume of the

solute at the normal boiling point in cm^3/gm-mole, and x is an association factor.

Use of the Wilke-Chang correlation requires accurate determination of the viscosity of amines. Experimental viscosity data were obtained for all the amines except MDEA, which was calculated by van Velzen's correlation (24, 25). Table II shows the viscosity of the various amines and Table III presents the calculated diffusivity of the acidic gases in alkanolamines.

Solubility data of the acidic gases in pure amines are generally unavailable. However, the measurement of transient rates of reaction of the acidic gases in the reacting amines provide reasonably accurate values of solubility, and this mode of approximation has been employed satisfactorily by some authors (3).

TABLE II

VISCOSITY OF ALKANOLAMINES

Amine	Viscosity at 27 C (cP)
MEA	15.10 (25, 27)
DEA	505 (25, 27)
DGA	31.20 (25, 27)
DIPA	407 (27)
DMEA	4.51 (26)
MDEA	203 (24, 25)

TABLE III

DIFFUSIVITY OF ACIDIC GASES IN AMINES AT 27 C

Amine	D_{CO_2} (10^{-8} . cm/s)	D_{COS} (10^{-8} . cm/s)
MEA	---	150
DEA	---	5.84
DGA	122	95.20
DIPA	14.7	11.40
DMEA	687	535
MDEA	23.9	18.60

CHAPTER V

RESULTS AND DISCUSSION

This chapter is divided into three sections. In the first section, the identification and an understanding of the mechanism of reaction products formation are presented and is followed by the determination of kinetic rate constants. The third segment emphasizes the reaction rates and relative efficiency of the various amines with respect to the acidic gases.

Reaction Between Carbonyl Sulfide

and Monoethanolamine

The transient rate of reaction data of carbonyl sulfide in monoethanolamine is presented in Table VII (Appendix B). The reaction proceeded at a rapid rate and the final product was green in color. Appendix D presents some of the techniques employed to identify the solid phase. Figures 3 and 4 (Appendix B) show the ^{1}H-NMR spectra of 20% MEA (80% solvent) in $DCCl_3$ and D_2O, respectively. For convenience, the MEA skeletal structure is labeled as

$$N\!-\!\underset{\alpha}{C}\!-\!\underset{\beta}{C}\!-\!OH \qquad\qquad (5.1)$$

In Figure 3, the peak labeled No. 1 is a proton associated with $DCCl_3$ and peaks numbered 2 and 4 are the β and α protons, respectively. The protons of the N atom and OH group are represented by the broad peak

No. 3. Peaks No. 6 and No. 7 in Figure 4 are the α and β protons, respectively, in D_2O solvent. D_2O undergoes a rapid exchange with OH and N protons as indicated by peak No. 5.

The proton NMR scan of MEA and COS reaction products (solvent D_2O) is shown in Figure 5. Apparently a downfield shift of 0.2 ppm is observed for the α and β protons relative to pure MEA, and in the case of the N protons the triplet symmetry was not observed. This indicates the presence of a new species on the N atom. The reactions anticipated are:

$$2 \; HO \cdot CH_2 \cdot CH_2 \cdot NH_2 \; + \; COS \longrightarrow HO \cdot CH_2 \cdot CH_2 \cdot NHCOS \cdot NH_3 \cdot CH_2 \cdot CH_2 \cdot OH$$

$$(5.2)$$
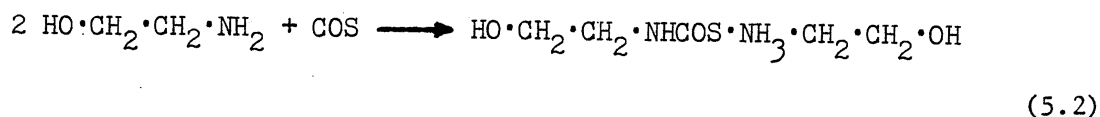
Pure MEA ^{13}C-NMR spectra in $DCCl_3$ and D_2O solvents are shown in Figures 6 and 7, respectively. Peaks No. 8 and No. 10 are those of the β carbon, and peaks No. 9 and No. 11 are the absorption responses of the α carbon. The unnumbered triplets in Figure 6 are the ^{13}C of solvent $DCCl_3$.

Figure 8 shows the ^{13}C-NMR spectrum of the reaction products in D_2O. β and α carbons are represented by labels No. 13 and No. 14, respectively. Monoethanolamine thiocarbamate exhibits a spectrum in which the α and β carbon nuclei and their respective protons are relatively more shielded due to the presence of a carbon atom in the environment of the central N atom. Equation (5.2) indicates that $R \cdot NH_2$ and $R \cdot NH_3^+$ ($R=CH_2 \cdot CH_2 \cdot OH$) are both present in the reaction product mixture and this is borne out in Figure 8 where label a indicates $R \cdot NH_2$ and $R \cdot NH_3^+$ is shown as label b. Peak No. 12 is the ^{13}C nucleus in the group COS^- and the α and β carbons of the $R \cdot NHCOS^-$ ion are represented by peak No. 15.

The overall reaction may be written as

$$R \cdot NH_2 + COS \longrightarrow m\ R \cdot NH_2 + n\ COS + (1-n)\ R \cdot NHCOS \cdot NH_3 \cdot R$$

$$(5.3)$$
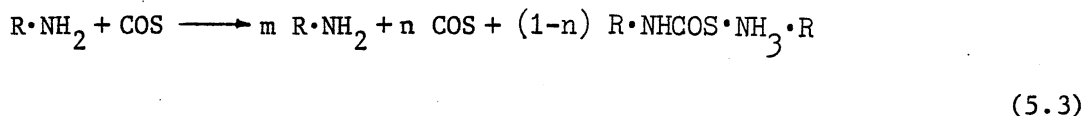
The reaction data in Table IV indicate that about 55% of the COS was unconverted whereas determination of the fraction of a is 0.58 and 0.68 in peaks No. 13 and No. 14, respectively. Based on the above data, a fair estimate of n is 0.6 and, as a consequence, m is calculated to be 0.2.

The reaction products are not completely regenerable because of the degradation of MEA thiocarbamate, with the addition of heat, into 2-oxazolidone and diethanolurea (Equations [2.17] and [2.18]). Detection of the -C=O group of oxazolidone and diethanolurea is generally within the 150-200 ppm range. Figure 8 does not show any signal within this range, which is not surprising because no additional heat was applied to the system except for the heat release of the exothermic forward reaction in Equation (5.3). If any oxazolidone or diethanolurea is produced, the amount is too small for the relatively insensitive ^{13}C-NMR to detect it.

Solubility of Methyl Mercaptan in Monoethanolamine

The solubility data of the methyl mercaptan-monoethanolamine system are presented in Table VIII. The ^{1}H-NMR spectrum of the mercaptan-amine system (DCCL$_3$ solvent) is shown in Figure 9. The absorption peaks centered at labels No. 18 and No. 21 are the protons of the β and α carbons, respectively. The OH and N protons are indicated by label No. 20 and peak No. 16 shows the DCCl$_3$ proton. -SH and -CH$_3$ protons are indicated by No. 17 and No. 19, respectively. The NMR spectra were obtained with 20% of the reaction sample dissolved in D$_2$O which may not be adequate for the carbon-13 NMR scan to compute a sharp absorption response. Figure 10

does not yield any new information and the conclusion is that the weak

basicity of MEA does not allow the ionization of methyl mercaptan into

H^+ and CH_3S^- ions. However, a hydrogen bond interaction probably occurs

of the type

$$H_2N \cdot CH_2CH_2OH$$
$$\vdots$$
$$HS \cdot CH_3 \qquad\qquad (5.4)$$

Reaction Between Carbonyl Sulfide
and Diethanolamine

Pure DEA samples were scanned for proton and carbon-13 (D_2O solvent)

and are presented in Figures 11 and 12, respectively.

The skeleton structure of DEA is

$$H\!-\!N \begin{array}{c} CH_2 \cdot CH_2 \cdot OH \\ \alpha \quad \beta \\ CH_2 \cdot CH_2 \cdot OH \end{array}$$
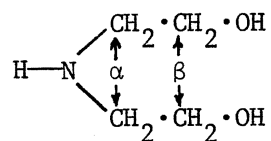
Peak No. 1 shows the rapid exchange of OH and N protons with D_2O.

The triplets centered at No. 2 are β protons followed by α protons at

position 3 (Figure 11). In Figure 12, labels No. 4 and No. 5 indicate β

and α carbon nuclei, respectively. Since the twin α and β carbon nuclei

are in identical magnetic environments, their absorption peaks are ob-

served at the same position in the ^{13}C-NMR spectrum.

The reaction products were miscible in D_2O and analyzed for proton

and carbon-13. Protons of the α and β carbons were found with a down-

field shift of 0.5 ppm. This would occur if a new species attracts elec-

trons of the nitrogen atom which subsequently draws electrons from the α

environment and, as a result, the α nuclei attract the electric field of the β environment.

Further information was obtained from the ^{13}C-NMR spectrum (Figure 14). Peaks labeled No. 10 and No. 11 are β and α carbon nuclei, respectively. Conversion of COS was only about 10% of the original COS concentration, as shown in Table IX (Appendix B). Peak No. 9 is the -COSH product formed according to the following reaction:

$$2 \ (HO \cdot CH_2 \cdot CH_2)_2 N \cdot H + COS \ ----- \ (HO \cdot CH_2 \cdot CH_2)_2 NCOS \cdot NH_2 (CH_2 \cdot CH_2 \cdot OH)_2$$

$$(5.5)$$
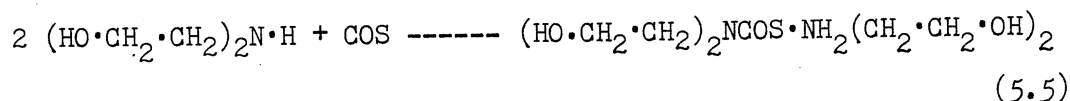
The β carbon nuclei in the DEA molecule exhibit an upfield shift of about 3 ppm in Figure 14. However, the shift is within the range of experimental error of sample preparation for NMR analysis.

Solubility of Methyl Mercaptan in Diethanolamine

The transient rate of absorption of mercaptan in DEA is presented in Table X (Appendix B). In the 30 minutes of residence time the mercaptan solubility was less than 10%. The proton NMR and carbon-13 NMR spectra of the product mixture are shown in Figures 15 and 16, respectively. No information could be deduced from the two spectra which resembled pure DEA scans. The relatively large viscosity of liquid DEA results in large liquid phase resistance to solute transport, thus leading to poor absorption efficiency.

Reaction Between Hydrogen Sulfide and Diglycolamine

Analyses of pure DGA in $DCCl_3$ solvent for protons and carbon-13 nuclei are presented in Figures 17 and 18, respectively. The structural formula is

$$H_2N \cdot \underset{\alpha}{CH_2} \cdot \underset{\beta}{CH_2} \cdot O \cdot \underset{\gamma}{CH_2} \cdot \underset{\delta}{CH_2} \cdot OH$$
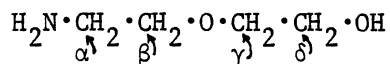
The $DCCl_3$ proton absorption peak is represented by label No. 1 in Figure 17. The set of peaks labeled No. 2 are the β and α protons, respectively. Peak No. 4 is the response of the δ protons and the N and OH protons are represented by label No. 3. In the ^{13}C-NMR spectrum (Figure 18) the magnetic similarity of the β and γ carbon nuclei environment results in two absorption peaks almost at the same position (peak No. 6). Peaks No. 7 and No. 8 are the δ and α carbon nuclei, respectively. DGA was also analyzed for ^{13}C in D_2O solvent (Figure 19). As in the case of $DCCl_3$ solvent, peaks No. 9, No. 10, No. 11, and No. 12 represent γ, β, δ, and α carbon nuclei, respectively.

The rate of reaction data for the H_2S-DGA system are shown in Table XI. The ^1H-NMR spectrum of this system is presented in Figure 20. The absorption peaks were found to be shifted downfield by 0.2 ppm. In Figure 20, peaks labeled No. 14, No. 15, and No. 16 are γ/β protons, N/OH protons, and α protons, respectively. The close proximity of the absorption peaks makes the correct assignment of the -SH proton difficult. The reaction may be expressed as

$$H_2S + H_2 \cdot N \cdot CH_2 \cdot CH_2 \cdot O \cdot CH_2 \cdot CH_2 \cdot OH \rightleftarrows HO \cdot CH_2 \cdot CH_2 \cdot O \cdot CH_2 \cdot CH_2 \cdot NH_3SH$$

(5.6)
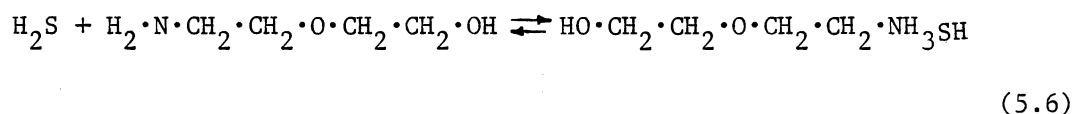
The carbon-13 NMR spectrum of H_2S-DGA system is presented in Figure 21. The scan is identical to the pure DGA ^{13}C-NMR scan as no new carbon species were determined in the reaction product.

Reaction Between Carbon Dioxide and Diglycolamine

Table IX shows the transient reaction rate of the CO_2-DGA system. The proton scan was not of sharp resolution due to the high viscosity of the reaction product. Figure 22 presents the ^{13}C-NMR spectrum of CO_2-DGA product sample. A carbamate peak was observed at 165 ppm (No. 17). Peaks labeled No. 18 and No. 20 are the γ and β carbon nuclei, and δ and α carbon nuclei are represented by No. 21 and No. 23, respectively. The unnumthree peaks are the absorption peaks of $DCCl_3$. The reaction based on the NMR study is

$$2 \ HO \cdot CH_2 \cdot CH_2 \cdot O \cdot CH_2 \cdot CH_2 \cdot NH_2 + CO_2 \longrightarrow$$

$$(5.7)$$

$$HO \cdot CH_2 \cdot CH_2 \cdot O \cdot CH_2 \cdot CH_2 \cdot NHCOO \cdot NH_3 \cdot CH_2 \cdot CH_2 \cdot O \cdot CH_2 \cdot CH_2 \cdot OH$$
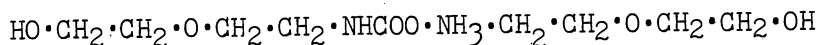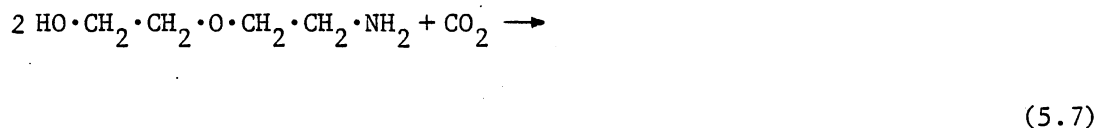
Peaks No. 19 and No. 22 seem to be the β and α carbon nuclei of the protonated amine specified in Equation (5.7). This is also borne out by taking the ratio of peaks No. 22 and No. 23 and comparing it with the conversion from Table IX. The ratio is 0.31, and the fraction of CO_2 gas consumed is 0.315 (Table IX). Thus the ^{13}C-NMR spectrum adequately represents the reaction scheme in Equation (5.7).

Reaction Between Carbonyl Sulfide and Diglycolamine

The proton scan of the COS-DGA system was not sharply resolved at even 10% sample strength in D_2O. Table XIII shows the rate of reaction profile of the COS-DGA system. The ^{13}C-NMR spectrum revealed some new information for this system (Figure 23). The anticipated reaction is of the form

$$HO \cdot CH_2 \cdot CH_2 \cdot O \cdot CH_2 \cdot CH_2 \cdot NH_2 + COS \longrightarrow HO \cdot CH_2 \cdot CH_2 \cdot O \cdot CH_2 \cdot CH_2 \cdot NH \cdot COSH$$
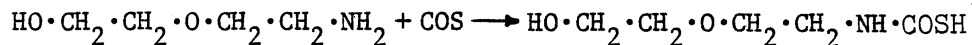
$$(5.8)$$

In Figure 23, the peaks labeled No. 24 and No. 25 are the γ and β carbon nuclei, respectively. Peak No. 28 is that of the δ carbon and the α carbon is represented by peak No. 29.

The COS^- peak, as in the case of MEA in Figure 8, is represented by the label No. 26. The β and γ carbon nuclei of the DGA thiocarbamate (Equation [5.8]) are represented by peak No. 27 and the α carbon of the carbamate by No. 30. In this case, the ratio of peaks No. 30 and 29 is 0.22, whereas the amount of COS reacted according to the experimental run is 28% (Table XIII).

Methyl Mercaptan Absorption in Diglycolamine

Methyl mercaptan absorption data are presented in Table XIV and the proton and carbon-13 spectra are shown in Figures 24 and 25, respectively. The ^{13}C-NMR spectrum did not yield any new information and the proton scan of the CH_3SH-DGA system is basically similar to that of pure DGA except for an upfield shift of 0.2 ppm. A hydrogen bonding type of interaction could play a role in this system. It may be of the form

$$HO \cdot CH_2 \cdot CH_2 \cdot O \cdot CH_2 \cdot CH_2 \cdot NH_2$$
$$\vdots$$
$$H-S-CH_3$$

$$(5.9)$$
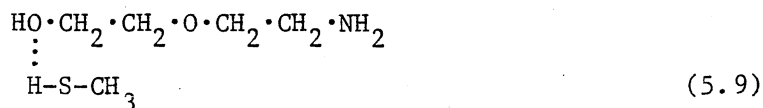
Reaction Between Hydrogen Sulfide
and Diisopropanolamine

The pure DIPA ^1H-NMR spectra in $DCCl_3$ and D_2O are presented in Figures 26 and 27, respectively. The skeletal arrangement of DIPA is

$$\begin{array}{c} \text{OH} \\ | \\ {}_{\alpha}\text{C}-\overset{}{\text{C}}-\text{C-} \\ -\text{N} \quad {}_{\beta}\quad {}_{\gamma} \\ \text{C}-\overset{}{\text{C}}-\text{C-} \\ | \\ \text{OH} \end{array} \qquad (5.10)$$

In Figure 26, the peaks centered at No. 1 are the N and OH protons. The lack of sharp resolution may be du to the multiple OH absorption response. The peaks centered at label No. 2 are the β protons followed by the α and γ protons at positions No. 3 and No. 4, respectively. The peaks centered at No. 5 are the result of the exchange of protons of OH and N atom with the D_2O solvent. The β, α, and γ proton absorptions are reflected by peaks No. 6, No. 7, and No. 8, respectively.

The reaction between DIPA and H_2S is expected to proceed in the form

$$(CH_2 \cdot CHOH \cdot CH_2)_2 NH + H_2S \longrightarrow (CH_3 \cdot CHOH \cdot CH_2)_2 NH_2 SH \qquad (5.11)$$
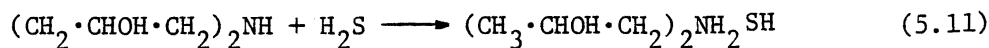
The peaks labeled No. 9, 11, and 12 in Figure 28 are ^1H absorption response of the β, α, and γ protons, respectively. The nitrogen and hydroxyl protons (No. 10) show an upfield shift of 1 ppm.

The carbon-13 NMR spectra of pure DIPA in $DCCl_3$ and D_2O solvents are presented in Figures 29 and 30, respectively. The β carbon nuclei are indicated by labels 13, 14, 19, and 20; the α carbon nuclei by 15, 16, 21, and 22, whereas the γ carbon nuclei are shown as No. 17, 18, 23, and 24, respectively.

The reaction sample was also examined for carbon-13 and Figure 31 shows the ^{13}C-NMR. No new information was revealed from the carbon-13 scan. Table XV presents the transient rate of reaction data of the H_2S-DIPA system. Conversion was determined to be less than 10% within the 30 minutes of residence time. Pure DIPA has a freezing point of 107.6 F and as a result the reaction was initiated at 110 F so that DIPA entered the

reaction flask as a liquid. However, at the end of the reaction period the temperature dropped below the freezing point of DIPA and some of the liquid amine was observed to solidify and settle at the bottom of the flask.

Reaction Between Carbon Dioxide
and Diisopropanolamine

Table XVI presents the rate of reaction data for the CO_2-DIPA system. The proton and carbon-13 spectra of this system are shown in Figures 32 and 33, respectively. No shift was observed in the proton scan. DIPA carbamate was observed in the carbon-13 spectrum (No. 31). The reaction scheme is of the following form:

$$CO_2 + 2(CH_3 \cdot CHOH \cdot CH_2)_2 \cdot NH \longrightarrow$$

$$(CH_3 \cdot CHOH \cdot CH_2)_2 \cdot NCOO \cdot NH_2 \cdot (CH_2 \cdot CHOH \cdot CH_3)_2 \qquad (5.13)$$
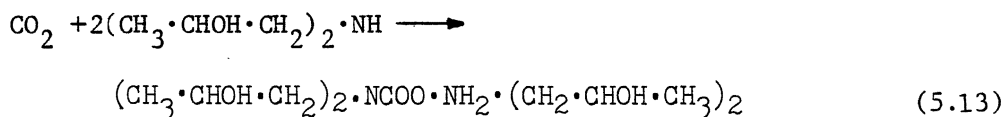
The β carbon nuclei are represented by labels No. 33 and 34, the α carbon nuclei by No. 36 and 37, and the γ carbon nuclei by No. 38 and 39, respectively. The β carbon nuclei of the carbamate ion (Equation [5.12]) are shown by peak No. 32. $DCCl_3$ solvent shows three absorption peaks centered at about 77 ppm.

The reaction scheme specified in Equations (5.12) and (5.13) is consistent with the conclusions from the carbon-13 NMR spectrum of the reaction product sample.

Reaction Between Carbonyl Sulfide
and Diisopropanolamine

The pressure-time profile of COS interaction with DIPA is presented

in Table XVII. The reaction rate closely follows that of CO_2 with DIPA; hence a similar reaction scheme was postulated:

$$(CH_3 \cdot CHOH \cdot CH_2)_2 \cdot NH + COS \longrightarrow (CH_3 \cdot CHOH \cdot CH_2)_2 \cdot N \cdot \underset{\underset{SH}{|}}{C} = O \qquad (5.14)$$

No significant shift was revealed in the proton scan of the product sample (Figure 34).

An important aspect of the DIPA reaction with COS and CO_2 is the problem of steric hindrance of the isopropanol groups which hamper the transport of COS and CO_2 molecules to the vicinity of the nitrogen atom. For this reason, DIPA is not as effective as other primary and smaller chained secondary amines for removal of COS. Processes employing DIPA as a solvent require longer residence times relative to other commonly used amines.

The carbon-13 spectrum of the COS-DIPA reaction product system is presented in Figure 35. Apart from the absorption responses for the various carbon nuclei of DIPA, an additional peak was observed which was attributed to the 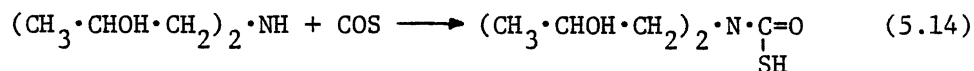thiocarbamate carbon (No. 40). The β carbon nuclei of the unreacted amine are represented by labels No. 41 and 42, the α carbon nuclei by No. 43 and 44, and the γ carbon nuclei by peaks No. 45 and 46, respectively. The formation of diisopropanolamine thiocarbamate is the only reaction detected by NMR spectroscopy.

Solubility of Methyl Mercaptan
in Diisopropanolamine

Diisopropanolamine is not a strong base and does not facilitate the dissociation of methyl mercaptan. However, a strong hydrogen bond is speculated between the N atom of the DIPA molecule and the CH_3SH protons.

Table XVIII (Appendix B) presents the transient absorption data of mercaptan in DIPA. The proton and carbon-13 spectra are shown in Figures 36 and 37, respectively. In the carbon-13 spectrum, a mercaptan peak was not observed and no shift was noticed of DIPA carbon nuclei. The proton scan revealed that the nitrogen and hydroxyl protons were not sharply resolved, although the methyl and the methylene group were unaffected. This is speculated to be due to a hydrogen bonding of the form

$$(CH_3 \cdot CHOH \cdot CH_2)_2 \cdot NH \atop \vdots \atop H-S-CH_3 \qquad (5.15)$$
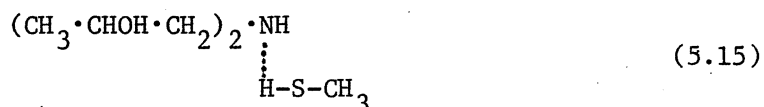
In Figure 36, the peaks centered at label No. 47 are β protons. The lump designated as label No. 48 is the -OH proton absorption response. The α protons are represented by label No. 49. There is a distinct separation in the shifts of the nitrogen proton as compared to the shift of hydroxyl protons. Peak No. 50 represents the nitrogen proton. The γ protons are represented by the set of peaks centered at position No. 51. Equation (5.15) shows the probable hydrogen bonding interaction site between the mercaptan and diisopropanolamine molecules.

Solubility of Methyl Mercaptan

in Methyldiethanolamine

Table XIX (Appendix B) presents the solubility data of methyl mercaptan in methyldiethanolamine. The skeletal structure of MDEA is

$$\begin{array}{c} HO \cdot CH_2 \cdot CH_2 \\ \gamma \quad \beta \quad \diagdown \\ \quad \quad N \cdot CH_3 \\ HO \cdot CH_2 \cdot CH_2 \diagup \end{array} \qquad (5.16)$$

Figure 38 shows the proton spectrum of pure MDEA in $DCCl_3$. Peak No. 1 is the absorption peak of the OH proton followed by a triplet (No. 2) of γ protons. The α and β protons are shown by a triplet centered at position No. 3 and a quintuplet centered at No. 4, respectively.

The carbon-13 spectrum of pure MDEA (Figure 39) shows γ and β carbon nuclei at positions No. 5 and No. 6, respectively. Peak No. 7 is the α carbon nucleus. The magnetic field similarity of each pair of γ and β carbons is exhibited by two peaks at the same position.

The proton spectrum of the CH_3SH-MDEA system is presented in Figure 40. Peaks No. 9, No. 10, and No. 11 are the γ, β, and α protons, respectively. Only the hydroxyl proton shows a downfield shift of 0.1 ppm (No. 8).

The ^{13}C-spectrum (Figure 41) does not reflect any absorption response for the mercaptan carbon nucleus, presumably due to the low product sample concentration (20%).

The downfield shift of the OH proton may be explained in terms of hydrogen bonding interaction between the oxygen atom of the amine and the mercaptan proton as illustrated in Equation (5.17):

$$HO \cdot CH_2 \cdot CH_2 \diagdown$$
$$N \cdot CH_3$$
$$HO \cdot CH_2 \cdot CH_2 \diagup$$
$$\vdots$$
$$H \cdot S \cdot CH_3$$

(5.17)
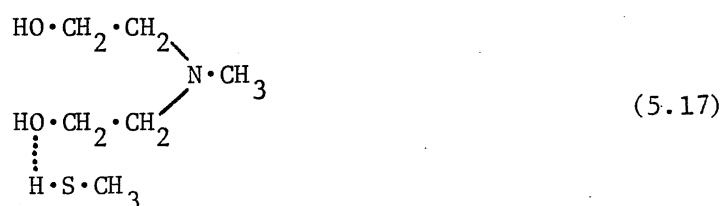
Reaction Between Carbon Dioxide

and Methyldiethanolamine

Table XX shows the reaction data for the CO_2-MDEA system. Figure 42 presents the MDEA-CO_2 system ^{1}H-NMR spectrum in which the OH proton is at label

No. 15. The triplets centered at No. 16 and No. 17 are γ and β protons, respectively. Peak No. 18 indicates the absorption response of the α proton.

The carbon-13 spectrum of the MDEA-CO_2 system (Figure 43) shows a 1 ppm downfield shift for γ carbon (No. 19) and a 2 ppm downfield shift for β carbon nuclei (No. 20). The two shifts indicate a weak interaction between a CO_2 molecule and an MDEA molecule of the form

$$(OH \cdot CH_2 \cdot CH_2)_2 \overset{\vdots}{N} \cdot CH_3 \atop O=C=O \tag{5.18}$$
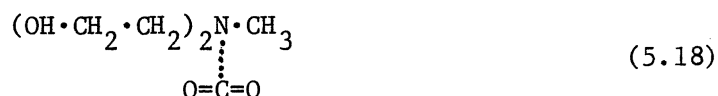
This form of interaction would alter the electric field of the central nitrogen atom, reducing its shielding. The nitrogen atom in turn attracts the α and β electrons, resulting in the 2 ppm downfield shift for the α and β protons. The β nuclei also reduce the shield of the γ carbon nuclei (1 ppm downfield shift).

The proton scan of the MDEA-CO_2 system did not reveal any shift with respect to the pure MDEA. A weak Lewis acid-base interaction is the probable reaction and the resulting complex is relatively unstable and decomposes into the original reactants.

Reaction Between Carbonyl Sulfide

and Methyldiethanolamine

The transient reaction data of the COS-MDEA system are presented in Table XXI. Figures 44 and 45 are the ^{1}H and ^{13}C-NMR spectra, respectively, of the COS-MDEA system. No new peak nor shift is observed in either of the two scans. However, an interaction scheme is proposed similar to the carbon dioxide and methyldiethanolamine reaction:

$$(HO\ CH_2\ CH_2)_2 \overset{\displaystyle N}{\underset{\displaystyle S=C=O}{\vdots}} CH_3 \tag{5.19}$$

This product is a weak Lewis acid-base complex and is not as stable as the thiocarbamate product synthesized in the case of primary and secondary amines.

<div align="center">

Reaction Between Hydrogen Sulfide
and Methyldiethanolamine

</div>

The proton NMR spectrum of the H_2S-MDEA system is shown in Figure 46. The two triplets centered at positions No. 28 and No. 30 are the γ and β protons, respectively. The peaks centered at No. 31 are the α protons. The response of the hydroxyl protons are not of good resolution and shows an upfield shift of 0.6 ppm.

The acid-base interaction in the MDEA-H_2S system is of the form

$$H \cdot SH + (HO \cdot CH_2 \cdot CH_2)_2 N \cdot CH_3 \longrightarrow (HO \cdot CH_2 \cdot CH_2)_2 NHCH_3\ SH$$

$$\tag{5.20}$$
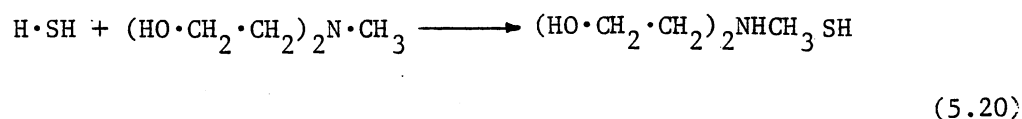
The upfield shift may occur due to the ionic attraction between the protonated amine and the dissociated SH^- ion. Table XXII presents the reaction kinetics data of the MDEA-H_2S system.

<div align="center">

Reaction Between Hydrogen Sulfide
and Dimethylethanolamine

</div>

The reaction data of the H_2S-DMEA system is shown in Table XXIII. Pure DMEA proton scans in $DCCl_3$ and D_2O are shown in Figures 48 and 49, respectively. Peaks No. 1 and No. 4 are the absorption responses of the hydroxyl proton, and the triplets at positions No. 2 and No. 5 are the γ
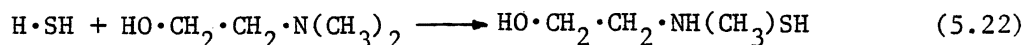
protons. The superimposed triplets and the quintuplets No. 3 and No. 6 are the β and α protons, respectively.

The skeletal structure of DMEA is

$$\text{HO} \cdot \underset{\gamma}{\text{CH}_2} \cdot \underset{\beta}{\text{CH}_2} \cdot \underset{\alpha}{\text{N(CH}_3)_2} \qquad (5.21)$$

The carbon-13 NMR spectra of pure DMEA in $DCCl_3$ and D_2O solvents are illustrated in Figures 50 and 51, respectively. Peaks No. 7 and No. 10 are the γ carbon nucleus, positions No. 8 and No. 11 is the β carbon nucleus, and labels No. 9 and No. 12 represent the twin α carbon nuclei.

The ^{1}H-NMR spectrum of the H_2S-DMEA system ($DCCl_3$ solvent) is shown in Figure 52. The proposed overall reaction is of the form

$$\text{H} \cdot \text{SH} + \text{HO} \cdot \text{CH}_2 \cdot \text{CH}_2 \cdot \text{N(CH}_3)_2 \longrightarrow \text{HO} \cdot \text{CH}_2 \cdot \text{CH}_2 \cdot \text{NH(CH}_3)\text{SH} \qquad (5.22)$$

Examination of Figure 52 for this product indicates a new peak (No. 13) not present in the pure DMEA spectrum (Figure 48). This peak is assigned to the new proton associated with the N atom (Equation [5.22]). The peaks labeled No. 14, No. 15, and No. 16 are the hydroxyl, γ, α, and β protons, respectively. The hydroxyl proton is shifted upfield by a significant amount (1.5 ppm). This would occur in case of a strong interaction (ionic bond) between the protonated amine and the dissociated SH⁻ ion.

<div align="center">

Reaction Between Carbon Dioxide

and Dimethylethanolamine

</div>

The proton scan of CO_2-DMEA (Figure 53) did not reveal any new absorption peaks or any significant shifts. The kinetic rate data are presented in Table XXIV. Release of carbon dioxide gas pressure over the

reaction flask at the end of an experimental run triggered an effervescense in the liquid product mass. This resulted in poor NMR scans of proton and carbon-13 (Figures 53 and 54). No conclusive evidence of a reaction or its mode could be made. However, the formation of a weak Lewis acid-base complex in a manner similar to the CO_2-MDEA reaction system is very likely.

<div align="center">

Reaction Between Carbonyl Sulfide

and Dimethylethanolamine

</div>

Table XXV presents the kinetic data of the COS-DMEA reaction system. The proton scan of the product sample (Figure 55) shows the hydroxyl proton at peak No. 17; the triplets centered at No. 18 and No. 19 are the γ and β protons, respectively. The six α protons are centered at peak No. 20.

In the ^{13}C-NMR spectrum (Figure 56), the γ and β carbon nuclei are located at positions No. 21 and No. 22, respectively, and the two α carbon nuclei at 45 ppm (No. 23). The reaction product is probably a weak Lewis acid-base complex of the form

$$HO \cdot CH_2 \cdot CH_2 \cdot \underset{\vdots}{N}(CH_3)_2 \qquad (5.23)$$
$$S=C=O$$

The lack of "labile" hydrogen atoms bonded to the N atom of a tertiary amine like DMEA results in an unstable product, unlike the secondary and primary amines which yield stable carbamates.

Solubility of Methyl Mercaptan

in Dimethylethanolamine

The solubility data of methyl mercaptan in DMEA are presented in

Table XXVI. Figure 57 shows the proton scan in which the hydroxyl proton

was of poor resolution. The mercaptan cannot be ionized in the weakly

basic DMEA liquid; hence the only recourse is an hydrogen bond type inter-

action which may be of the following form:

$$(CH_3)_2 N \cdot CH_2 \cdot CH_2 \cdot OH$$
$$\vdots$$
$$H \cdot S \cdot CH_3$$

$$(5.24)$$
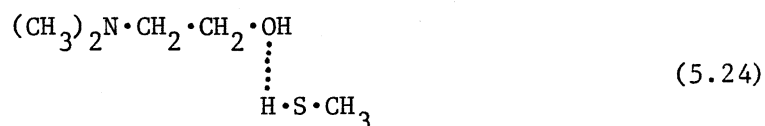
The carbon-13 spectrum of the CH_3SH-DMEA system is presented in Fig-

ure 58. The carbon atom of the mercaptan molecule was not revealed in

the ^{13}C-NMR spectrum, presumably due to the low concentration of the pro-

duct sample used for NMR analyses.

Determination of Rate Constants and

Mass Transfer Coefficients

The values of k_{AM}, as determined from Equation (4.8) for carbon di-

oxide reactions with alkanolamines are presented in Table IV, along with

calculated values of $\Delta P/Pt$ and solubility S.

The reaction rate parameters of DGA and DIPA with CO_2 are substan-

tially greater in magnitude than the two tertiary amines considered in

this study. DGA is apparently the most effective amine for CO_2 removal.

The kinetics of reaction between the various amines with COS is shown

in Table V. Carbonyl sulfide was always found to have slightly lower con-

version than carbon dioxide when reacted with the amines. MDEA and DMEA

TABLE IV

REACTION RATES OF CARBON DIOXIDE AT 27 C

Amine	(AM) Mol/Lit	$10^3 \cdot S$ Gm Mol/Atm-Cm^3	10^3 (d ln P/dt) 1/Sec	log k_{AM}	Log k_{AM} Literature
DGA	10.10	2.780	9.988	3.18	
DIPA	7.44	0.583	0.526	2.03	2.6 (3, 19)
MDEA	9.70	0.773	0.109	0.12	
DMEA	9.94	0.255	0.096	0.27	

TABLE V

REACTION RATES OF CARBONYL SULFIDE AT 27 C

Amine	(AM) Mol/Lit	$10^3 \cdot S$ Gm Mol/Atm-Cm^3	10^3(d ln P/dt) 1/Sec	Log k_{AM}	Log k_{AM} Literature
MEA	16.70	2.780	504	1.90	1.2 (3,19)
DEA	10.40	0.356	14.500	1.65	1.04 (19)
DGA	10.10	1.660	10.000	2.22	
DIPA	7.44	0.680	0.440	1.96	0.75 (19)
MDEA	9.70	0.821	0.097	0.03	
DMEA	9.94	1.160	0.077	0.05	

react slowly with COS with respect to the other amines. MEA, DIPA, and DGA were found to have rapid reactions rates with DGA being the most reactive.

The kinetic rate constants determined in Tables IV and V were compared with literature data. Sharma (19) reported several constants at 25 C, which are listed in Tables IV and V. Amine concentrations were in the range 20-30% in his experimental data. The agreement with published data was quite satisfactory despite the uncertainties existing in the determination of diffusivity coefficients, solubilities, and viscosities for some amines. The error in the computation of rate constants in Tables IV and V is unlikely to be greater than 20%.

Mass transfer coefficient calculations for CH_3SH in the various amines are presented in Table VI. DGA is found to be the best solvent with a value of 14.08×10^{-6} gm.mol/cm^2-atm-sec for $k_L S$ which is a good indicator of solvent efficiency. Amines with lower viscosity at room temperature were better mercaptan absorbents. The efficiency of mercaptan absorption may be expressed as

$$DGA > DMEA > MEA > MDEA > DEA > DIPA \ .$$
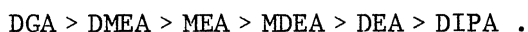
Efficiency and Relative Preference of

Alkanolamines for Acid-Gases

The relative rates of reaction for acidic gases reaction with monoethanolamine are $CH_3SH < COS$ for a time duration of 30 minutes. Figure 59 combines the experimental results of Batt (13) and this study; the relative rates of reaction then becomes $CH_3SH < COS < CO_2 < H_2S$. Carbonyl sulfide is the only acidic gas to react irreversibly with MEA. The product

TABLE VI

MASS TRANSFER COEFFICIENT OF METHYL MERCAPTAN
IN ALKANOLAMINES AT 27 C

Amine	$10^3 \cdot d \ln P/dt$ 1/Sec	$10^3 \cdot S$ Gm·Mol/Atm-Cm^3	$10^6 \cdot S \cdot k_L$ Gm·Mol/Cm^2-Atm-Sec
MEA	5.94	1.45	9.69
DEA	0.04	0.47	3.81
DGA	10.27	1.51	14.10
DIPA	3.61	0.39	3.72
MDEA	4.74	0.60	5.23
DMEA	9.50	1.37	11.50

is monoethanolamine thiocarbamate, a solid at room temperature and green in color.

Examination of the chemical structures of carbonyl sulfide and carbon dioxide indicate they are both linear molecules and, as their reactions with bases are similar, a close relationship is expected in the rates of reaction of the two acid-gases with alkanolamines. Figure 59 shows that the profiles of CO_2 and COS curves are close to each other as compared to other acidic gases (within 10%).

The other primary amine studied is diglycolamine, and Figure 60 shows the experimental results for H_2S, CO_2, CH_3SH, and COS reactions with DGA. Again, the similarity in COS and CO_2 reactions is evident from Figure 60. The relative rates, in the case of DGA, are in the order $H_2S < CH_3SH < COS < CO_2$. All the reactions were exothermic and, in the case of CO_2 and COS, most of the reaction is complete within the first two minutes of exposure of liquid amine to the acidic gases.

Diglycolamine is the more efficient primary amine in reacting with methyl mercaptan, while monoethanolamine is a better chemical solvent in the case of hydrogen sulfide. No significant difference was found in the reactions of CO_2 and COS with the two primary amines.

Diethanolamine was reacted with carbonyl sulfide and carbon dioxide, and Figure 61 illustrates the rates of reaction of the two acidic gases. The relative rates of reaction are $COS < CH_3SH$. Tables IX and X (Appendix B) indicate that the reactions of DEA with CH_3SH is less exothermic than with COS.

Figure 62 shows the experimental results of diisopropanolamine with the various acidic gases. The relative rates are $H_2S < CH_3SH < COS < CO_2$. The rates of reaction of CO_2 and COS with DIPA were within 5% of each

other at the end of 30 minutes of residence time. However, the initial rate of reaction is much faster in the case of CO_2 than with COS.

A comparison of the performance of secondary amines with CH_3SH and COS gases is illustrated in Figure 61. The mercaptan solubility of both DEA and DIPA were similar. However, DIPA is a more effective solvent in removal of COS than DEA.

The two tertiary amines investigated are methyldiethanolamine and dimethylethanolamine. Figure 63 shows the kinetic pressure data of MDEA reactions with COS, H_2S, and CH_3SH acid-gases. H_2S removal is more pronounced than the other gases. This selectivity is due to the fact that the carbamate formation option is unavailable in the case of tertiary amines. The relative preference of MDEA is $H_2S > COS > CO_2 > CH_3SH$. Although the reaction rates of COS and CO_2 in MDEA were close to each other, COS conversion was more than that of CO_2, contrary to the reactions of primary and secondary amines.

Figure 64 presents the experimental reaction data of H_2S, CO_2, COS, and CH_3SH. As in the case of MDEA, COS conversion was higher than CO_2. The rate of acidic gas removal by DMEA is in the order of $H_2S > COS > CH_3SH > CO_2$.

An attempt was made to correlate experimental acidic gas pressure data to the time elapsed. Of the various forms of equations tried, an Antoine type of expression gave a surprisingly good fit. The Antoine equation used is of the form

$$\ln P = A + B/(t + C) \qquad (5.25)$$

The constants of the equation are A, B, and C. P and t are pressure on the system in psia units and time elapsed in minutes, respectively.

Table XXVII (Appendix B) presents the constants A, B, and C of the various acidic gas-alkanolamine systems along with the maximum and average absolute deviation.

CHAPTER VI

CONCLUSIONS AND RECOMMENDATIONS

Conclusions

The following conclusions may be drawn from the results of this study:

1. Carbon dioxide reaction with DGA, DEA, and DIPA yielded the respective carbamate. Tertiary amines, MDEA and DMEA, did not form carbamates. Instead, a weak Lewis acid-base interaction occurs with carbon dioxide. The calculation of kinetic rate constants indicates that DGA and DIPA are very good reactive solvents for CO_2, and MDEA and DMEA are poor solvents.

2. The reactions between COS and tertiary amines, as in the case of CO_2, indicate formation of unstable weak Lewis acid-base complexes. Primary amines (MEA and DGA) and secondary amines (DEA and DIPA) synthesize their respective thiocarbamates. The rate constants show that DGA, DIPA, and MEA are effective reagents for COS removal.

3. Alkanolamine reaction with H_2S yields a bisulfide complex. The rate of reaction of H_2S with alkanolamine is instantaneous relative to CO_2 and COS reactions.

4. No conclusive evidence of a reaction between CH_3SH and the alkanolamines was found. However, a strong hydrogen bond type of interaction was revealed between the mercaptan proton and the oxygen and nitrogen atoms of the alkanolamines. Calculation of $k_L S$, the product of mass

transfer coefficient and solubility, show that DGA, MDEA, and DMEA are the most effective absorbents of methyl mercaptan.

5. The stirred vessel is a viable method for determining kinetic rate parameters as well as liquid and gas phase mass transfer coefficients.

Recommendations

The following recommendations are attractive options for further investigation:

1. The kinetics of acidic gases reactions with alkanolamines may be studied by the measurement of liquid phase amine concentration at various time intervals. This will help in determining the order of reactions between acidic gases and amines where ambiguity exist in the literature.

2. The effect of hydrolysis of CO_2 and COS in aqueous amine solutions may be investigated.

3. Increasing the number of acquisitions in carbon-13 NMR analyses should improve the response of the absorption peaks, leading to better understanding of product molecular structures, especially in the case of low product conversion.

BIBLIOGRAPHY

(1) Kohl, A., and F. Reisenfeld. Gas Purification. Third Edition.
        Houston, Texas: Gulf Publishing Co., 1979.

(2) Maddox, R. N. Gas and Liquid Sweetening. Second Edition.
        Campbell Petroleum Series, Norman, Oklahoma, 1977.

(3) Danckwerts, P. V., and M. M. Sharma. "The Absorption of Carbon Di-
        oxide Into Solutions of Alkalis and Amines." The Chemical
        Engineer, CE 244 (Oct., 1966).

(4) Ammons, H. L., and D. M. Sitton. "Operating Data From a Commercial
        MDEA Gas Theater." Univ. of Okla. Gas Cond. Conf., Norman,
        Oklahoma, March 2-4, 1981.

(5) Weber, S., and G. McClure. "New Amine Process for FCC." Oil and
        Gas Journal, Vol. 79, No. 23 (June, 1981), pp. 160-163.

(6) McClure, G. P., and D. C. Morrow. "Amine Process Removes COS From
        Propane Economically." Oil and Gas Journal, Vol. 77, No. 27
        (July, 1979), pp. 106-108.

(7) Landry, J. E. "The Effect of a Second Order Chemical Reaction on
        the Absorption of Methyl Mercaptan in a Laminar Liquid Jet."
        (Unpublished Ph.D. thesis, Louisiana State Univ., 1966.)

(8) Sigmund, P. W., K. F. Butwell, and A. J. Wussler. "HS Process Re-
        moves H_2S Selectively." Hydrocarbon Processing, Vol. 60, No. 5
        (May, 1981), p. 119.

(9) Astarita, G. Mass Transfer With Chemical Reaction. New York:
        Elsevier Publishing Company, 1967.

(10) Danckwerts, P. V., and K. M. McNeil. "The Absorption of Carbon Di-
        oxide Into Aqueous Amine Solutions and the Effect of Cataly-
        sis." Trans. Instn. Chem. Engr., Vol. 45 (1967), p. T 32.

(11) Sharma, M. M., and P. V. Danckwerts. "Fast Reactions of CO_2 in
        Alkaline Solutions." Chem. Eng. Sci., Vol. 18 (1963), p. 729.

(12) Hikita, H. et al. "The Kinetics of Reactions of CO_2 With MEA, DEA
        and TEA by a Rapid Mixing Method." The Chem. Eng. Journal,
        Vol. 13 (1977), pp. 7-12.

(13) Batt, W. T. "Monoethanolamine Reactions With Selected Acid Gases."
      (Unpublished M.S. thesis, Oklahoma State Univ., 1979.)

(14) Laddha, S. S., and P. V. Danckwerts. "Reaction of CO_2 With Ethanol-
      amines Kinetics From Gas Absorption." Chem. Eng. Sci., Vol.
      36, No. 3 (1981), pp. 479-82.

(15) Hikita, H. et al. "Absorption of Carbon Dioxide Into Aqueous Mono-
      ethanolamine Solutions." A. I. CH. E. J., Vol. 25, No. 5
      (1979), pp. 793-800.

(16) Nguyen, Y. N. "Carbon Dioxide Transport and Reaction Mechanisms in
      Ethanolamine Solutions." (Unpublished Ph.D. thesis, Univ. of
      Rochester, 1979.)

(17) Sada, E., H. Kumazawa, and M. A. Butt. "Absorption With Consecutive
      Reaction: Absorption of Carbon Dioxide Into Aqueous Amine
      Solutions." Can. J. Chem. Eng., Vol. 54 (1976), p. 421.

(18) Sharma, M. M., and P. V. Danckwerts. "Absorption of Carbonyl Sul-
      fide in Amines and Alkalis." Chem. Eng. Sci., Vol. 19 (1964),
      pp. 991-92.

(19) Sharma, M. M. "Kinetics of Reactions of Carbonyl Sulfide and Car-
      bon Dioxide With Amines and Catalysis by Bronsted Bases of the
      Hydrolysis of COS." Trans. Faraday Soc., Vol. 61 (1965), p.
      681.

(20) Pearce, R. L., J. L. Arnold, and C. K. Hall. "Studies Show Carbonyl
      Sulfide Problem." Hydrocarbon Proc. and Petro. Refiner, Vol.
      40, No. 8 (1961), p. 121.

(21) Danckwerts, P. V. Gas Liquid Reactions. New York: McGraw-Hill
      Book Co., 1970.

(22) Skoog, D. A., and D. M. West. Principles of Instrument Analysis.
      Second Edition. Philadelphia: Saunders Golden Series, 1980.

(23) Mattson, J. S., H. B. Mark, Jr., and H. C. MacDonald, Jr. Spectro-
      scopy and Kinetics. New York: Marcel Dekker, 1973.

(24) Van Velzen, D., R. L. Cardozo, and H. Langenkamp. "A Liquid Vis-
      cosity-Temperature-Chemical Constitution Relation for Organic
      Compounds." Ind. Eng. Chem. Fundam., Vol. 11, No. 1 (1972),
      pp. 20-25.

(25) Chen, D. H. "Prediction of Liquid Viscosity for N-Alkanes, N-Alco-
      hols and N-Alkanones." (Unpublished Ph.D. thesis, Oklahoma
      State Univ., 1981.)

(26) Al-Harbi, D. K. "Viscosity of Selected Hydrocarbons Saturated With
      Gas." (Unpublished Ph.D. thesis, Oklahoma State Univ., 1981.)

(27) GPSA Engineering Data Book. Ninth Edition (Revised).
          Texas: Gas Processors Association, 1973.

(28) Maddox, R. N. Private communication, June, 1982.

(29) Klein, J. P. "Developments in Sulfinol and ADIP Processes Increase
          Uses." Hydrocarbon Processing, Vol. 49, No. 9 (Sept., 1970),
          p. 247.

APPENDIX A

VOLUME AND SURFACE AREA DETERMINATION

The volume of the Claisen distillation flask was determined with distilled water as a reference. Three determinations of volume were obtained and they are 550.5 ml., 553.0 ml., and 554.0 ml., respectively. The reaction flask was filled with distilled water, with the thermometer, glass burette, and supply lines inserted as illustrated in Figure 2. Then it was discharged to a graduated cylinder of 100 ml. capacity. For measurements of less than a 100 ml., a graduated cylinder of capacity 25 ml. was employed.

The arithmetic mean of the three observations is 552.5 ml. and this value is retained as the flask volume. Precision in this method of determination is less than 1%.

The surface area of the gas-liquid interface was measured by pouring a known volume of india ink in the flask and then determining the surface diameter. The error in diameter observation is less than 1/16 in. The surface area was determined from the relation

$$A_s = \pi \cdot D^2 / 4$$

where A_s is the surface area, π is a constant, and D is the diameter. Figure 65 shows the relation of surface area with liquid volume in the reaction flask.

APPENDIX B

EXPERIMENTAL DATA

TABLE VII

MEA-COS REACTION SYSTEM

Time (min.)	Pressure (psig)	% of Initial Pressure (psia)	Temperature (°F)
0	20.0	100.0	90.5
1/3	15.0	85.6	
2/3	13.0	79.8	
1	12.5	78.4	118.0
2	12.0	76.9	114.0
3	11.8	76.4	110.0
4	11.6	75.8	106.0
5	11.5	75.5	105.0
10	10.7	73.2	97.0
15	10.5	72.6	94.0
20	10.4	72.3	92.0
25	10.3	72.0	91.0
30	10.2	71.7	91.0

Initial concentration of COS : 20 psig

Initial volume of MEA : 3.28 cm^3

Initial temperature of system : 90.5°F

TABLE VIII

MEA-CH$_3$SH REACTION SYSTEM

Time (min.)	Pressure (psig)	% of Initial Pressure (psia)	Temperature ($^{\circ}$F)
0	15.0	100.0	80.0
1	14.5	98.3	83.0
2	14.2	97.3	83.0
3	13.8	96.0	84.0
4	13.5	94.9	84.0
5	13.2	93.9	84.0
10	12.3	90.9	82.0
15	11.6	88.6	81.0
20	11.2	87.2	80.5
25	10.8	85.9	80.5
30	10.5	84.8	80.5
60	9.8	82.5	80.0

Initial concentration of CH$_3$SH : 15 psig

Initial volume of MEA : 2.94 cm^3.

Initial temperature of system : 80.0°F

TABLE IX

DEA-COS REACTION SYSTEM

Time (min.)	Pressure (psig)	% of Initial Pressure (psia)	Temperature ($^\circ$F)
0	20.0	100.0	86.0
1	19.7	99.1	92.0
2	19.5	98.6	92.0
3	19.4	98.3	92.5
4	19.3	98.0	93.0
5	19.2	97.7	94.0
10	18.9	96.7	88.0
15	18.5	95.7	86.0
20	18.0	94.2	86.0
25	17.7	93.4	86.0
30	17.4	92.5	85.0
45	17.0	91.4	84.0
60	16.6	90.2	82.0

Initial concentration of COS : 20 psig

Initial volume of DEA : 5.27 cm^3.

Initial temperature of system : 86.0°F

TABLE X

DEA-CH$_3$SH REACTION SYSTEM

Time (min.)	Pressure (psig)	% of Initial Pressure (psia)	Temperature (°F)
0	14.5	100.0	93.0
1	14.2	99.0	93.0
2	14.0	98.3	91.0
3	13.8	97.6	90.0
4	13.7	97.3	88.0
5	13.5	96.6	88.0
10	13.3	95.9	86.5
15	12.7	93.8	84.0
20	12.3	92.5	84.0
25	12.1	91.8	84.0
30	12.0	91.4	84.0

Initial concentration of CH$_3$SH: 14.5 psig

Initial volume of DEA : 4.78 cm^3.

Initial temperature of system : 93°F

TABLE XI

DGA-H_2S REACTION SYSTEM

Time (min.)	Pressure (psig)	% of Initial Pressure (psia)	Temperature (°F)
0	20.0	100.0	79.0
1	19.5	98.6	81.5
2	19.2	97.7	81.5
3	19.0	97.1	81.5
4	18.8	96.5	81.5
5	18.7	96.3	81.5
10	18.2	94.8	81.5
15	17.8	93.7	81.0
30	16.5	89.9	80.0
60	15.3	86.5	80.0

Initial concentration of H_2S : 20 psig

Initial volume of DGA : 5.44 cm^3.

Initial temperature of system : 79.0°F

TABLE XII

DGA-CO$_2$ REACTION SYSTEM

Time (min.)	Pressure (psig)	% of Initial Pressure (psia)	Temperature ($^\circ$F)
0	20.0	100.0	81.0
1/2	12.0	76.9	86.0
1	11.0	74.1	86.0
3/2	10.0	71.2	88.0
5/2	9.7	70.3	90.0
7/2	9.6	70.0	91.0
5	9.5	69.7	91.0
10	9.3	69.2	89.0
15	9.2	68.9	86.0
20	9.1	68.6	84.0
30	9.0	68.3	82.0

Initial concentration of CO$_2$: 20 psig

Initial volume of DGA: 5.4 cm^3.

Initial temperature of system: 81.0°F

TABLE XIII

DGA-COS REACTION SYSTEM

Time (min.)	Pressure (psig)	% of Initial Pressure (psia)	Temperature ($^\circ$F)
0	20.0	100.0	80.0
1/4	17.5	92.8	
1/2	15.0	85.6	
1	12.0	76.9	108.0
2	11.5	75.5	108.0
3	11.3	74.9	95.0
4	11.2	74.6	93.0
5	11.1	74.3	92.0
10	10.8	73.5	87.0
15	10.6	72.9	84.0
20	10.5	72.6	82.0
25	10.4	72.3	81.0
30	10.2	72.1	80.0

Initial concentration of COS:20 psig

Initial volume of DGA: 5.43 cm^3.

Initial temperature of system: 80.0°F

63

TABLE XIV

DGA-CH$_3$SH REACTION SYSTEM

Time (min.)	Pressure (psig)	% of Initial Pressure (psia)	Temperature (°F)
0	15.0	100.0	83.0
1	13.6	95.3	85.0
2	13.0	93.3	85.0
3	12.3	90.9	84.5
4	11.7	88.9	84.0
5	11.4	87.9	84.0
10	10.7	85.5	84.0
15	9.8	82.5	83.0
20	9.0	79.8	83.0
25	8.5	78.1	82.5
30	8.0	76.4	82.5

Initial concentration of CH$_3$SH: 15 psig

Initial volume of DGA: 4.86 cm^3.

Initial temperature of system: 83.0°F

TABLE XV

DIPA-H_2S REACTION SYSTEM

Time (min.)	Pressure (psig)	% of Initial Pressure (psia)	Temperature (°F)
0	20.5	100.0	91.5
1	19.9	99.7	91.5
2	19.5	97.2	94.0
3	19.3	96.6	92.5
4	19.1	96.0	92.0
5	19.0	95.7	91.8
10	18.6	94.6	91.8
15	18.4	94.0	91.0
30	18.0	92.9	90.5

Initial concentration of H_2S: 20.5 psig

Initial volume of DIPA: 7.3 cm^3.

Initial temperature of system: 91.5°F

TABLE XVI

DIPA-CO$_2$ REACTION SYSTEM

Time (min.)	Pressure (psig)	% of Initial Pressure (psia)	Temperature (°F)
0	18.0	100.0	
1	17.0	96.9	100.0
2	15.5	92.4	98.0
3	14.6	89.6	97.0
4	14.0	87.8	97.0
5	13.6	86.5	97.0
6	13.5	86.2	96.0
10	13.3	85.6	91.0
15	13.2	85.3	89.0
30	13.0	84.7	86.0
60	12.9	84.4	85.0

Initial concentration of CO$_2$: 18 psig

Initial volume of DIPA: 7.3 cm^3.

Initial temperature of system: 90.0°F

TABLE XVII

DIPA-COS REACTION SYSTEM

Time (min.)	Pressure (psig)	% of Original Pressure (psia)	Temperature (°F)
0	20.5	100.0	98.0
1	19.6	98.8	100.0
2	18.5	95.7	98.0
3	17.8	93.7	98.0
4	17.4	92.5	98.0
5	17.0	91.4	98.0
10	15.8	87.9	98.0
15	15.3	86.5	98.0
20	15.0	85.6	98.0
25	14.7	84.7	98.0
30	14.5	84.1	98.0

Initial concentration of COS: 20.5 psig

Initial volume of DIPA: 7.3 cm^3.

Initial temperature of system: 98.0°F

TABLE XVIII

DIPA-CH$_3$SH REACTION SYSTEM

Time (min.)	Pressure (psig)	% of Initial Pressure (psia)	Temperature (°F)
0	15.0	100.0	86.0
1	14.5	98.3	87.0
2	14.3	97.6	87.0
3	14.1	96.9	86.5
4	14.0	96.6	86.5
5	13.9	96.3	86.5
10	13.3	94.3	86.0
15	12.9	92.9	85.0
20	12.5	91.6	84.0
25	12.3	90.9	84.0
30	12.1	90.2	84.0

Initial concentration of CH$_3$SH: 15 psig

Initial volume of DIPA: 6.53 cm^3.

Initial temperature of system: 86.0°F

TABLE XIX

MDEA-CH$_3$SH REACTION SYSTEM

Time (min.)	Pressure (psig)	% of Initial Pressure (psia)	Temperature (°F)
0	15.0	100.0	80.5
1	14.7	98.7	85.5
2	14.4	98.0	85.0
3	14.1	96.9	84.0
4	13.8	96.0	84.0
5	13.4	94.6	82.0
25	11.5	88.2	81.0
30	11.3	87.5	81.0
60	10.0	83.2	81.0

Initial concentration of CH$_3$SH: 15 psig

Initial volume of MDEA: 5.63 cm^3.

Initial temperature of system: 80.5°F

TABLE XX

MDEA-CO_2 REACTION SYSTEM

Time (min.)	Pressure (psig)	% of Initial Pressure (psia)	Temperature (°F)
0	16.0	100.0	76.0
1	15.8	99.3	76.0
2	15.5	98.4	76.0
3	15.2	97.4	76.0
4	15.0	96.7	76.0
5	14.8	96.1	75.0
10	13.2	90.9	75.0
15	12.3	87.9	75.0
20	11.9	86.6	75.0
25	11.5	85.3	75.0
30	11.2	84.4	75.0

Initial concentration of CO_2: 16 psig

Initial volume of MDEA: 4.95 cm^3.

Initial temperature of system: 76.0°F

TABLE XXI

MDEA-COS REACTION SYSTEM

Time (min.)	Pressure (psig)	% of Initial Pressure (psia)	Temperature (°F)
0	20.0	100.0	82.0
1	19.8	99.4	84.0
2	19.6	98.8	84.0
3	19.4	98.3	84.0
4	19.0	97.1	84.0
5	18.4	95.4	84.0
10	16.8	90.8	83.0
15	15.8	87.9	82.5
20	15.1	85.9	82.0
25	14.3	83.6	82.0
30	13.5	81.3	80.5

Initial concentration of COS: 20 psig

Initial volume of MDEA: 6.28 cm^3.

Initial temperature of system: 82.0°F

TABLE XXII

MDEA-H_2S REACTION SYSTEM

Time (min.)	Pressure (psig)	% of Initial Pressure (psia)	Temperature ('F)
0	20.0	100.0	80.0
1/2	13.2	80.4	86.0
2	12.0	76.9	87.0
3	11.3	74.9	87.0
4	11.0	74.1	87.0
5	10.3	72.1	87.0
10	8.3	66.3	83.0
17	6.3	60.5	83.0
20	5.5	58.2	83.0
30	4.0	53.9	82.0

Initial concentration of H_2S: 20 psig

Initial volume of MDEA: 5.50 cm^3.

Initial temperature of system: 80.0'F

TABLE XXIII

DMEA-H_2S REACTION SYSTEM

Time (min.)	Pressure (psig)	% of Initial Pressure (psia)	Temperature (°F)
0	12.2	100.0	65.0
1/2	5.0	74.0	68.0
1	4.5	72.1	67.0
2	4.0	70.3	
3	3.3	67.7	
4	2.7	65.4	
5	2.2	63.6	
10	1.3	59.5	
15	0.8	57.6	
20	0.4	56.1	
25	0.0	54.6	
30	1"vacuum	53.9	

Initial concentration of H_2S: 12.2 psig

Initial volume of DMEA: 4.3 cm^3.

Initial temperature of system: 65°F

TABLE XXIV

DMEA-CO_2 REACTION SYSTEM

Time (min.)	Pressure (psig)	% of Initial Pressure (psia)	Temperature (°F)
0	20.2	100.0	79.0
1	20.0	99.4	79.0
2	19.8	98.9	80.0
3	19.6	98.3	80.0
4	19.5	98.0	80.0
5	19.4	97.7	80.0
6	19.3	97.4	80.3
7	19.2	97.1	80.3
8	19.0	96.6	80.3
9	18.8	96.0	80.8
10	18.7	95.7	80.8
15	18.6	95.4	81.0
20	18.4	94.8	80.0
25	18.3	94.6	79.8
30	18.2	94.3	79.8

Initial concentration of CO_2: 20.2 psig

Initial volume of DMEA: 5.46 cm^3.

Initial temperature of system: 79.0°F

TABLE XXV

DMEA-COS REACTION SYSTEM

Time (min.)	Pressure (psig)	% of Initial Pressure (psia)	Temperature (° F)
0	20.0	100.0	81.0
1	18.4	95.4	87.0
2	17.0	91.4	86.5
3	16.4	89.6	86.0
4	15.8	87.9	85.0
5	15.4	86.7	84.0
10	14.9	85.3	81.5
15	14.2	83.3	81.5
20	13.6	81.6	81.0
25	13.0	79.8	81.0
30	12.5	78.4	81.0

Initial concentration of CO_2: 20 psig

Initial volume of DMEA: 5.5 cm^3.

Initial temperature of system: 81.0°F

TABLE XXVI

DMEA-CH$_3$SH REACTION SYSTEM

Time (min.)	Pressure (psig)	% of Initial Pressure (psia)	Temperature (°F)
0	15.5	100.0	77.0
1/2	13.0	91.7	79.0
1	11.9	88.1	79.0
2	10.7	84.1	78.5
3	10.0	81.8	78.5
4	99.7	80.8	78.5
5	9.5	80.1	79.0
10	9.1	78.8	78.5
15	9.0	78.5	78.5
30	8.8	77.8	78.0

Initial concentration of CH$_3$SH: 15.5 psig

Initial volume of DMEA: 5.0 cm^3.

Initial temperature of system: 77.0°F

TABLE XXVII

ANTOINE EQUATION FIT FOR ACIDIC GAS AND ALKANOLAMINE SYSTEM

System	A	B	C	Average Error %	Maximum Error %
CH_3SH-MEA	3.1438	3.86E	15.74	0.116	0.21
COS-MEA	3.2265	0.112	0.38	1.08	2.17
COS-DEA	3.5991	11.000	-138.58	1.63	2.94
CH_3SH-DEA	3.7402	61.235	-160.8	0.653	1.47
H_2S-DIPA	3.4663	0.618	6.86	0.321	0.67
CO_2-DIPA	3.3026	0.385	2.02	0.933	2.44
COS-DIPA	3.3285	1.408	6.04	0.619	2.87
CH_3SH-DIPA	3.2796	0.9311	8.47	2.68	4.93
H_2S-DGA	3.3156	8.541	38.52	0.341	0.91
CO_2-DGA	3.165	0.089	0.26	0.375	0.92
COS-DGA	3.214	0.161	0.50	1.014	3.3
CH_3SH-DGA	3.2166	3.533	22.98	0.258	0.84
H_2S-MDEA	2.700	9.865	13.87	3.07	12.4
CO_2-MDEA	3.038	13.2	33.96	0.541	1.19
COS-MDEA	2.6344	111.0	121.52	0.512	1.25
CH_3SH-MDEA	3.0815	11.717	38.82	0.554	1.34
H_2S-DMEA	3.1879	4.592	0.46	1.92	3.38
CO_2-DMEA	3.4791	0.628	8.30	0.202	0.50
COS-DMEA	3.289	1.140	4.52	0.892	1.98
CH_3SH-DMEA	3.146	0.260	1.02	0.246	0.44
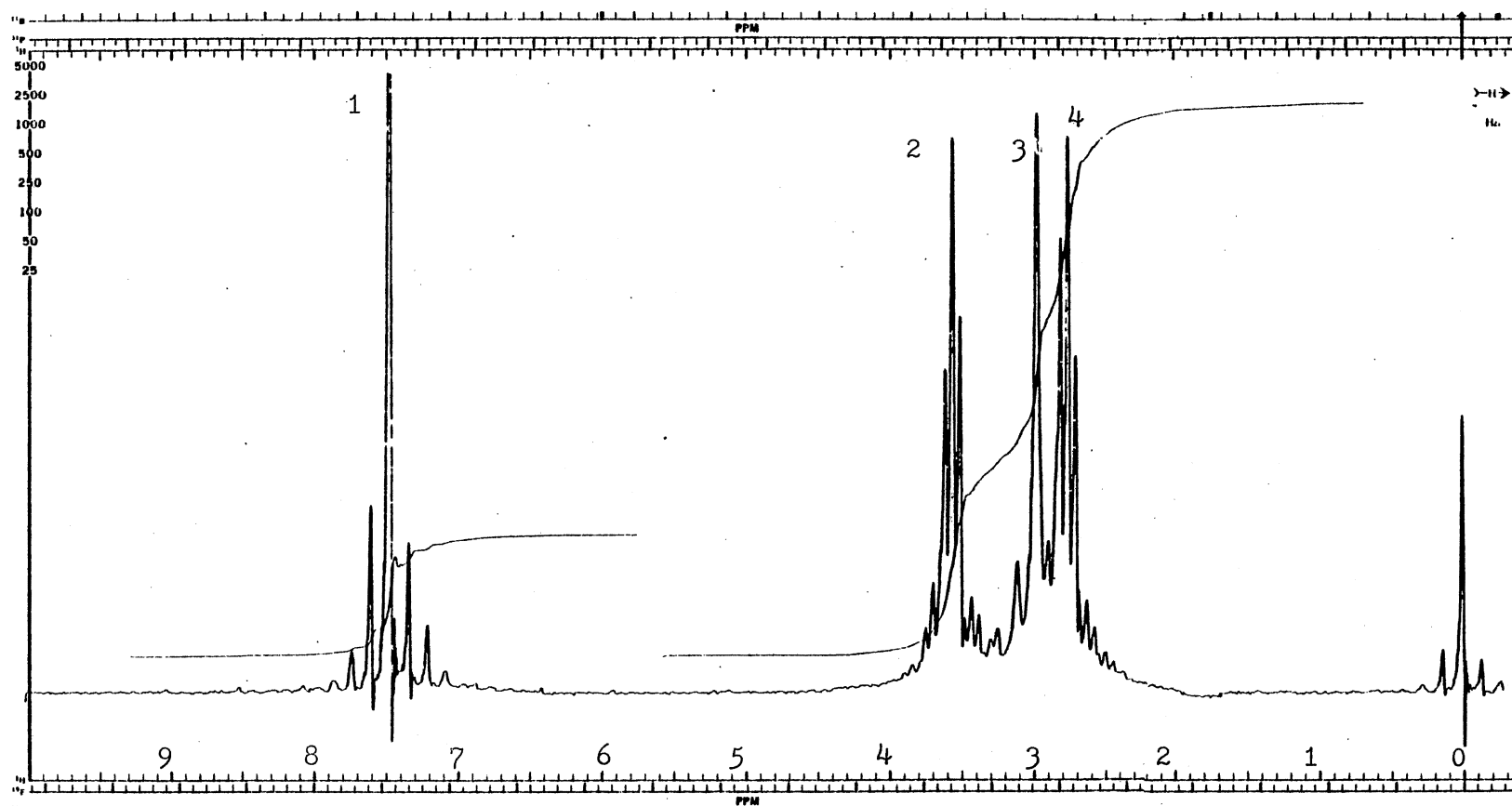
Figure 3. ^{1}H-NMR Spectrum of Pure MEA in $DCCl_3$ (20 % Sample)
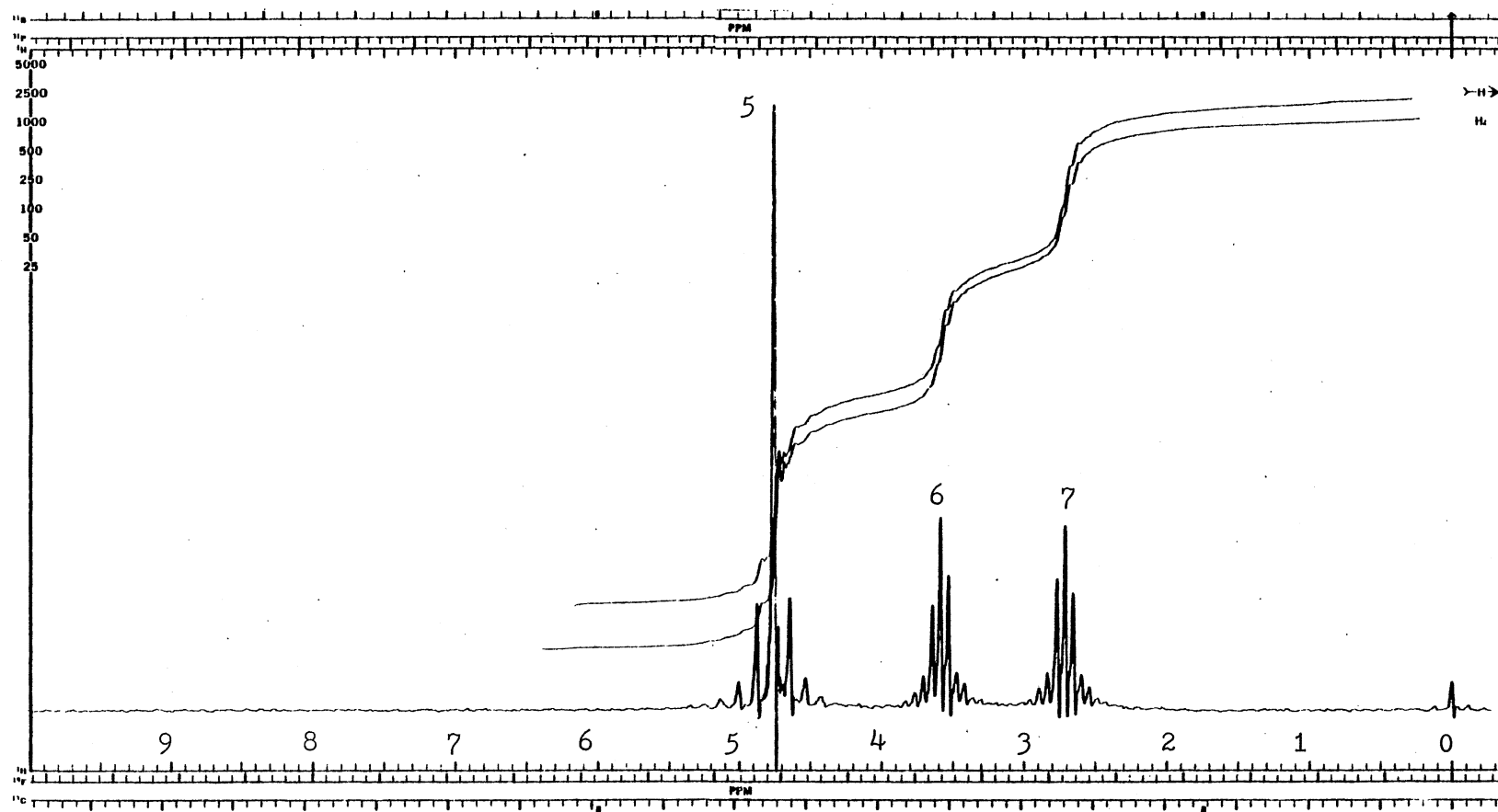
Figure 4. ^{1}H-NMR Spectrum of Pure MEA in D_2O (20 % Sample)
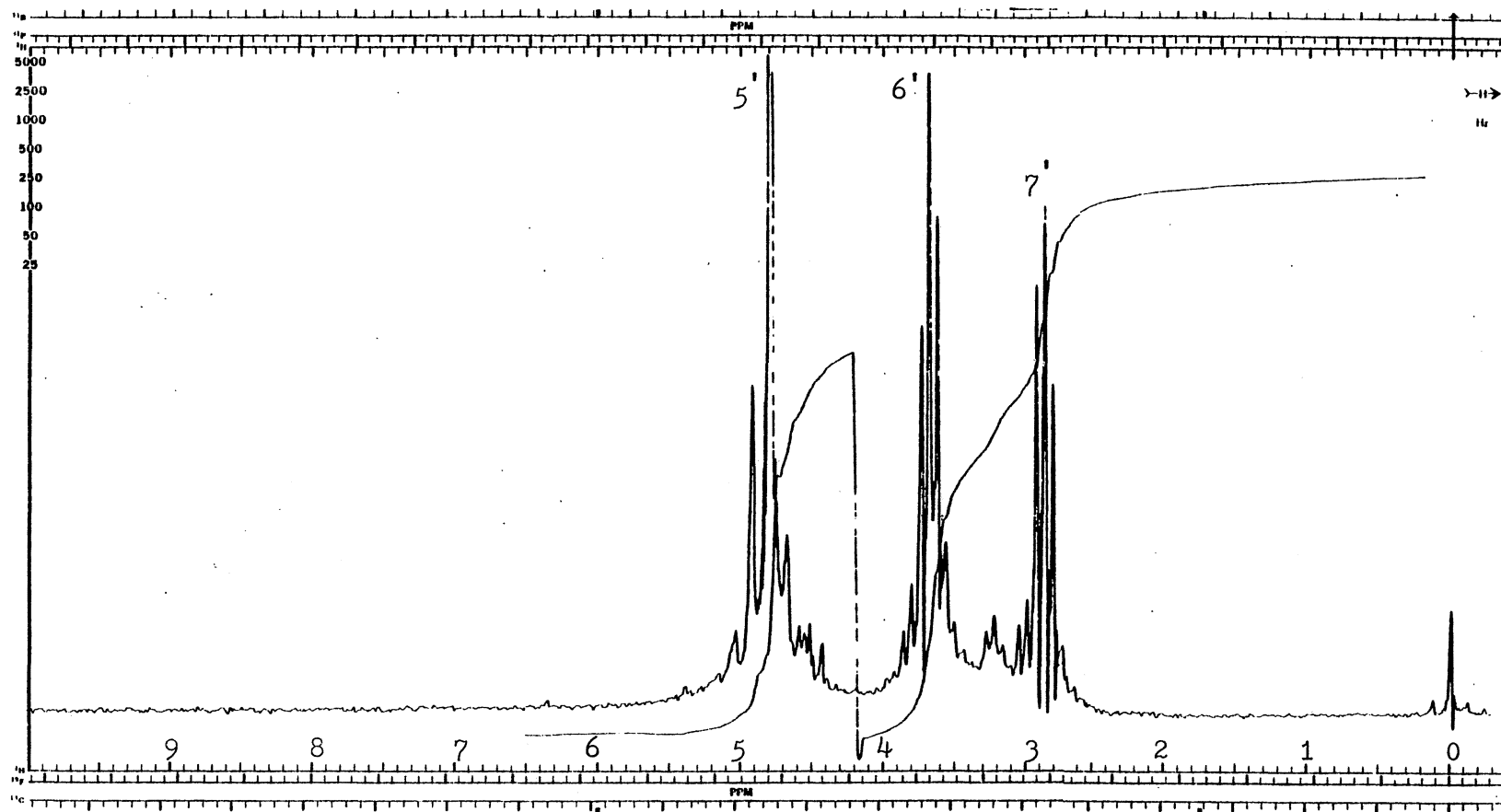
Figure 5. ^{1}H-NMR Spectrum of MEA-COS Reaction Products in D_2O (20 % Sample)
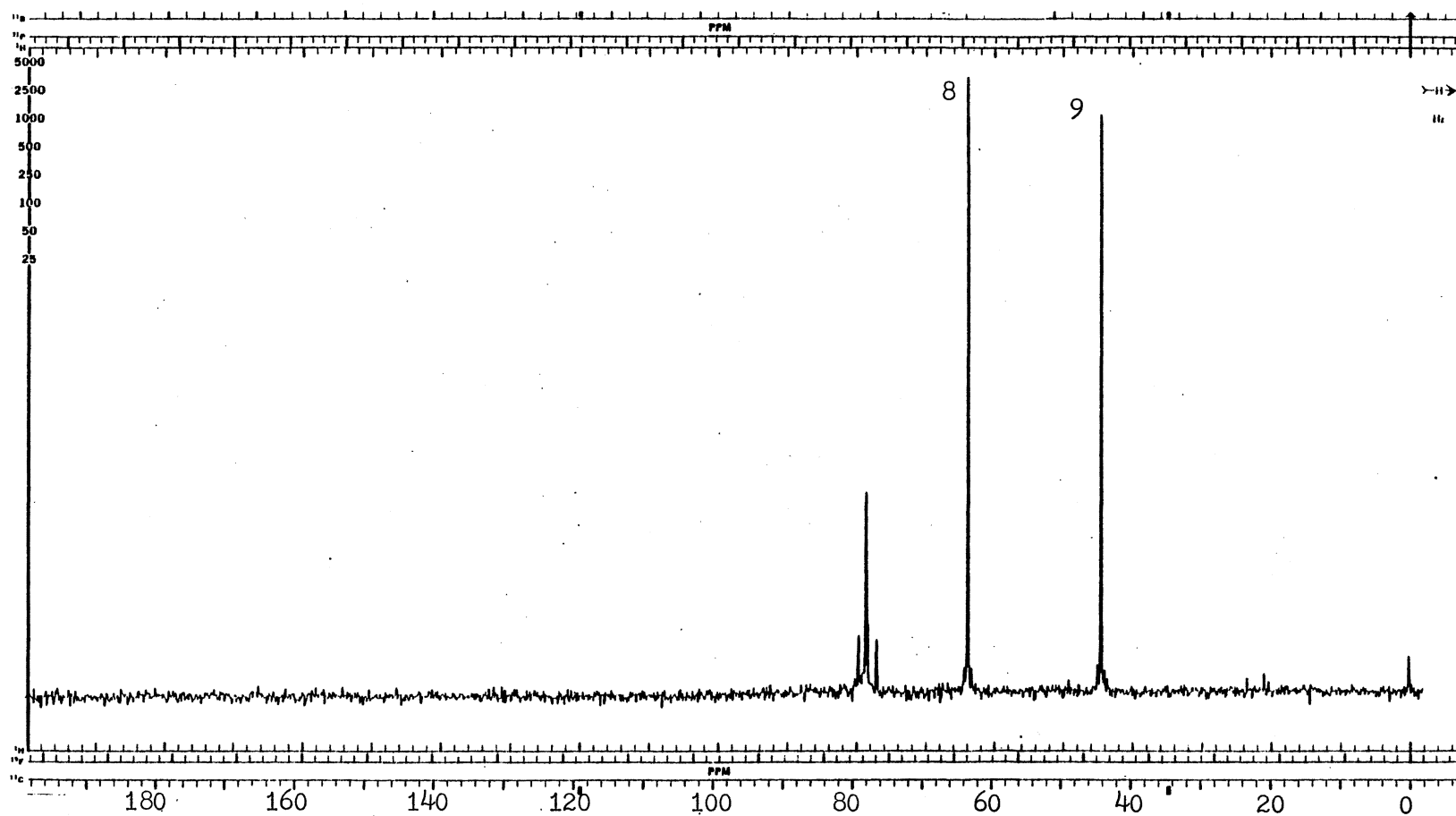
Figure 6. ^{13}C-NMR Spectrum of Pure MEA in DCCl$_3$ (20 % Sample)
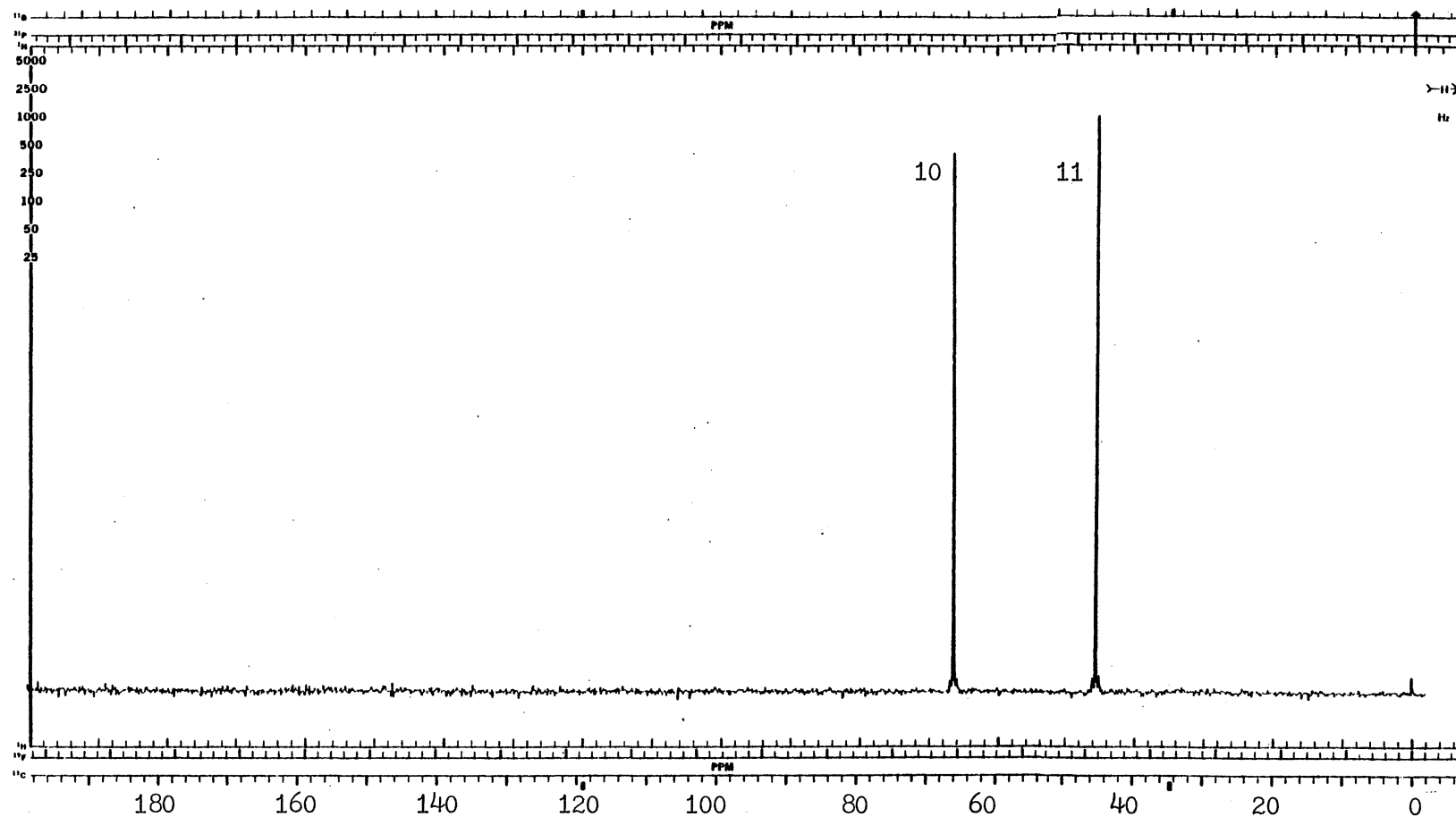
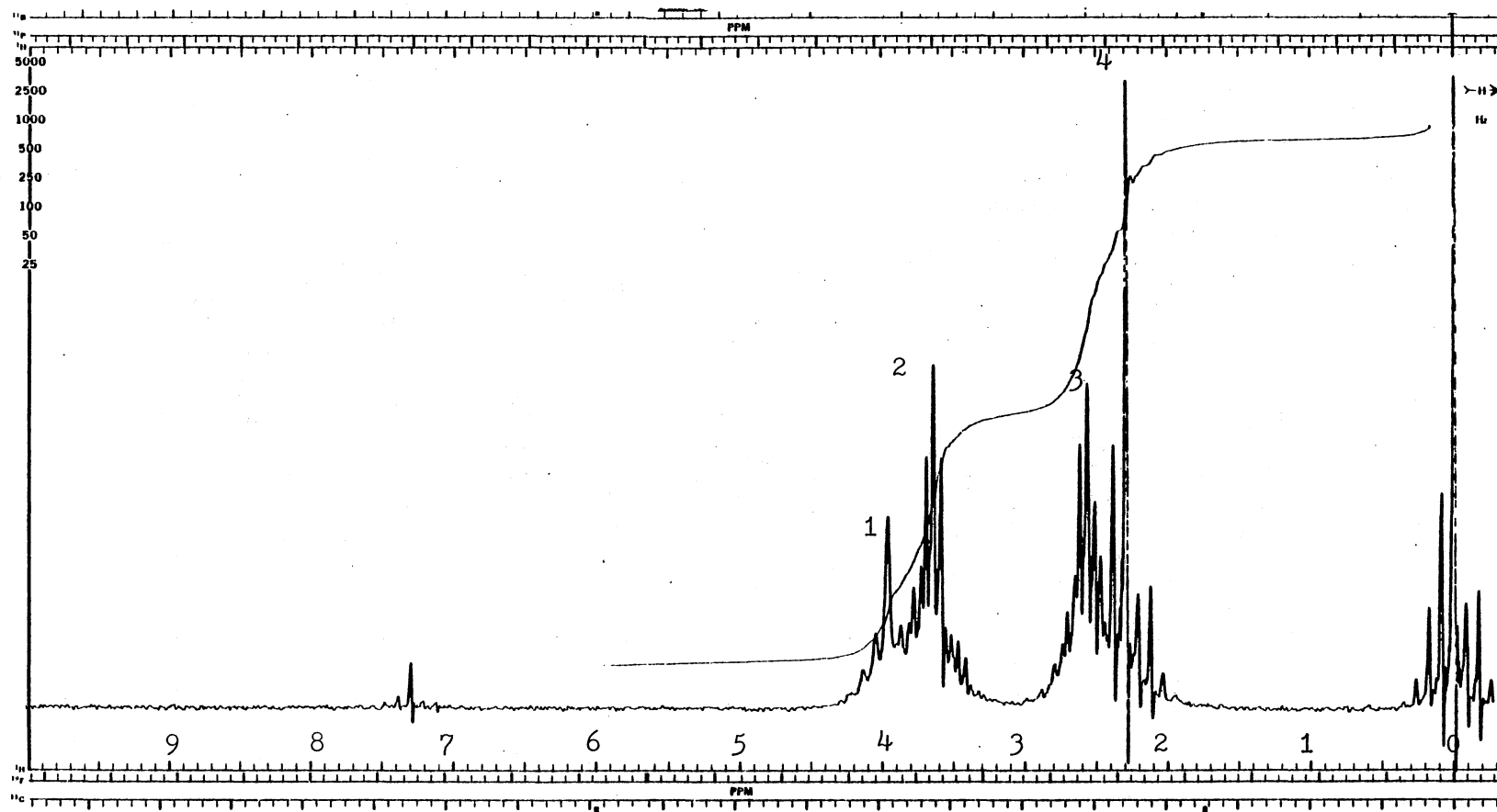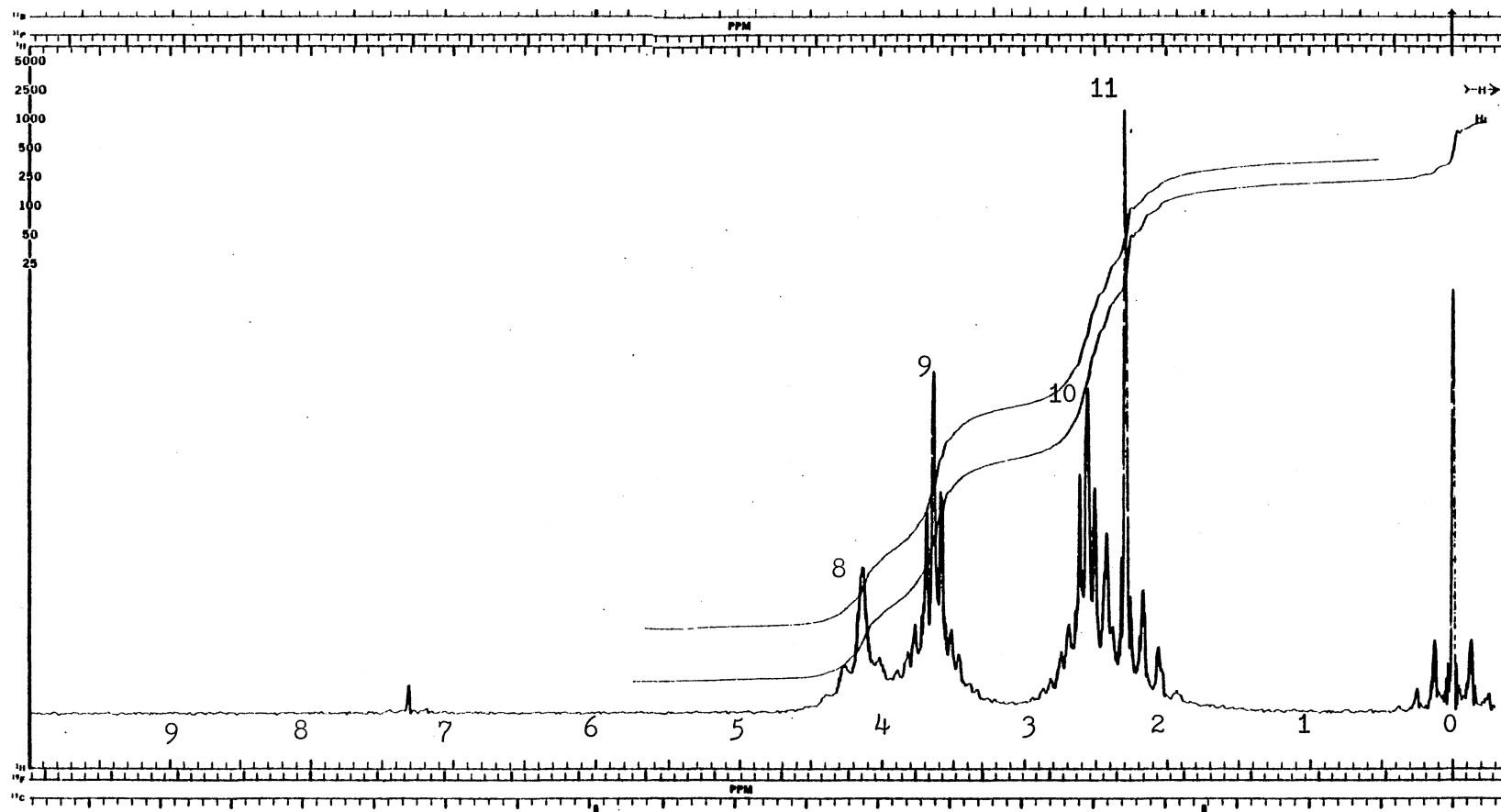Figure 7. ^{13}C-NMR Spectrum of Pure MEA in D_2O (20 % Sample)
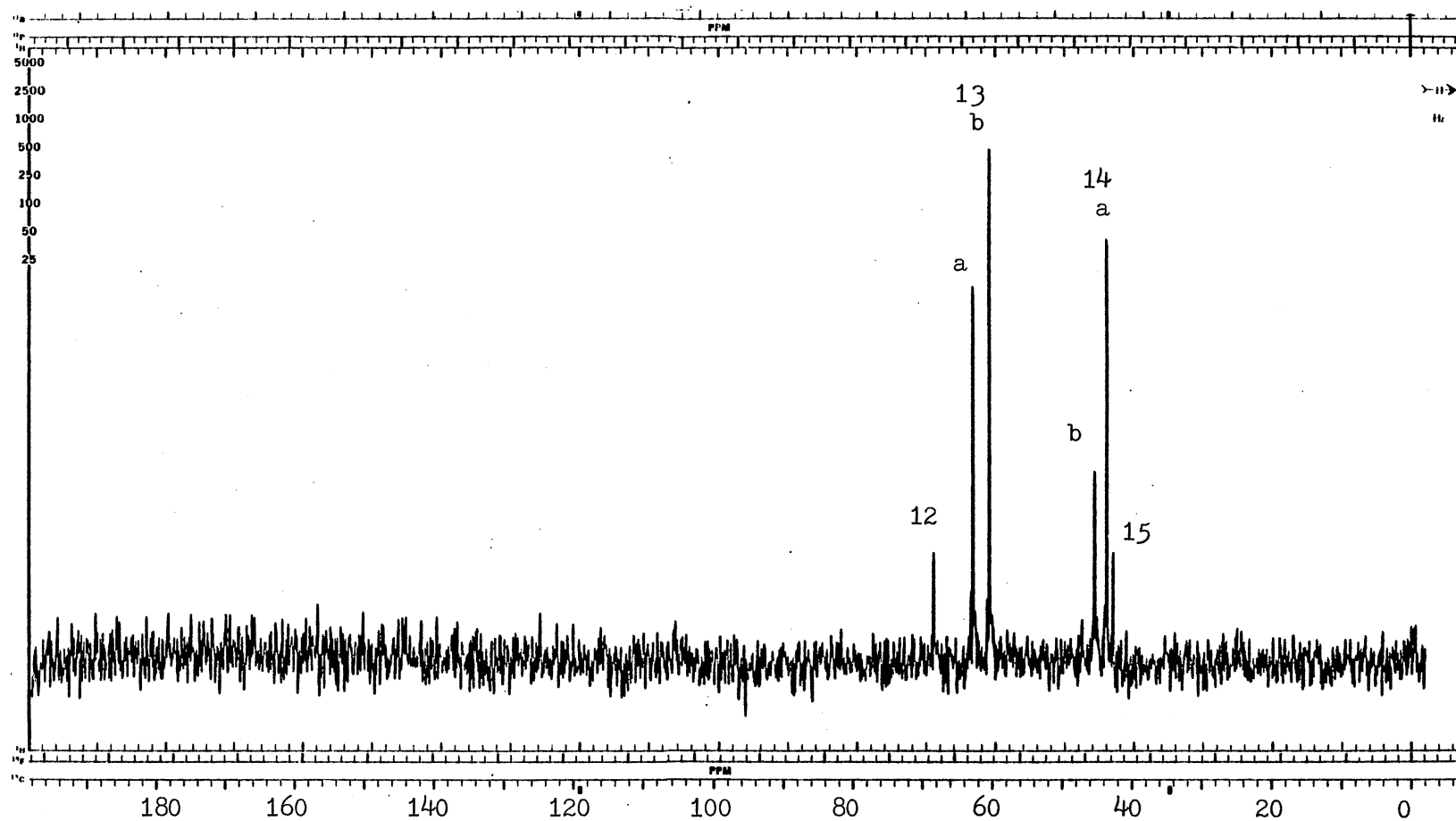
Figure 8. ^{13}C-NMR Spectrum of MEA-COS Reaction Products in D_2O (20 % Sample)
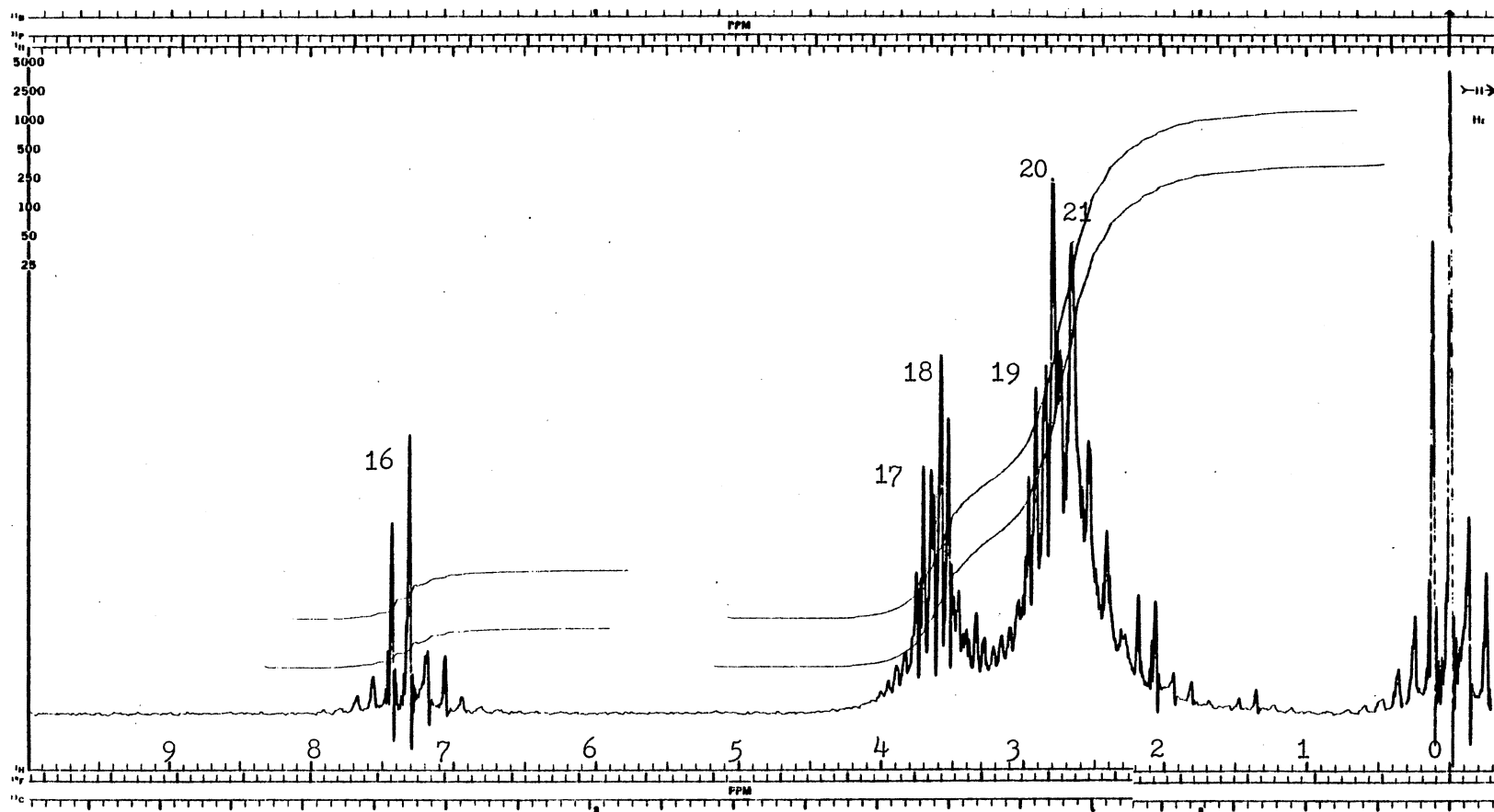
Figure 9. ^{1}H-NMR Spectrum of MEA-CH$_3$SH Absorption System (20 % Sample)
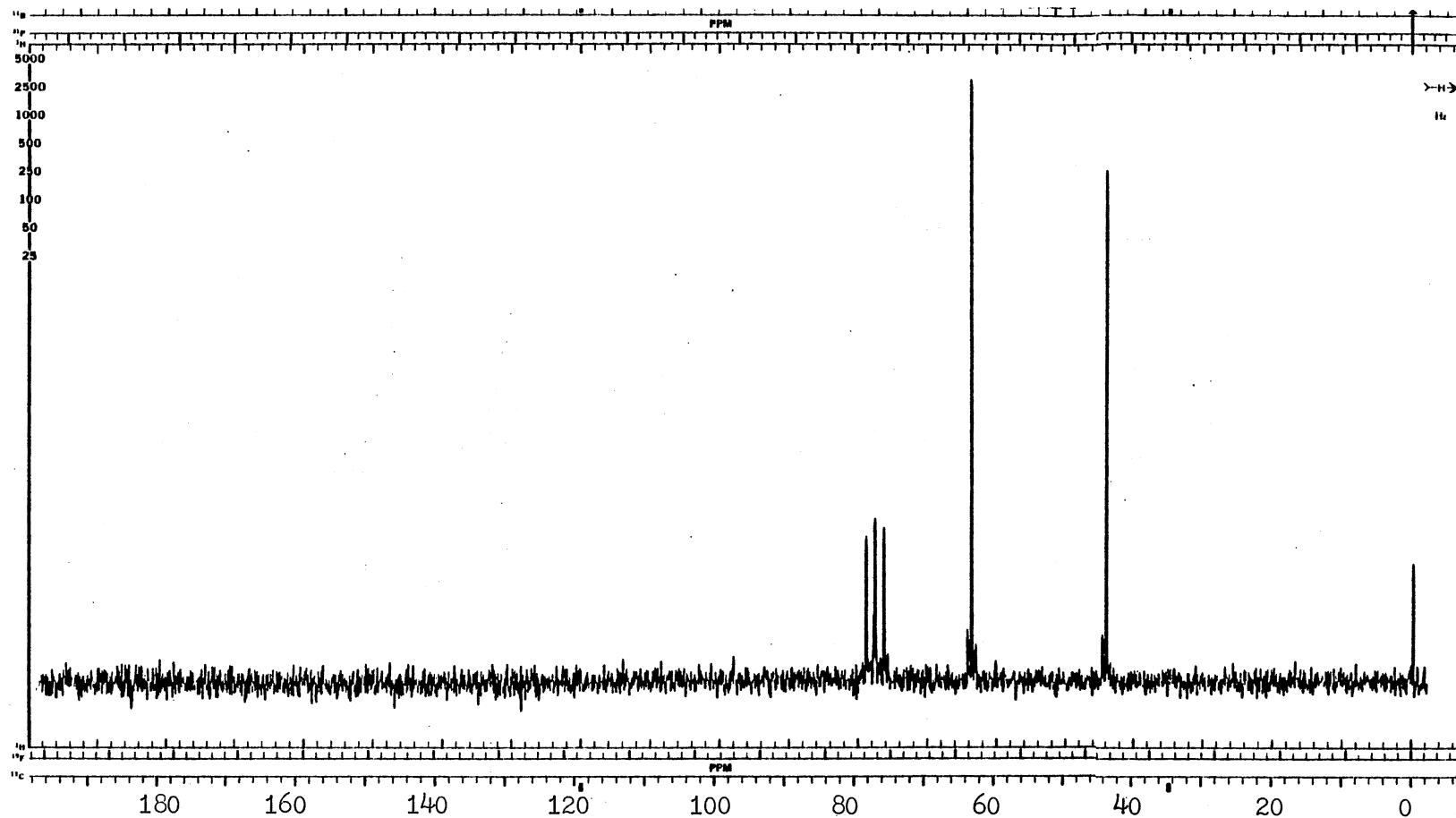
Figure 10. ^{13}C-NMR Spectrum of MEA-CH$_3$SH Absorption System (20 % Sample)
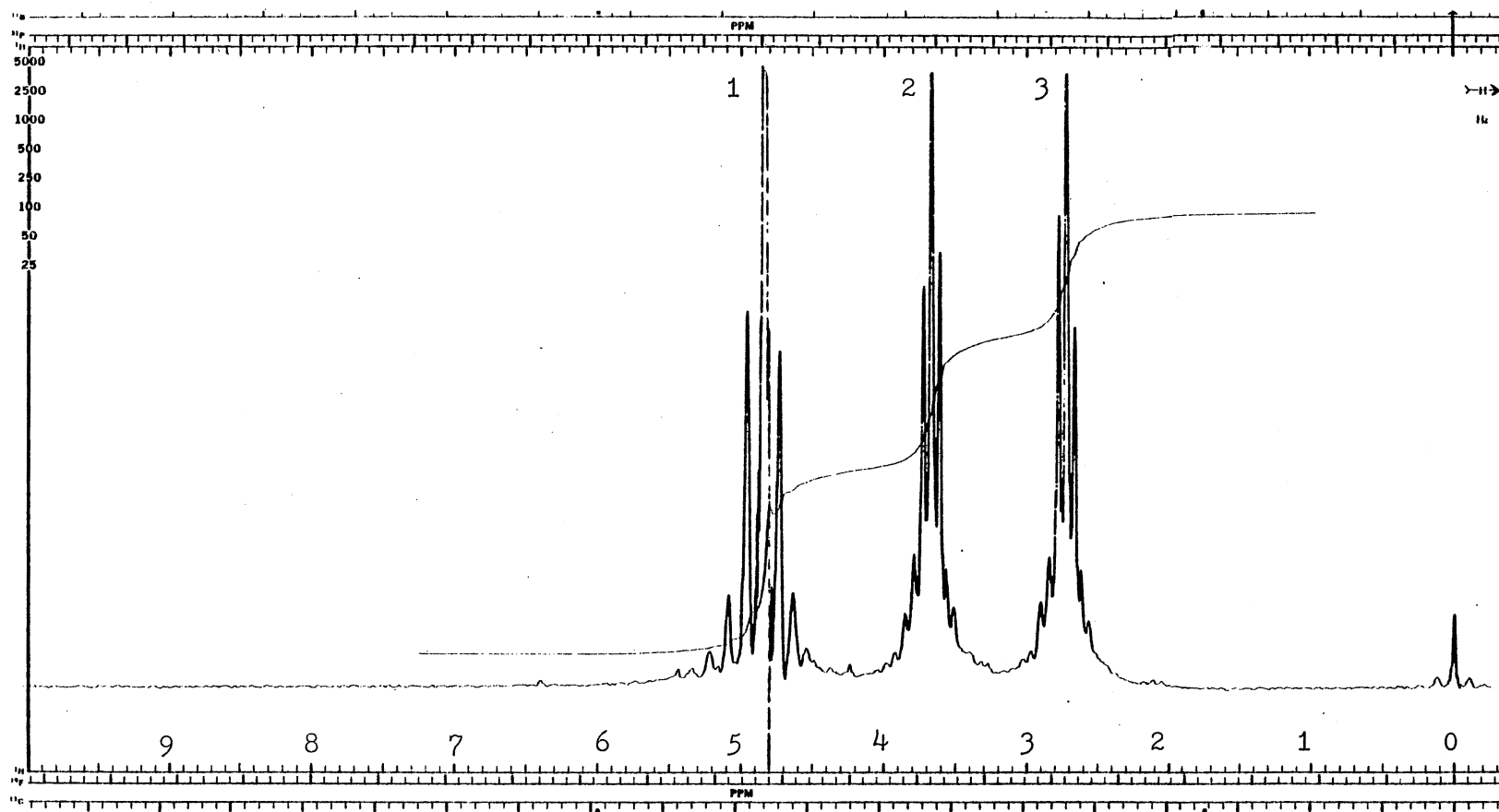
Figure 11. ^{1}H-NMR Spectrum of Pure DEA in D_2O (15 % Sample)
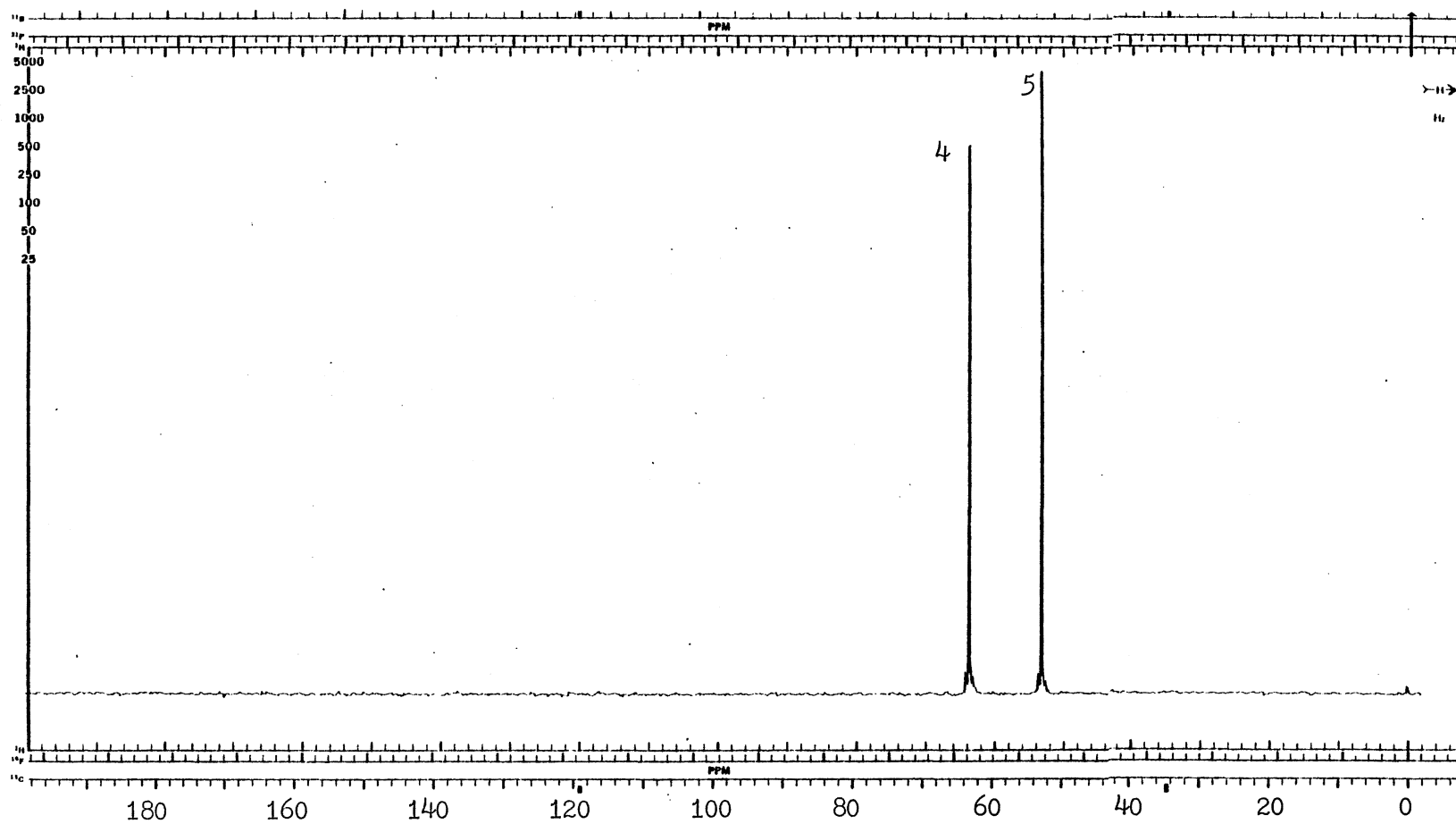
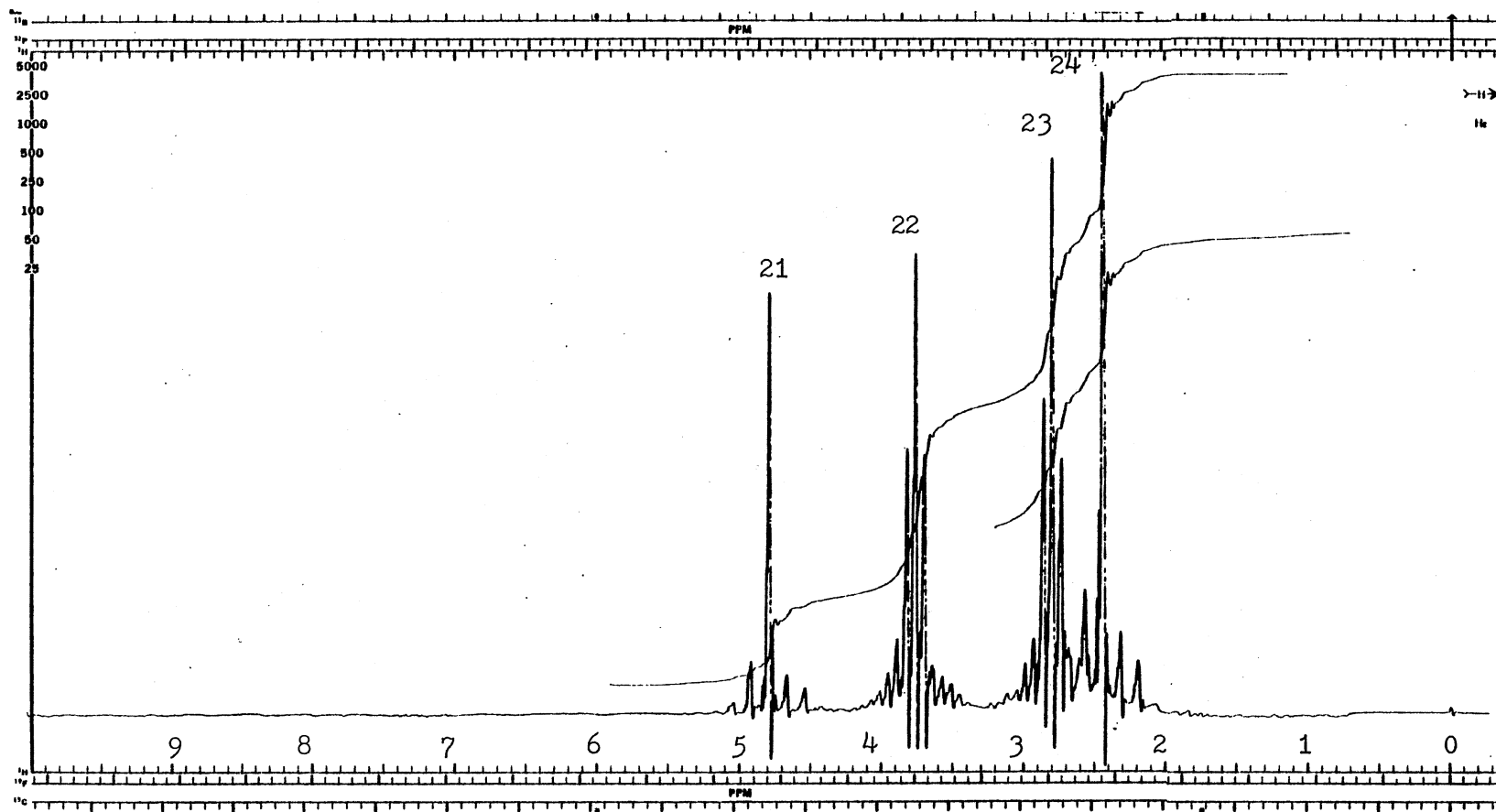Figure 12. ^{13}C-NMR Spectrum of Pure DEA in D_2O (15 % Sample)
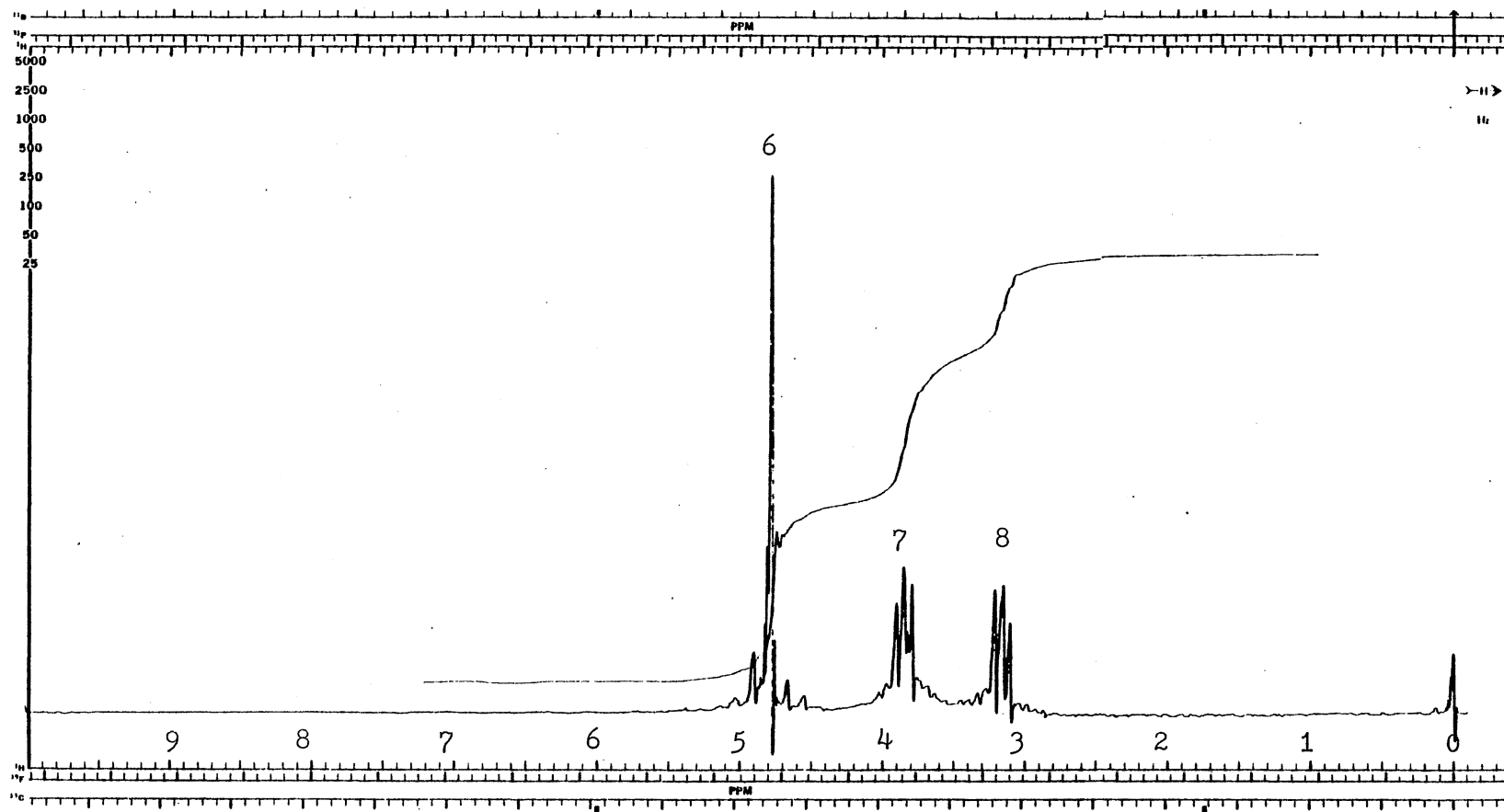
Figure 13. ^{1}H-NMR Spectrum of DEA-COS Reaction Products in D_2O (15 % Sample)
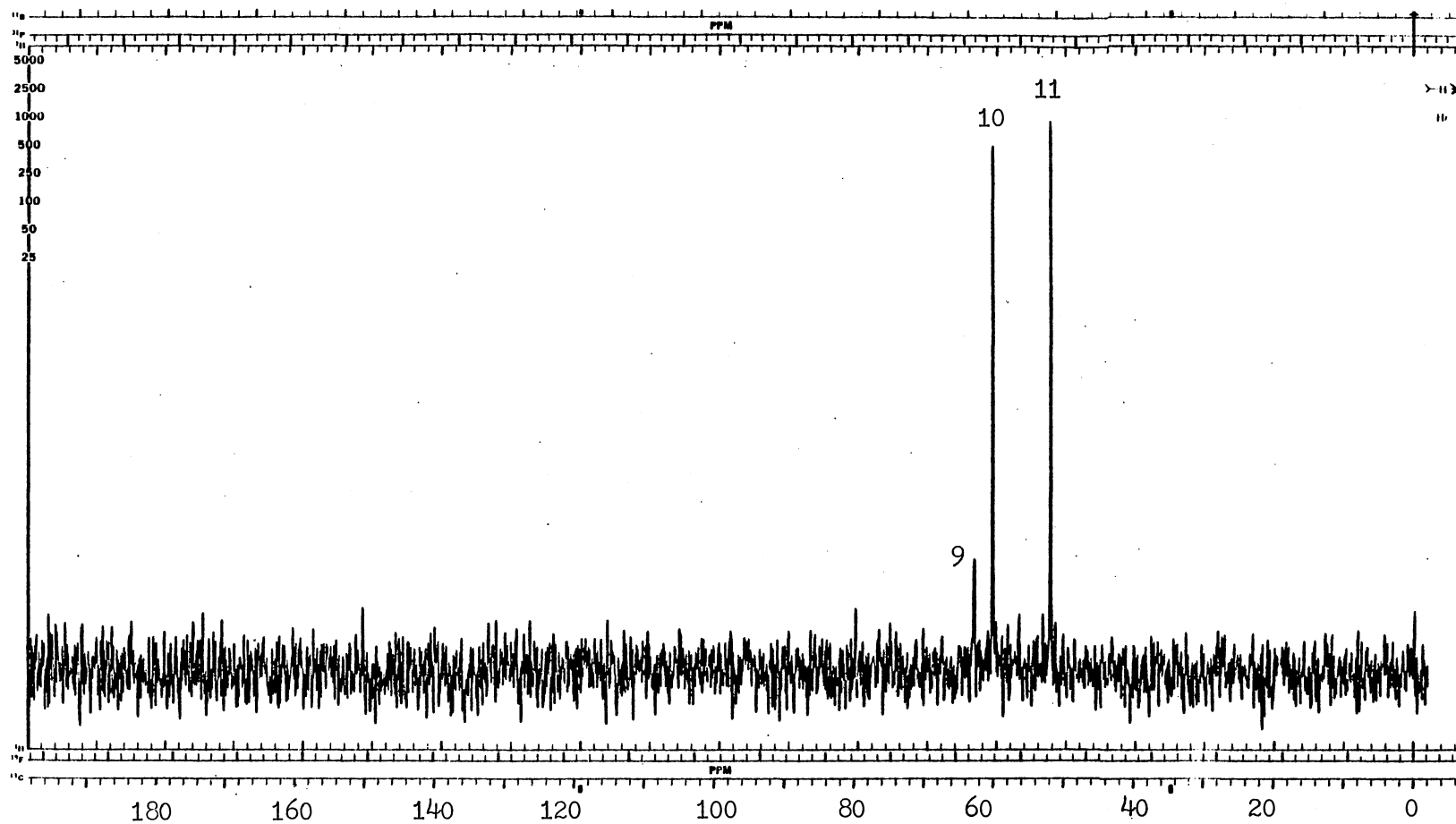
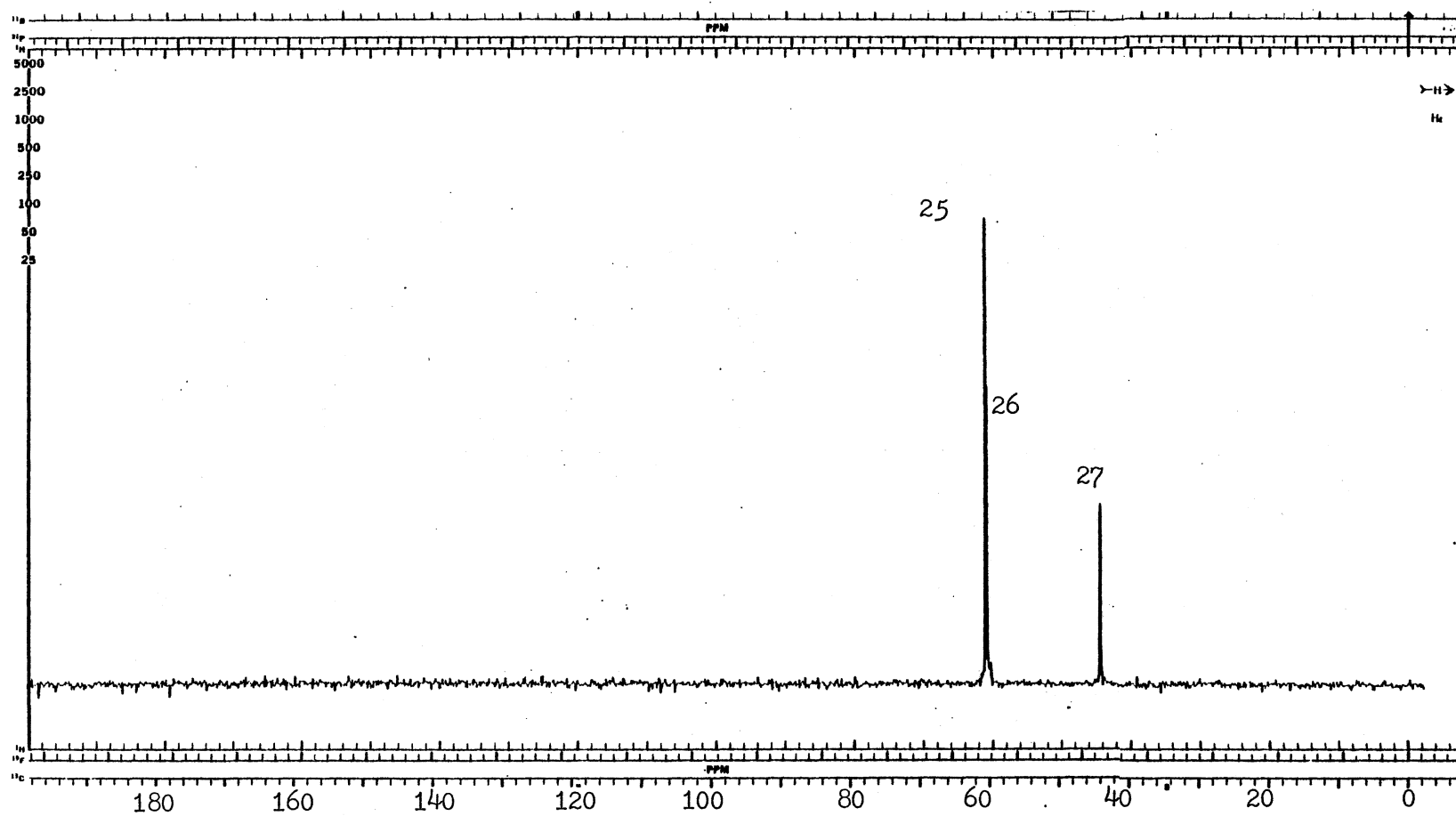Figure 14. ^{13}C-NMR Spectrum of DEA-COS Reaction Products in D_2O (15 % Sample)
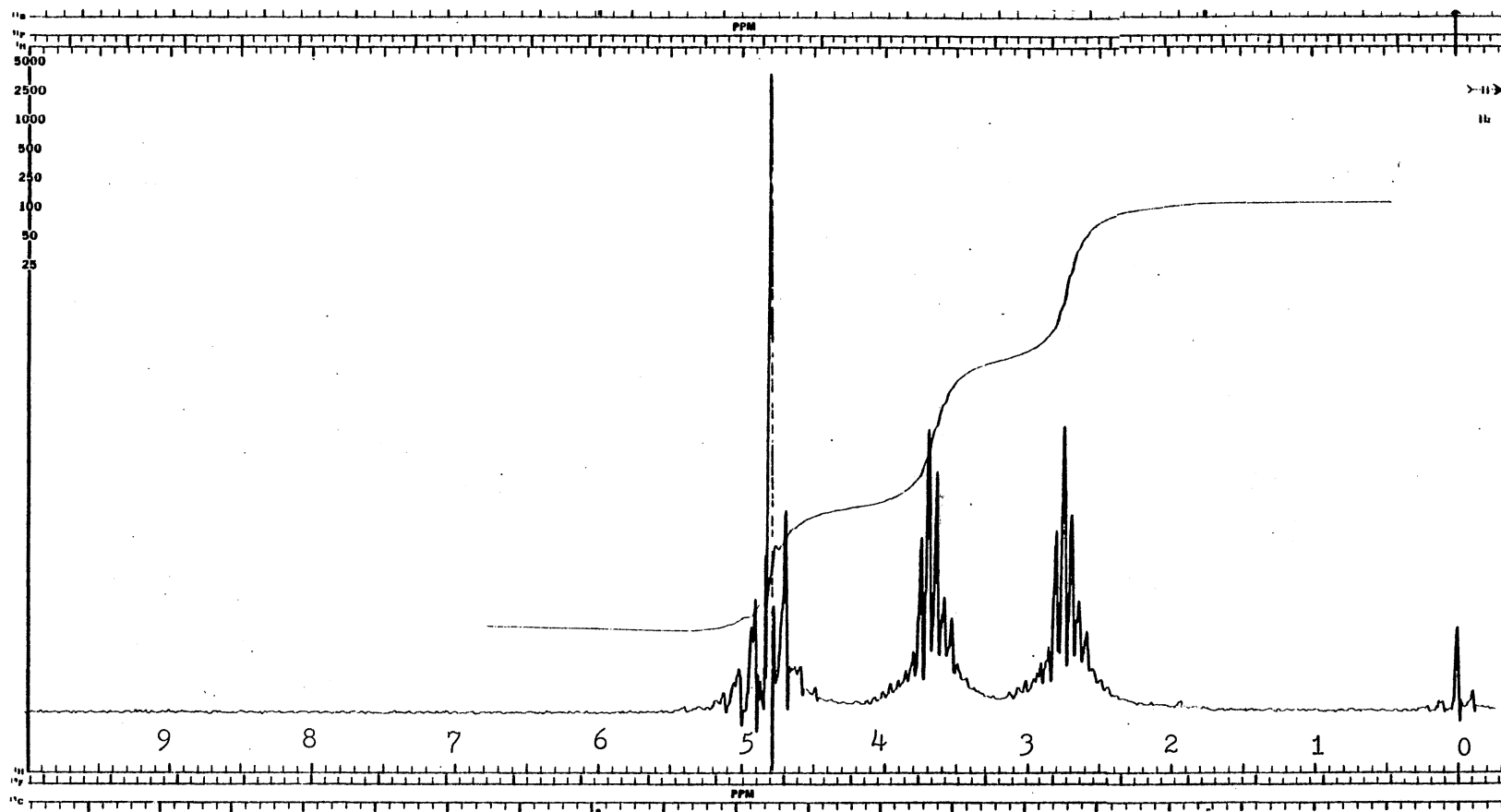
Figure 15. ^{1}H-NMR Spectrum of DEA-CH$_3$SH Absorption System in D$_2$O (15 % Sample)
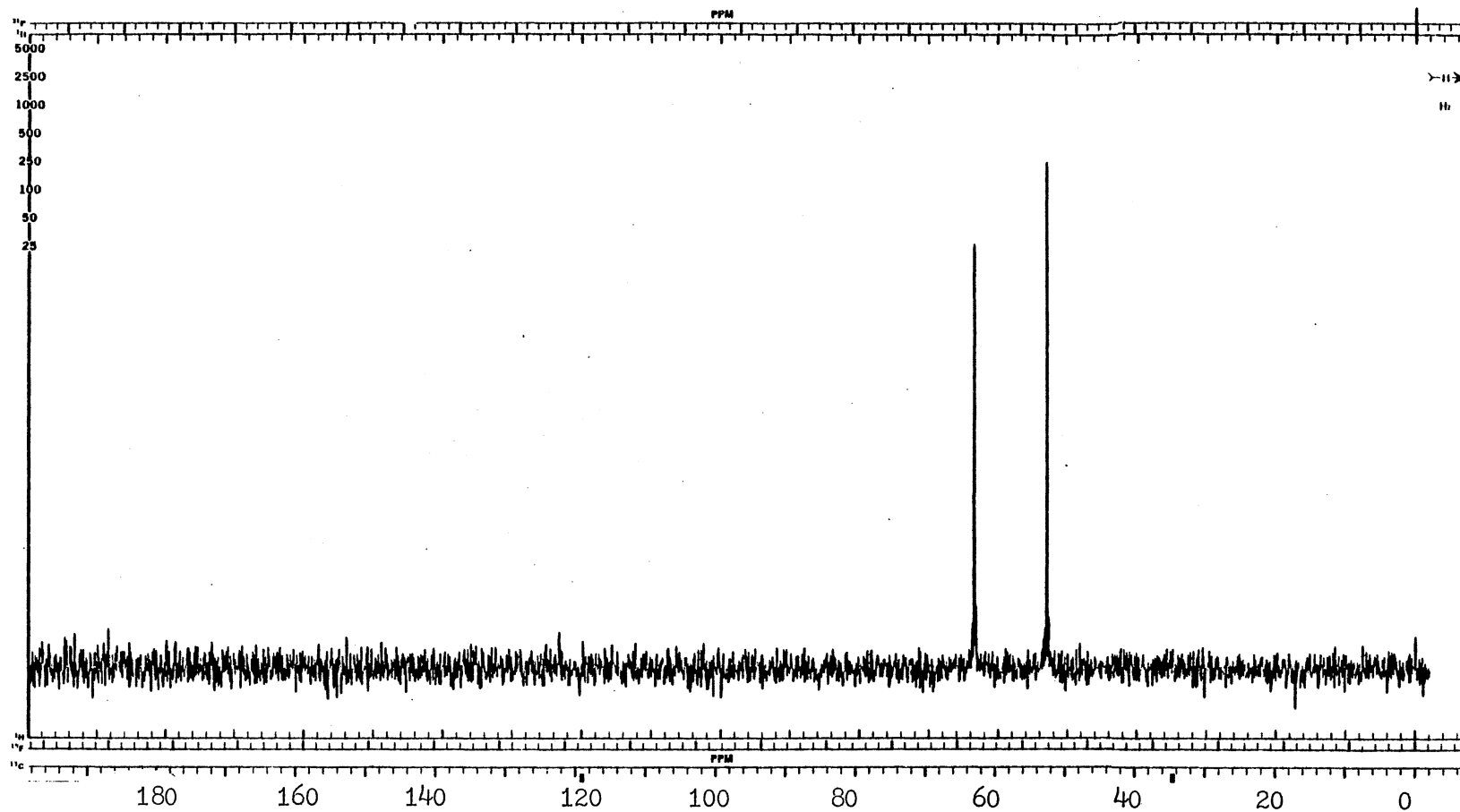
Figure 16. ^{13}C-NMR Spectrum of DEA-CH$_3$SH Absorption System in D$_2$O (15 % Sample)
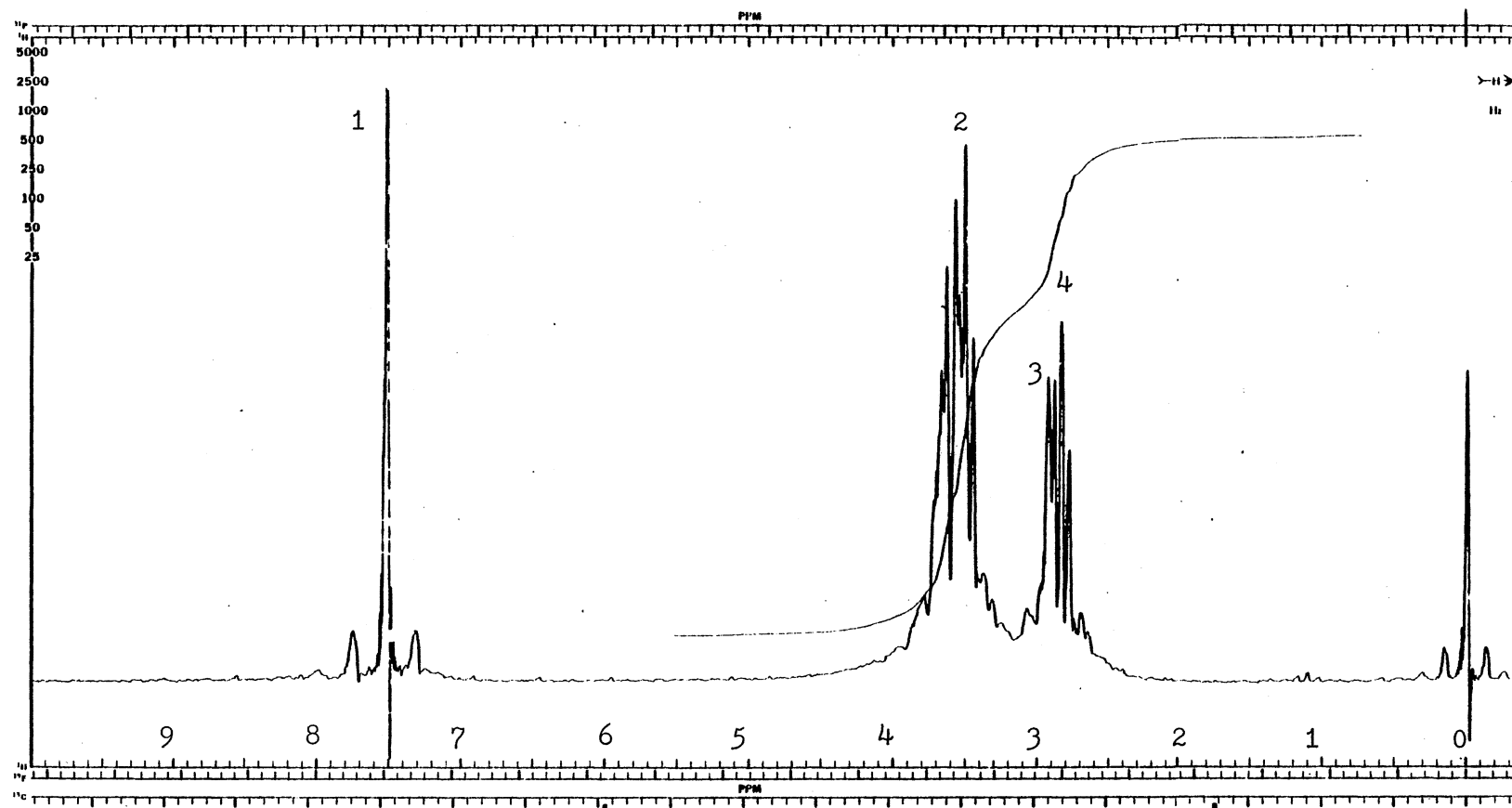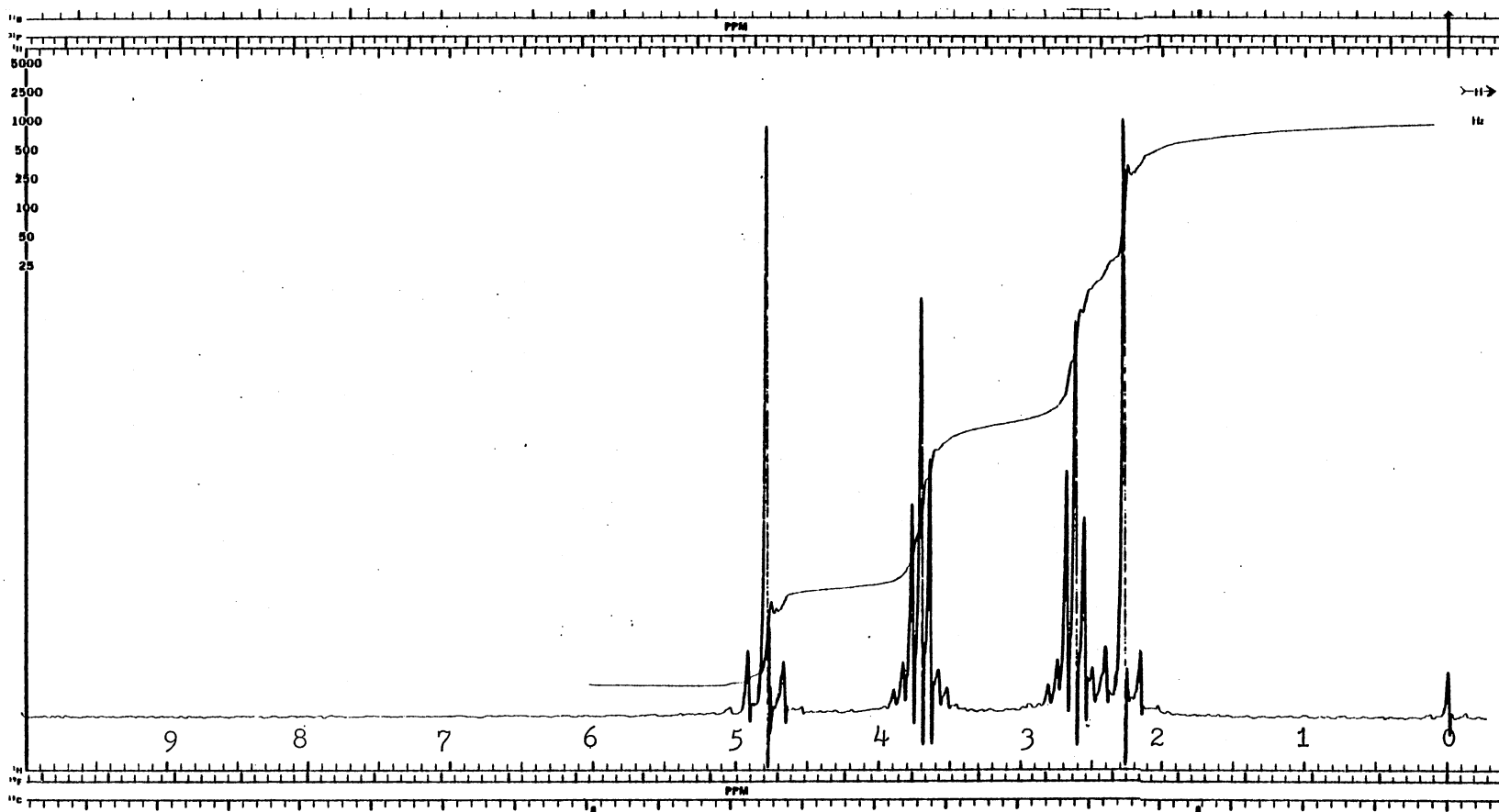
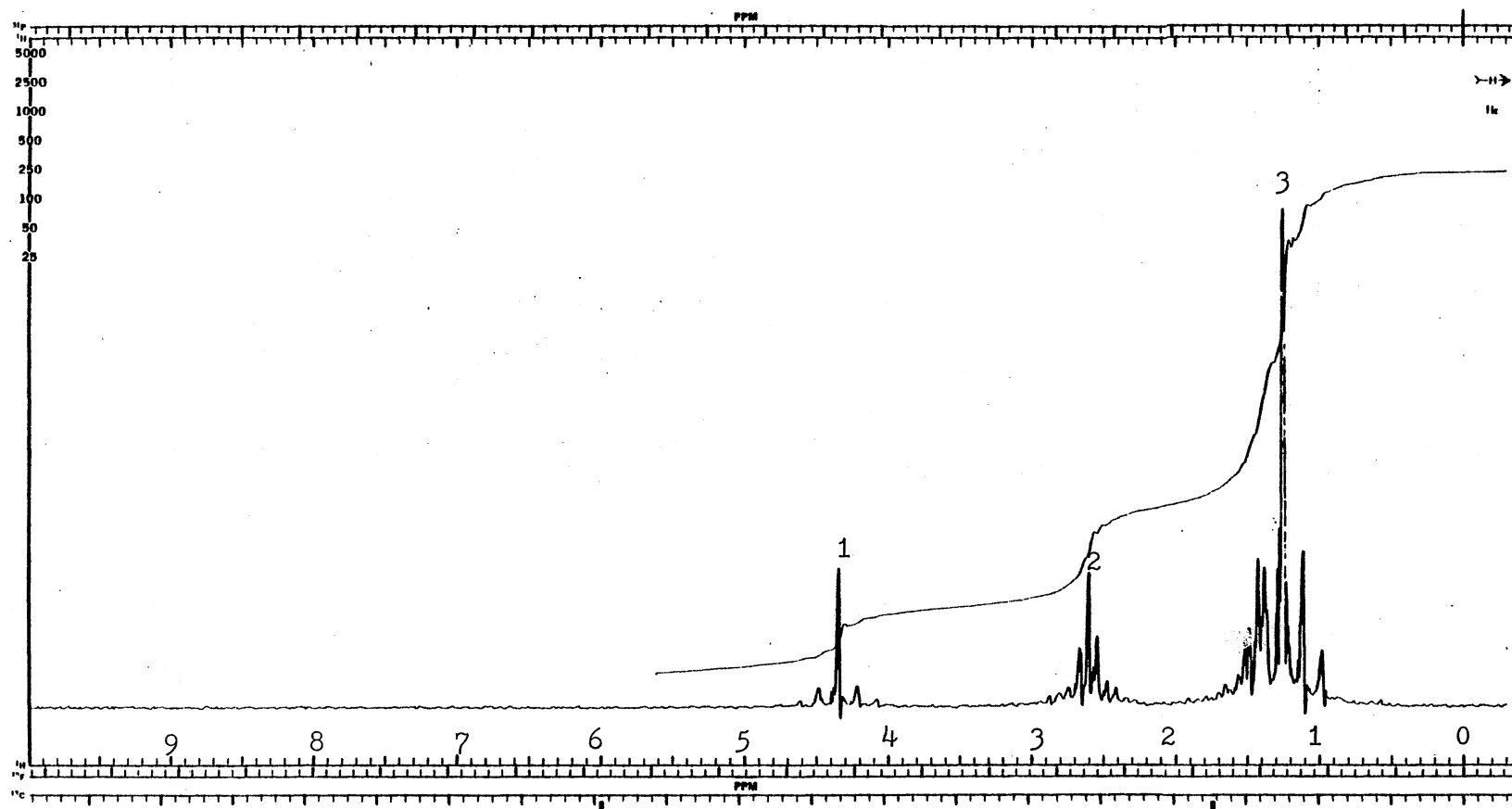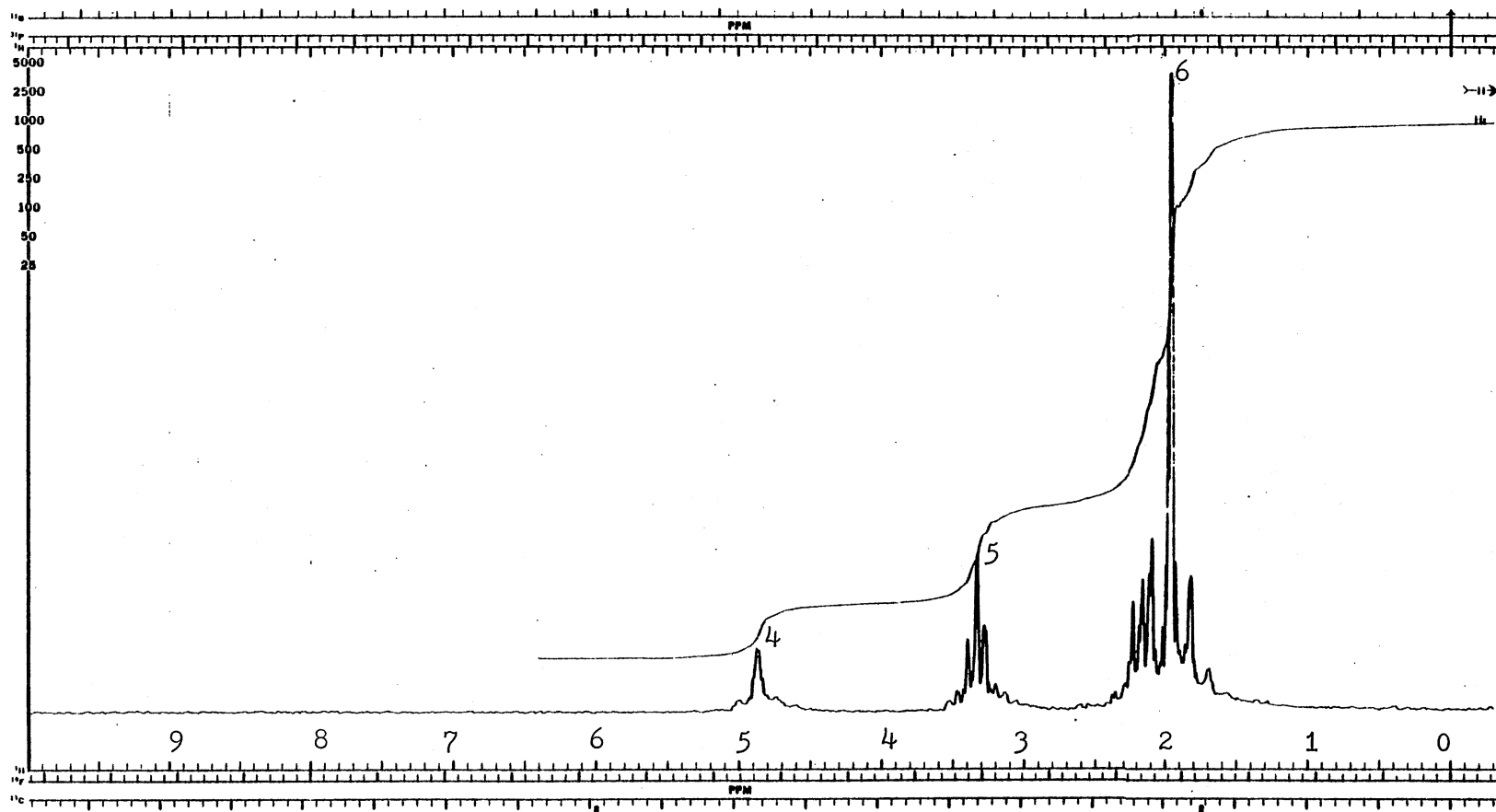Figure 17. ^{1}H-NMR Spectrum of Pure DGA in DCCl$_3$ (20 % Sample)
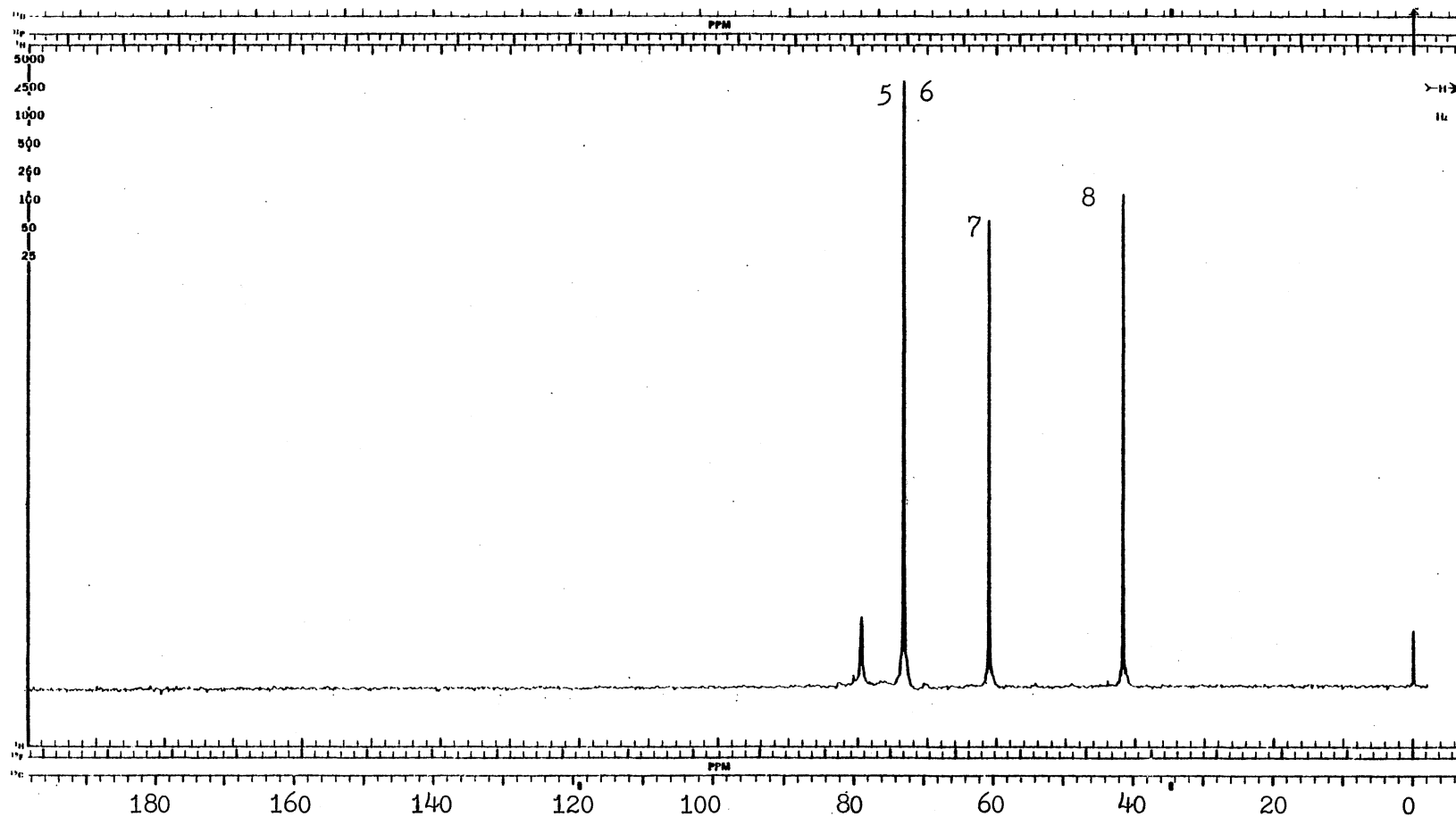
Figure 18. ^{13}C-NMR Spectrum of Pure DGA in DCCl$_3$ (20 % Sample)
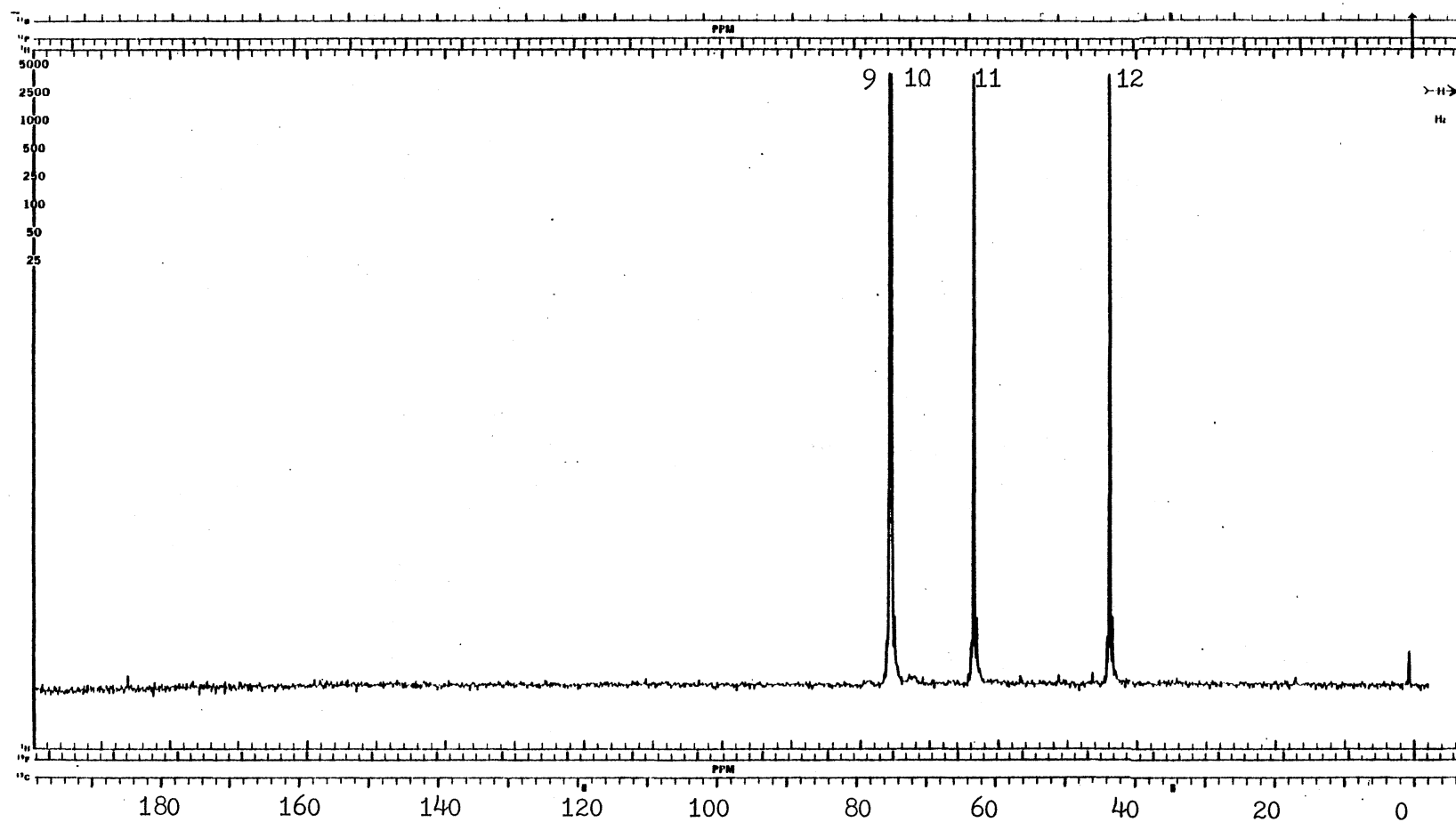
Figure 19. ^{13}C-NMR Spectrum of Pure DGA in D_2O (20 % Sample)
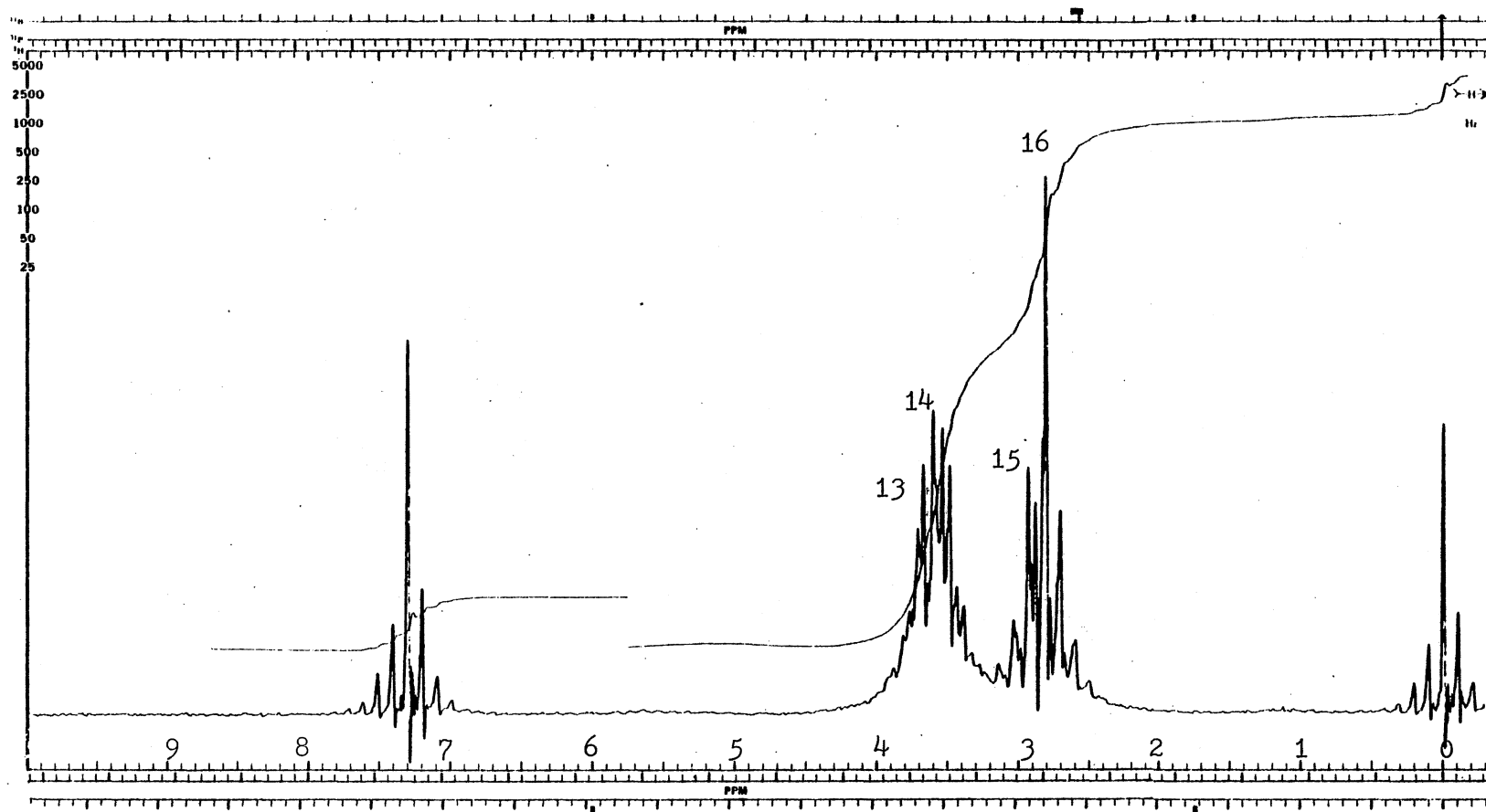
Figure 20. ^{1}H-NMR Spectrum of DGA-H$_2$S Reaction Products in DCCl$_3$ (20 % Sample)
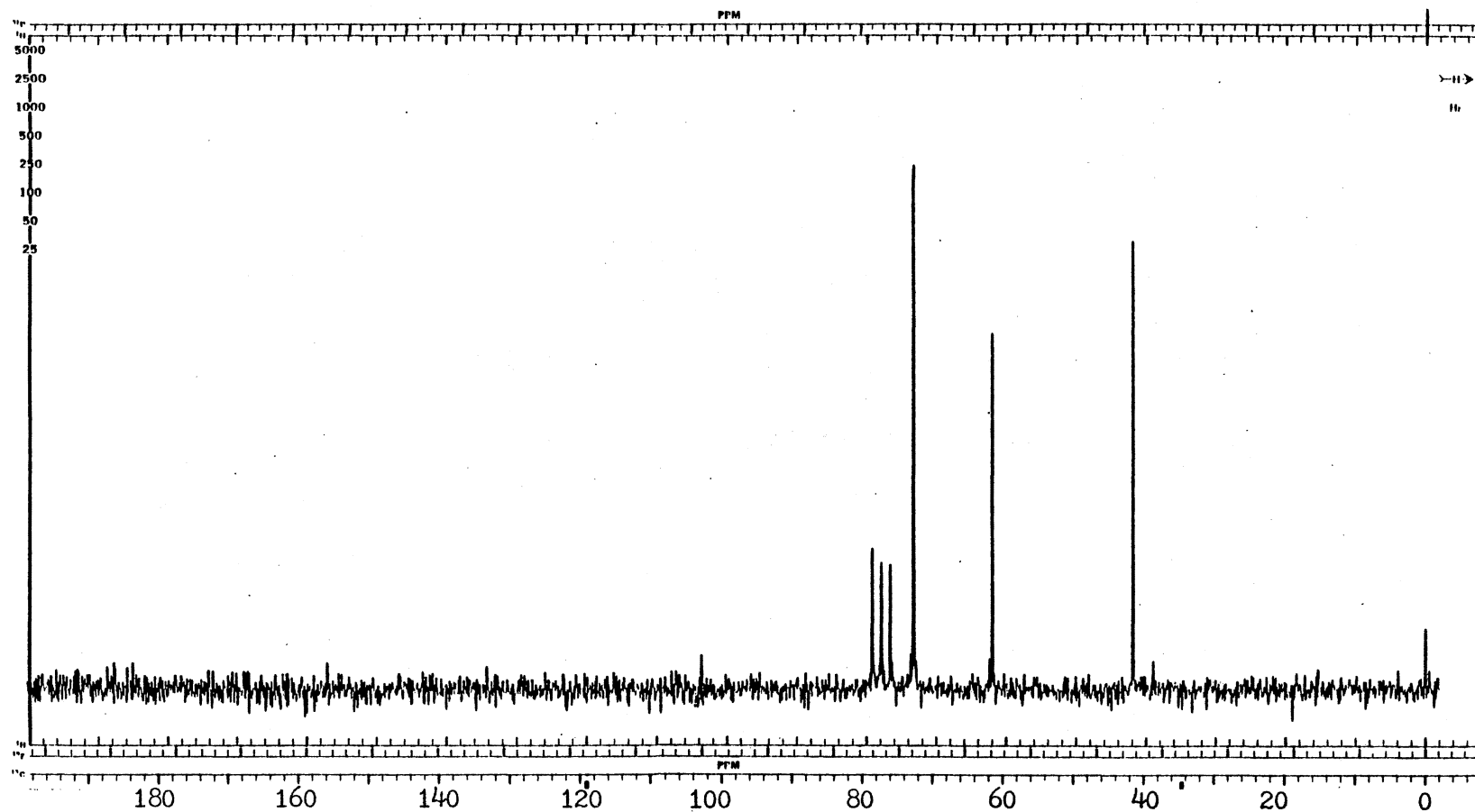
Figure 21. ^{13}C-NMR Spectrum of DGA-H$_2$S Reaction Products in DCCl$_3$ (20 % Sample)
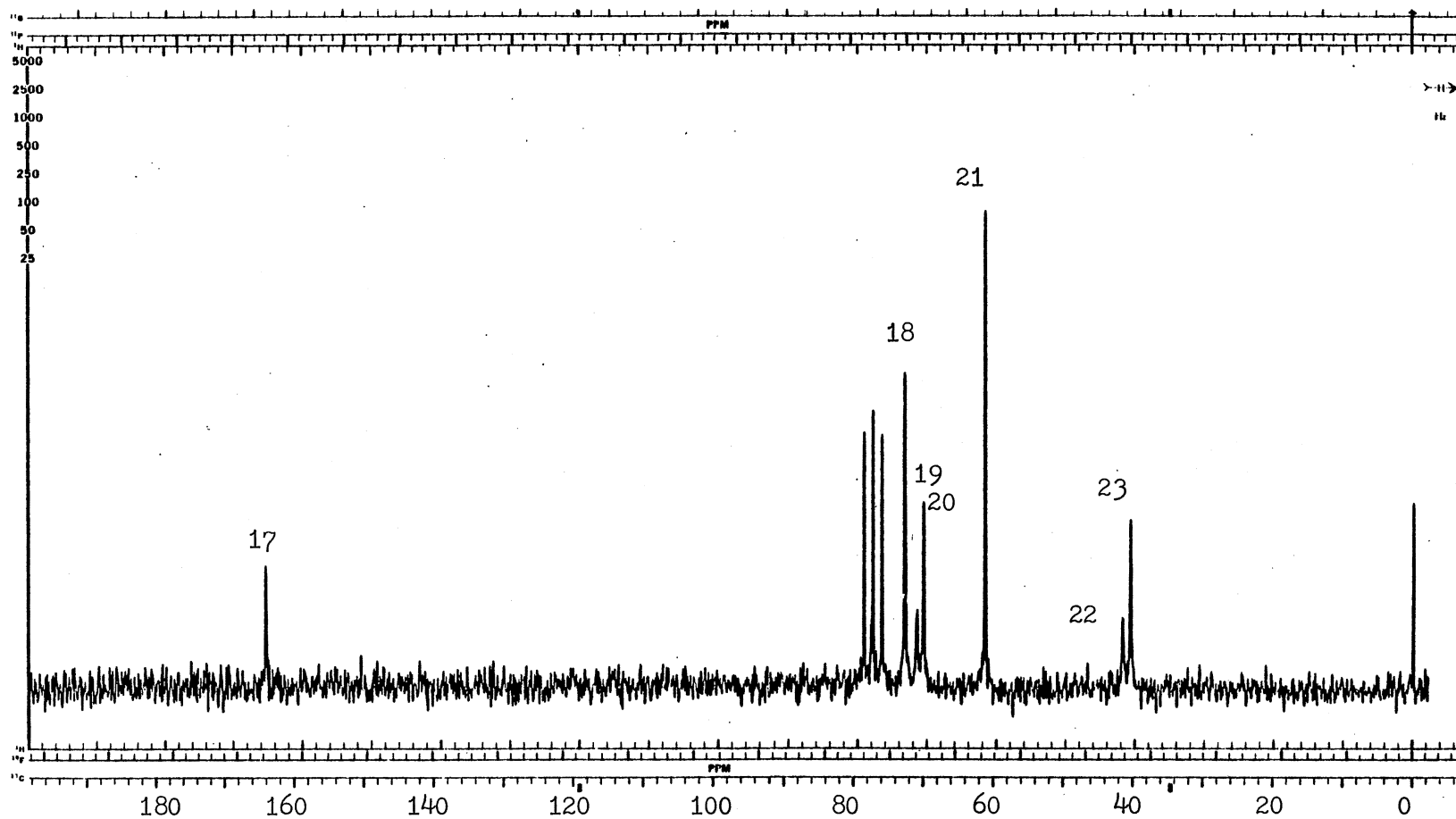
Figure 22. ^{13}C-NMR Spectrum of DGA-CO_2 Reaction Products in $DCCl_3$ (20 % Sample)
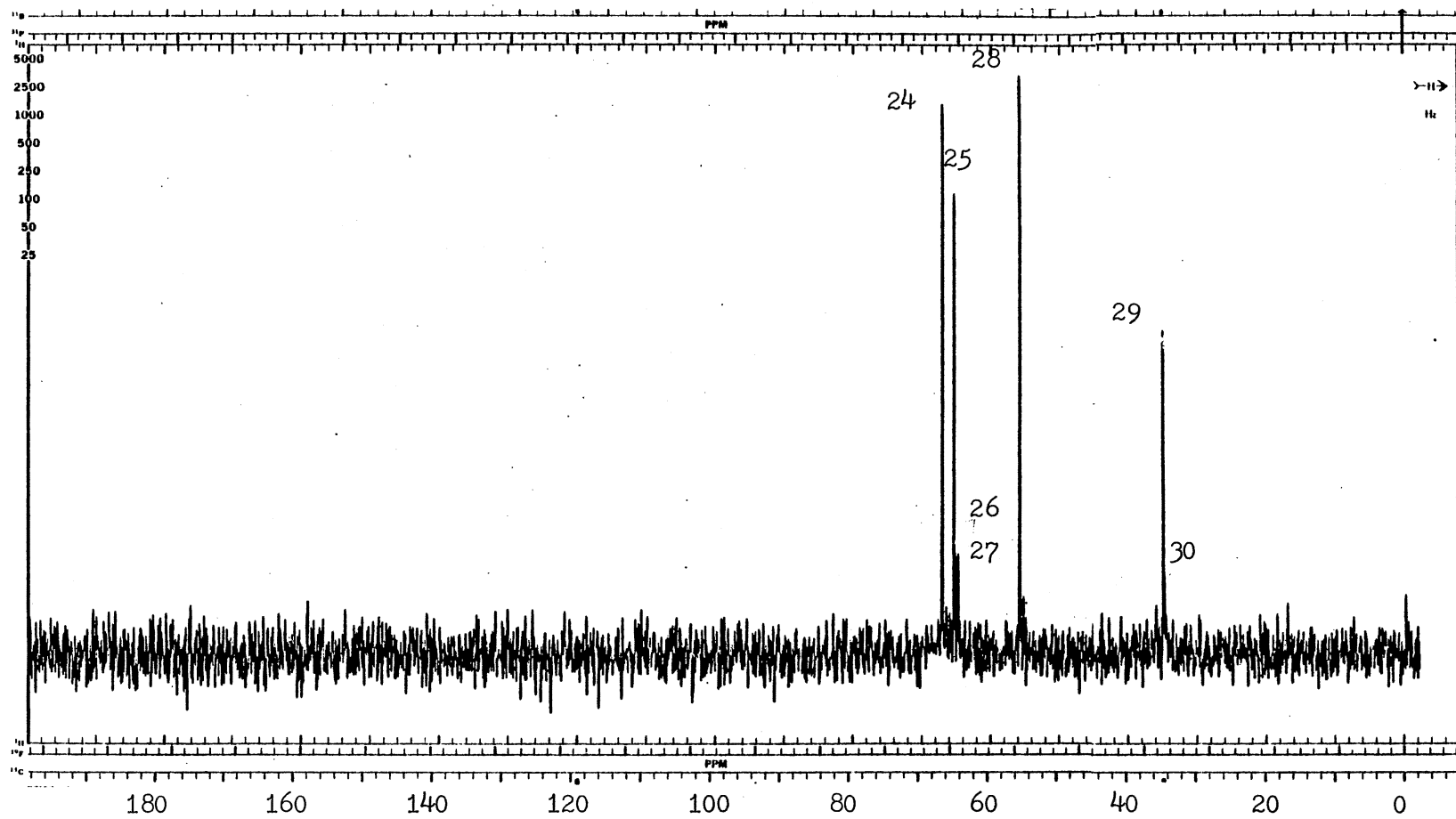
Figure 23. ^{13}C-NMR Spectrum of DGA-COS Reaction Products in D_2O (20 % Sample)
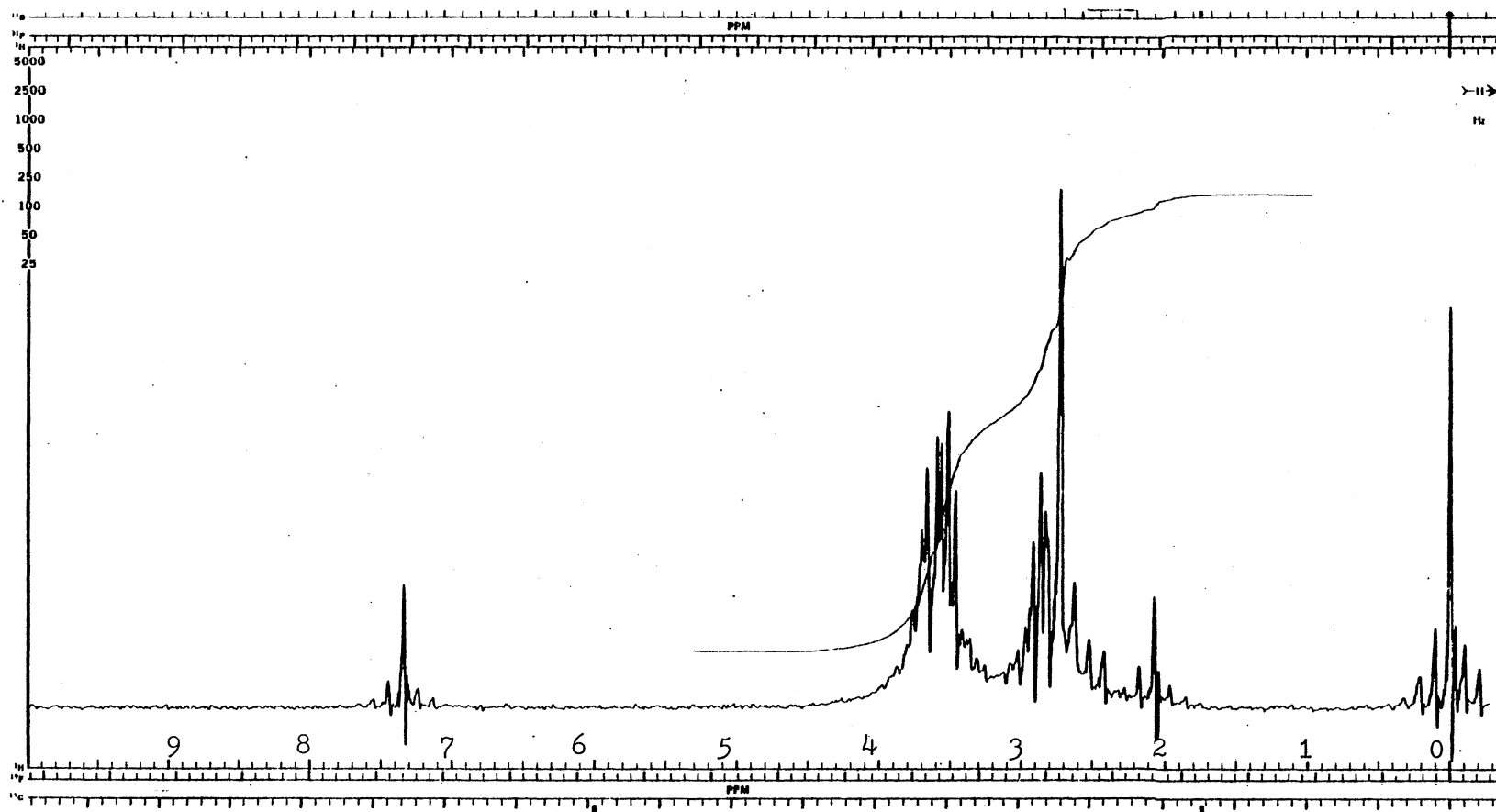
Figure 24. ^{1}H-NMR Spectrum of DGA- CH_3SH Reaction Products in $DCCl_3$ (20 % Sample)
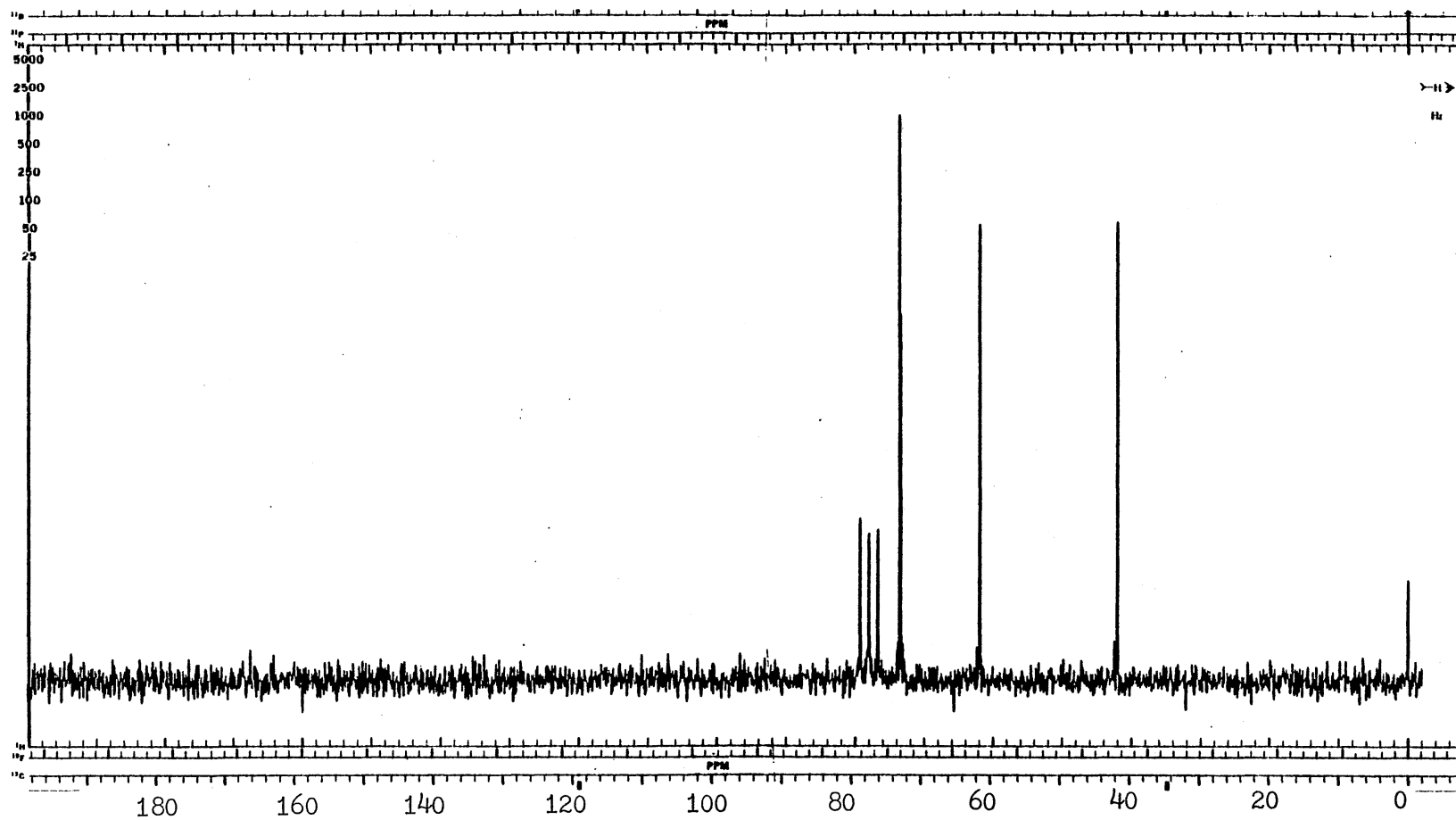
Figure 25. ^{13}C-NMR Spectrum of DGA-CH$_3$SH Absorption System in DCCl$_3$ (20 % Sample)
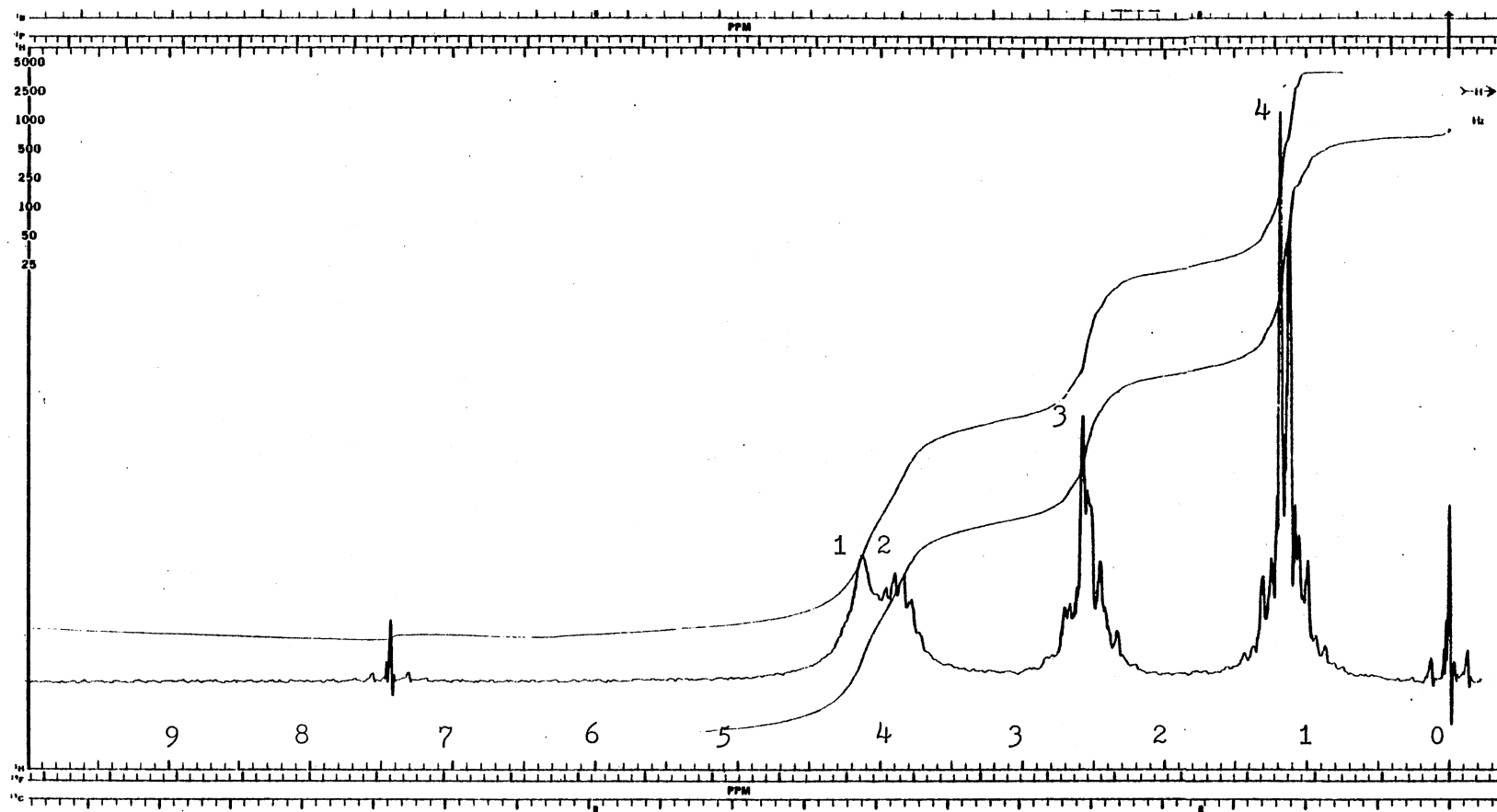
Figure 26. ^{1}H-NMR Spectrum of Pure DIPA in DCCl$_3$ (10 % Sample)
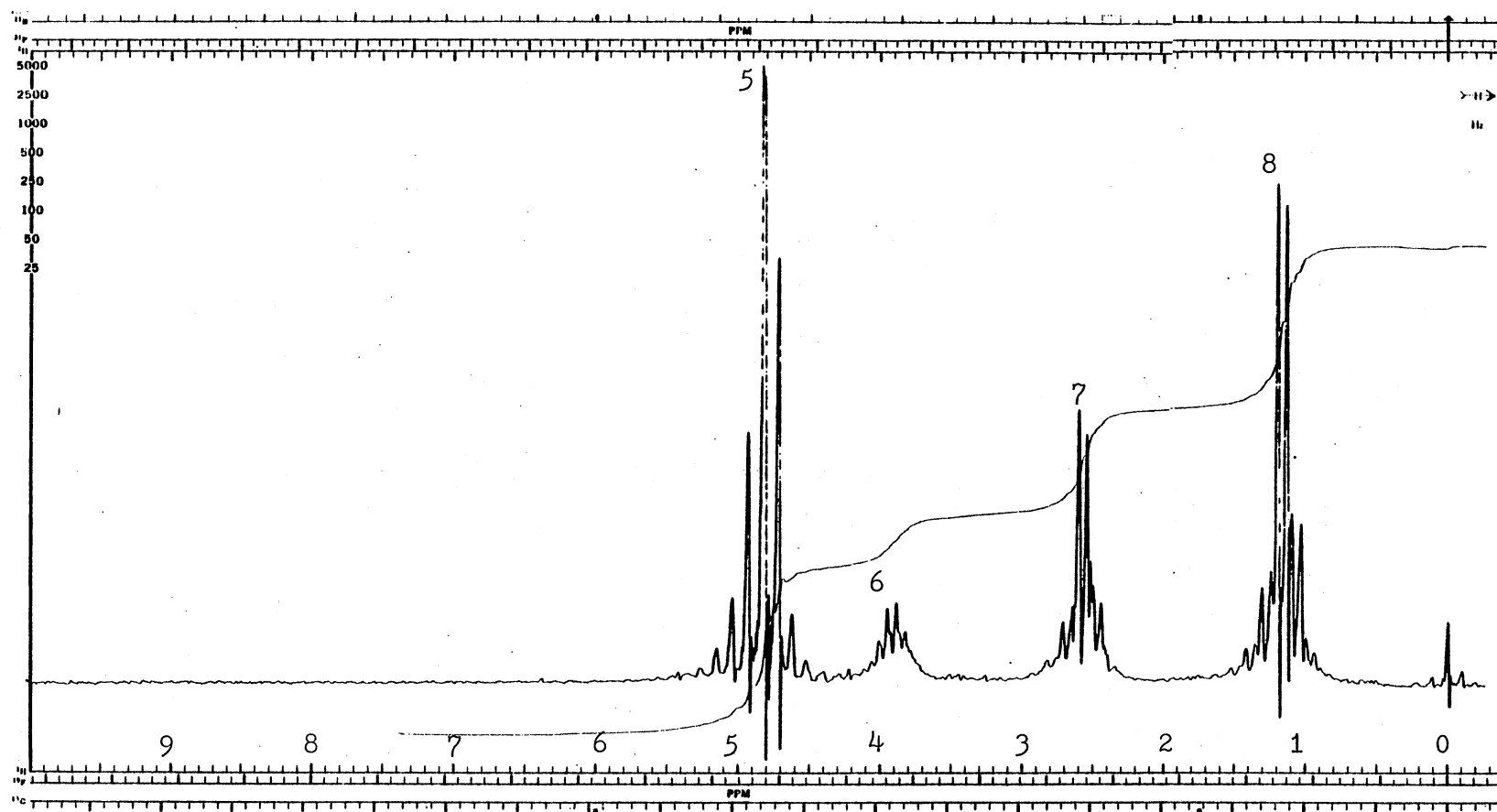
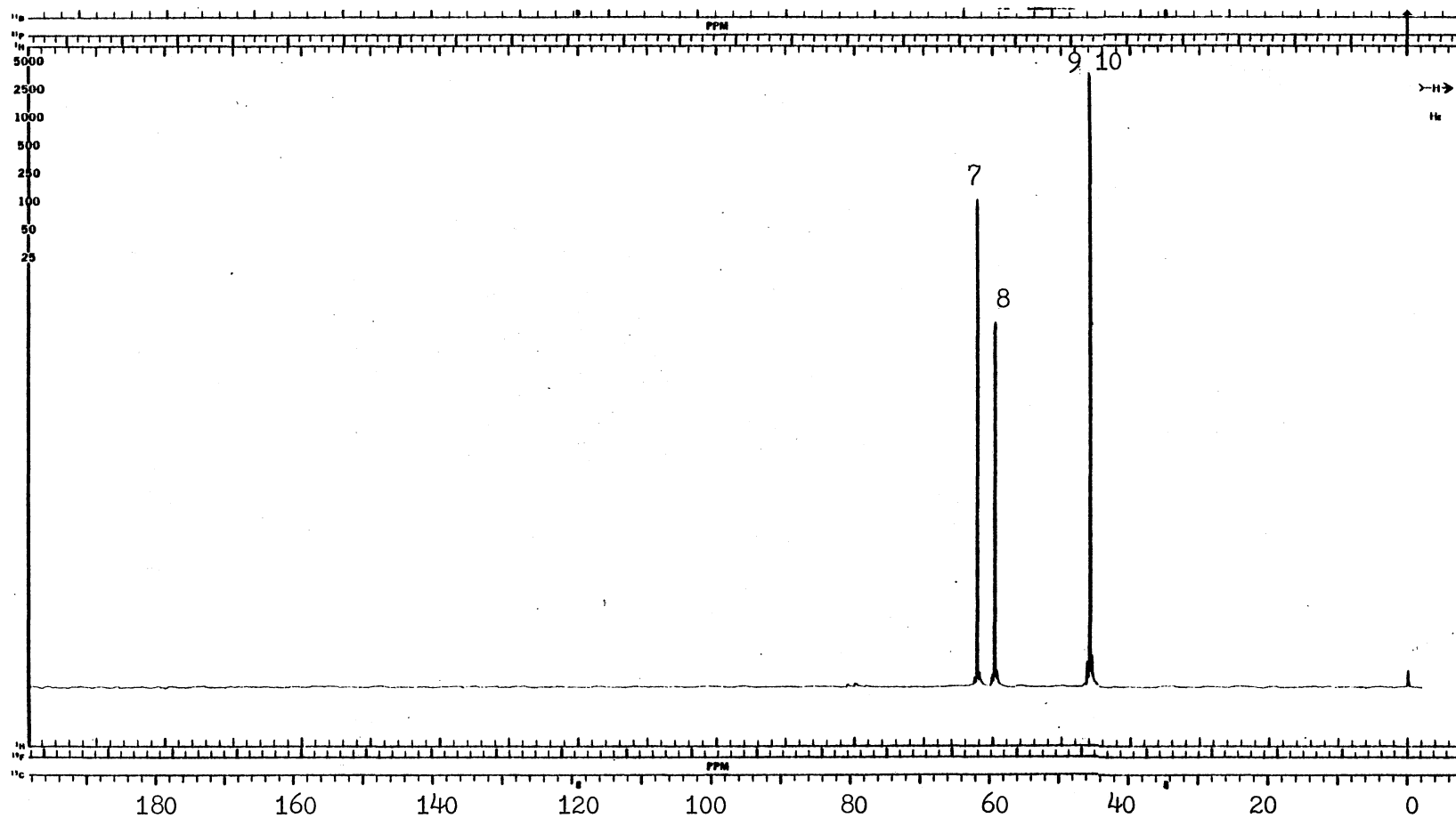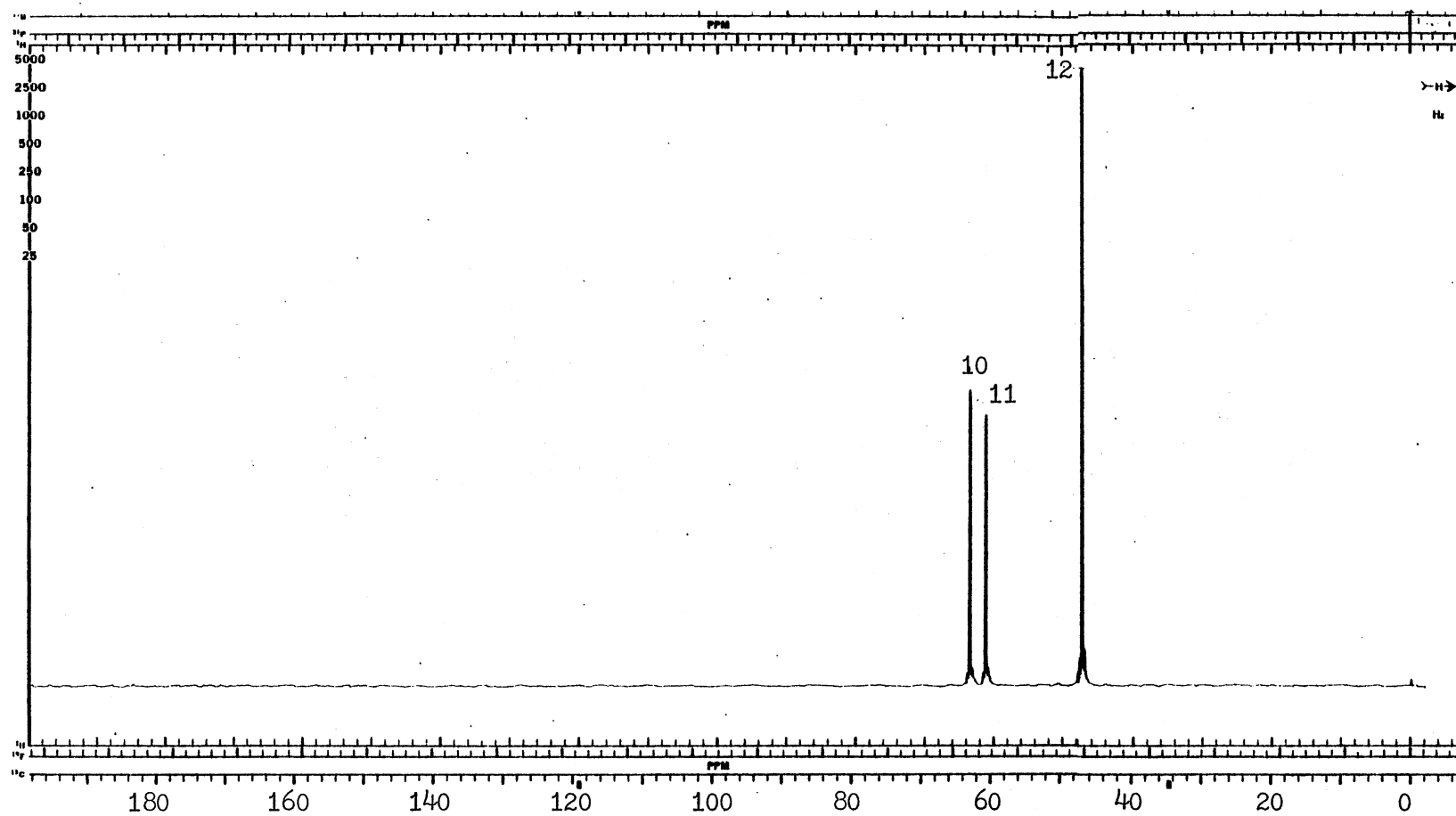Figure 27. ^{1}H-NMR Spectrum of Pure DIPA in D_2O (10 % Sample)
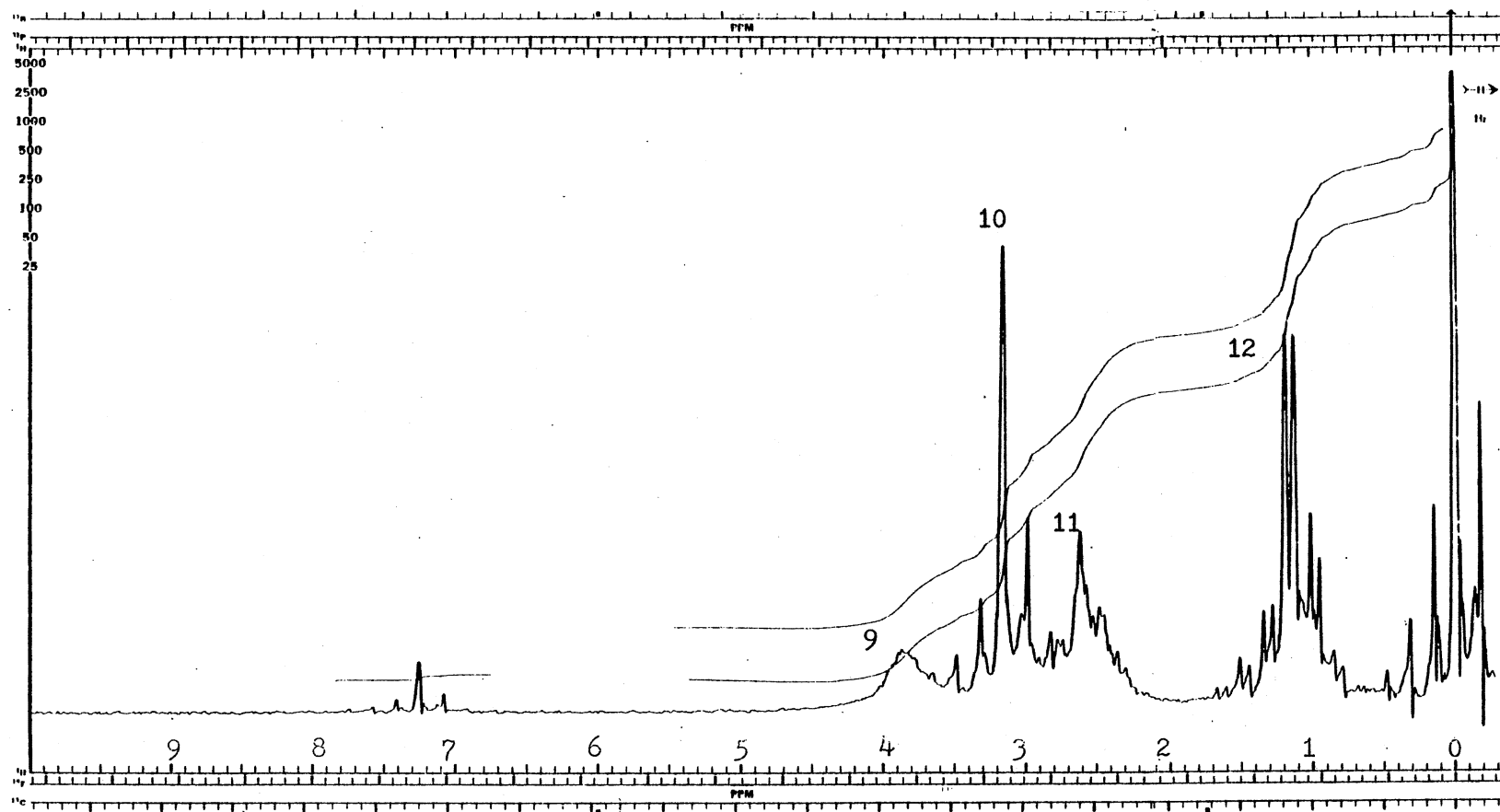
Figure 28. ^{1}H-NMR Spectrum of DIPA-H$_2$S Reaction Products in DCCl$_3$ (10 % Sample)
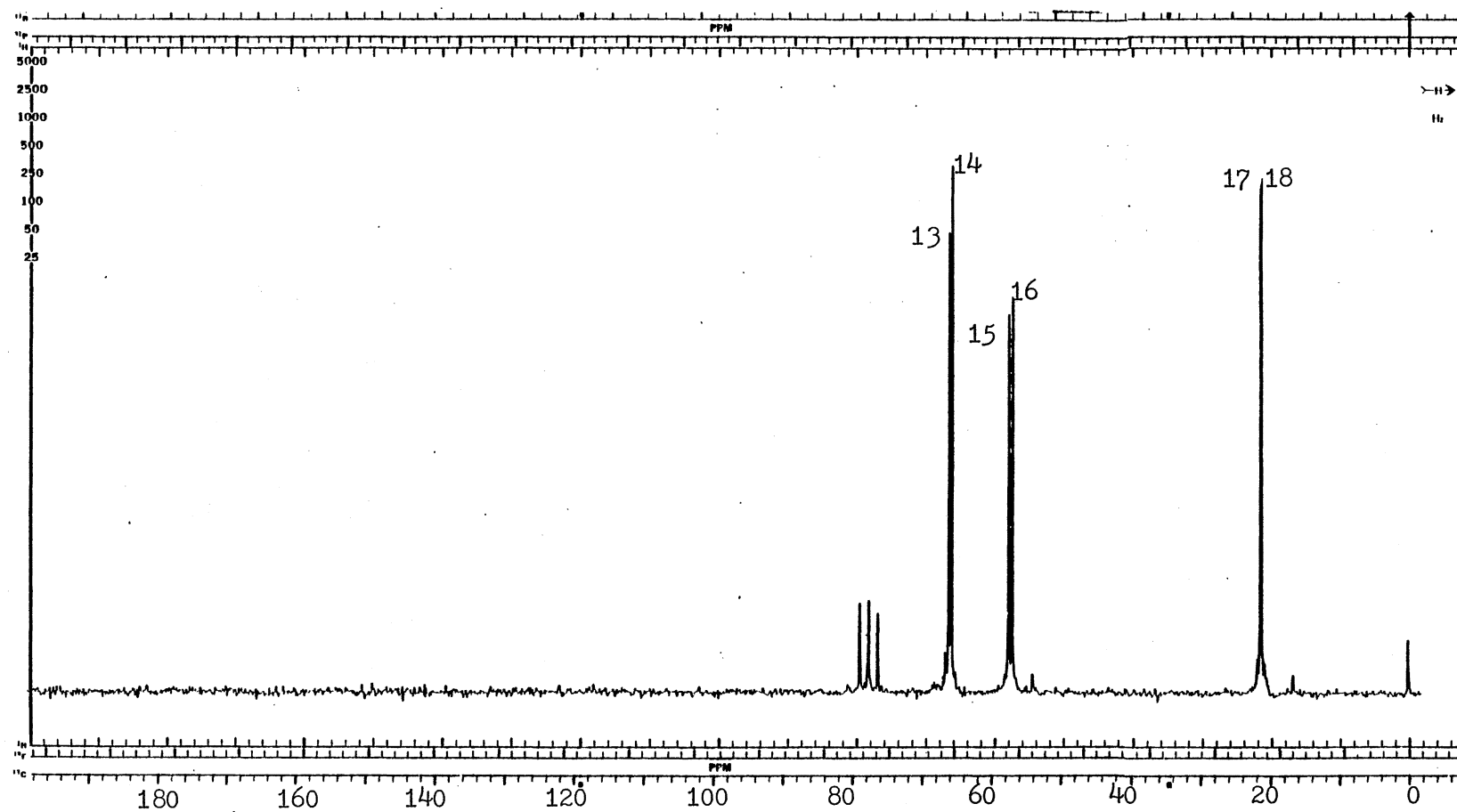
Figure 29. ^{13}C-NMR Spectrum of Pure DIPA in DCCl$_3$ (10 % Sample)
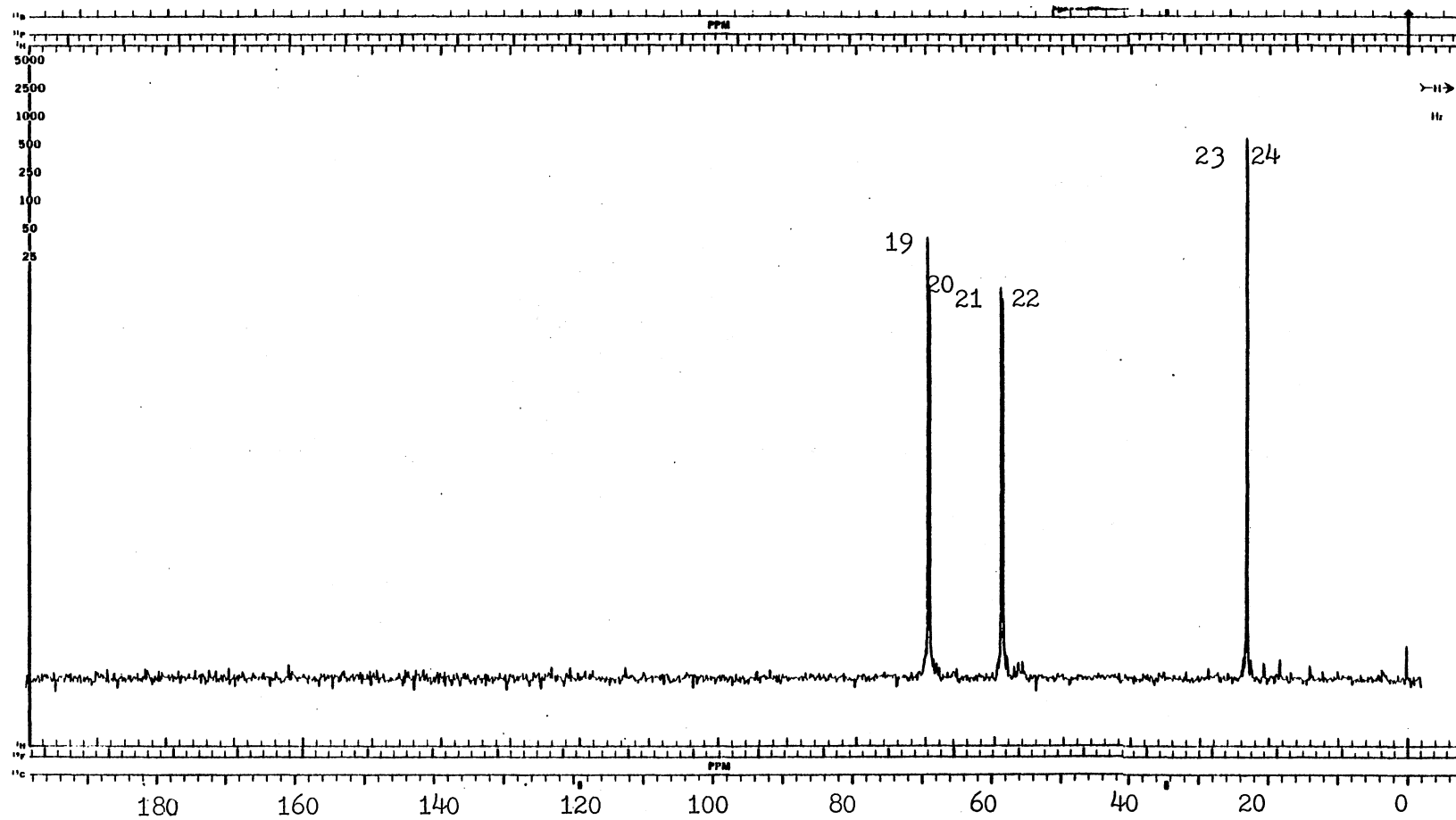
Figure 30. ^{13}C-NMR Spectrum of Pure DIPA in D_2O (10 % Sample)
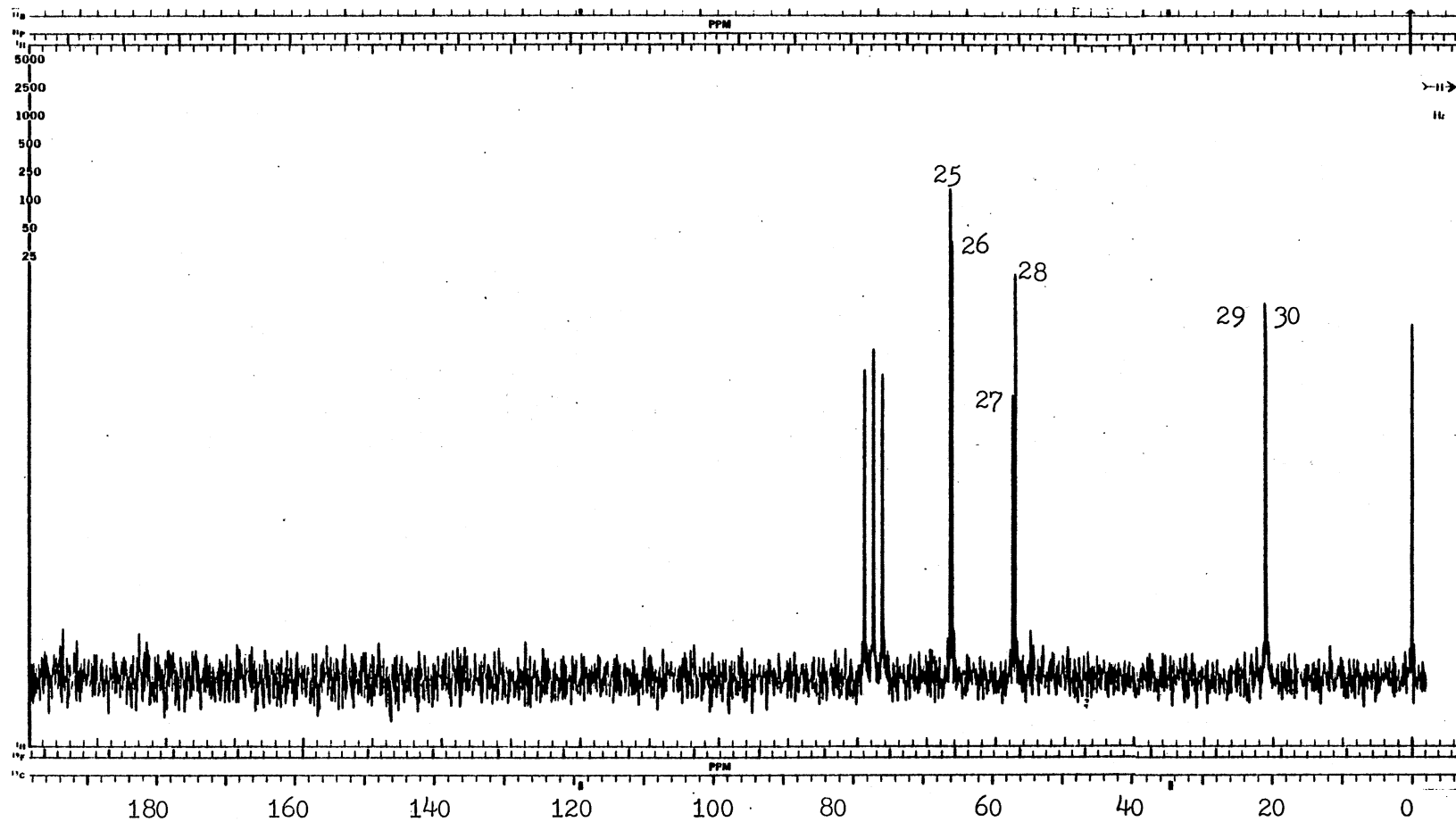
Figure 31. ^{13}C-NMR Spectrum of DIPA-H$_2$S Reaction Products in DCCl$_3$ (10 % Sample)
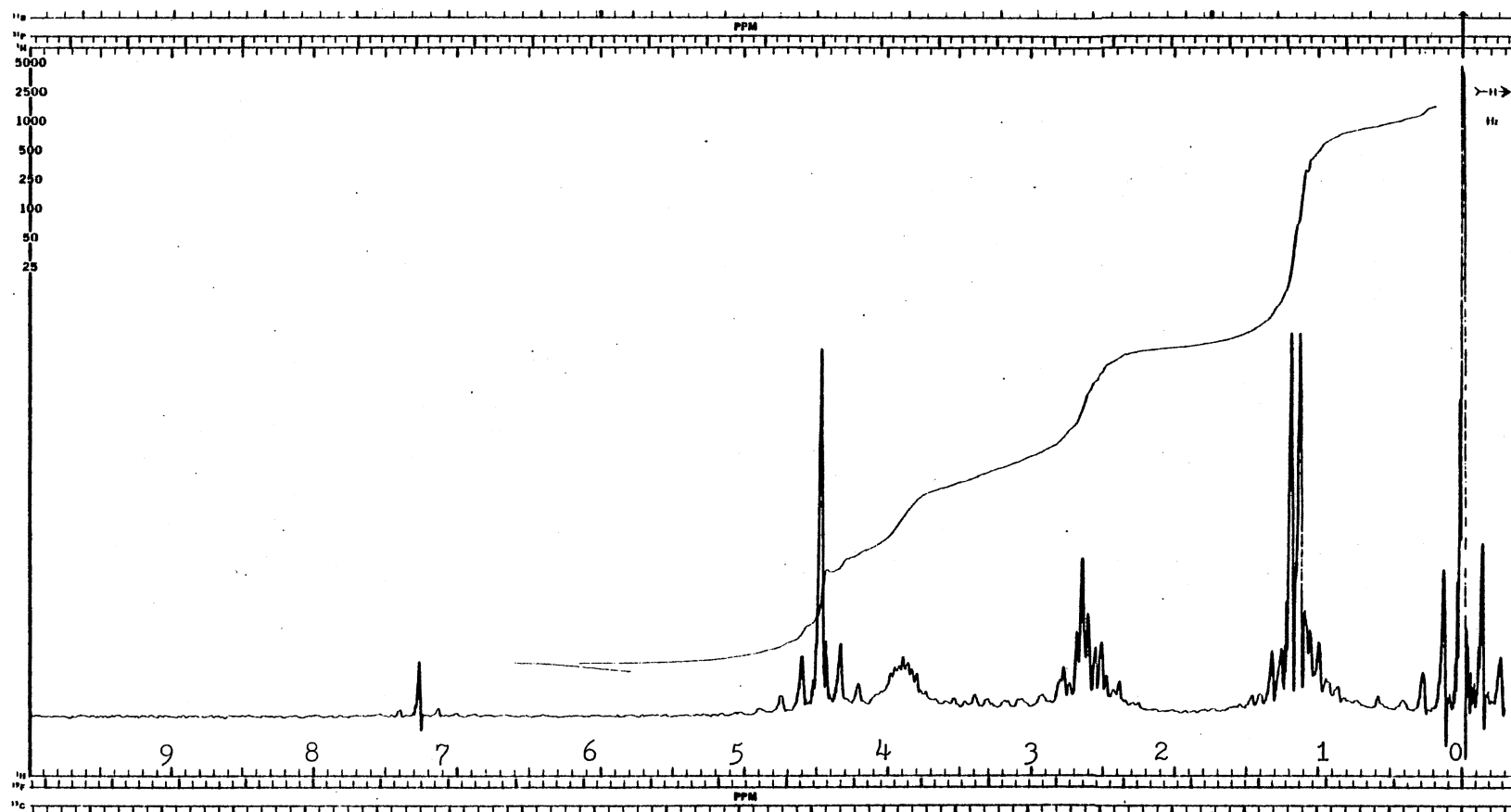
Figure 32. ^{1}H-NMR Spectrum of DIPA-CO$_2$ Reaction Products in DCCl$_3$ (10 % Sample)
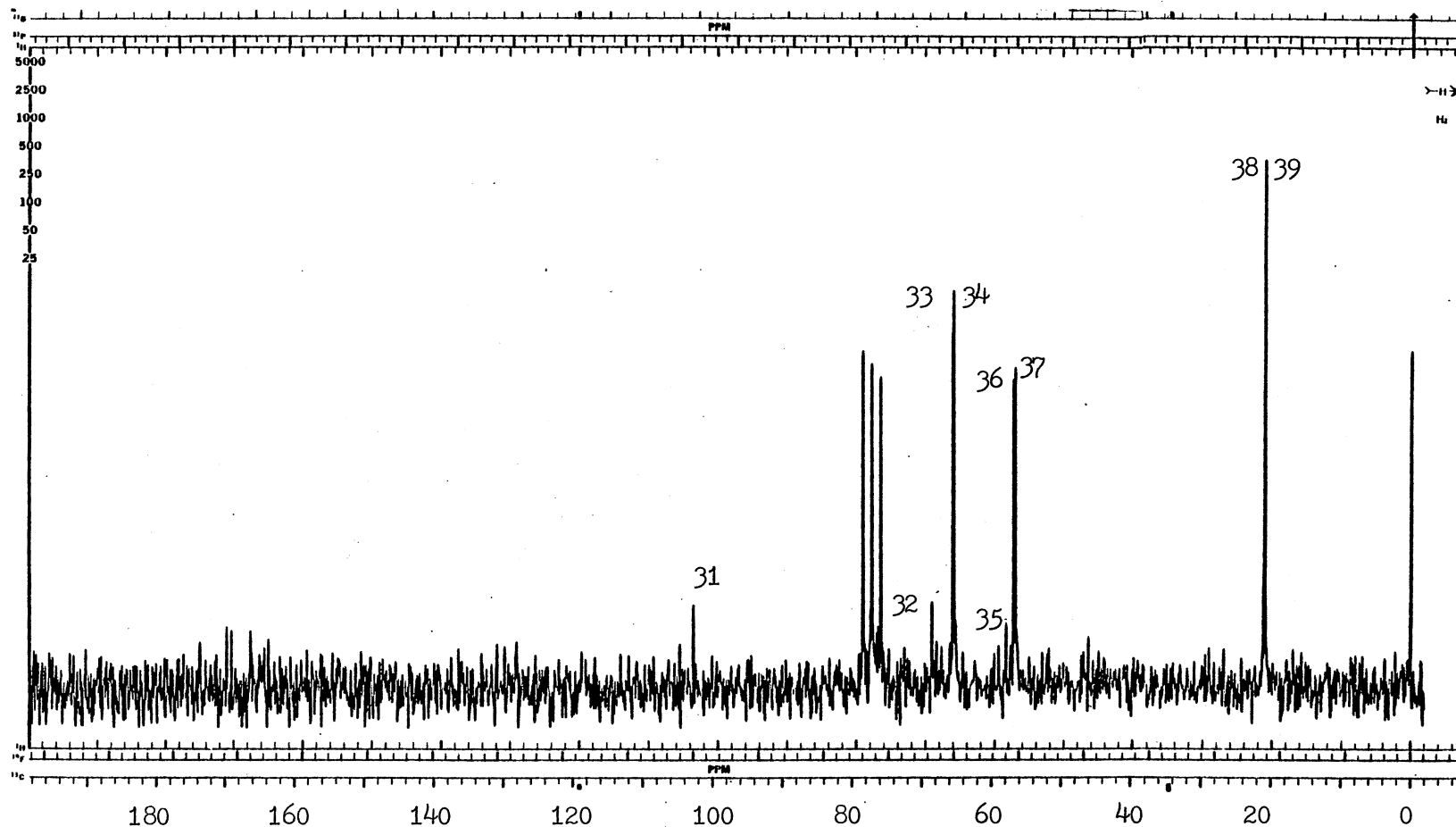
Figure 33. ^{13}C-NMR Spectrum of DIPA-CO$_2$ Reaction Products in DCCl$_3$ (10 % Sample)
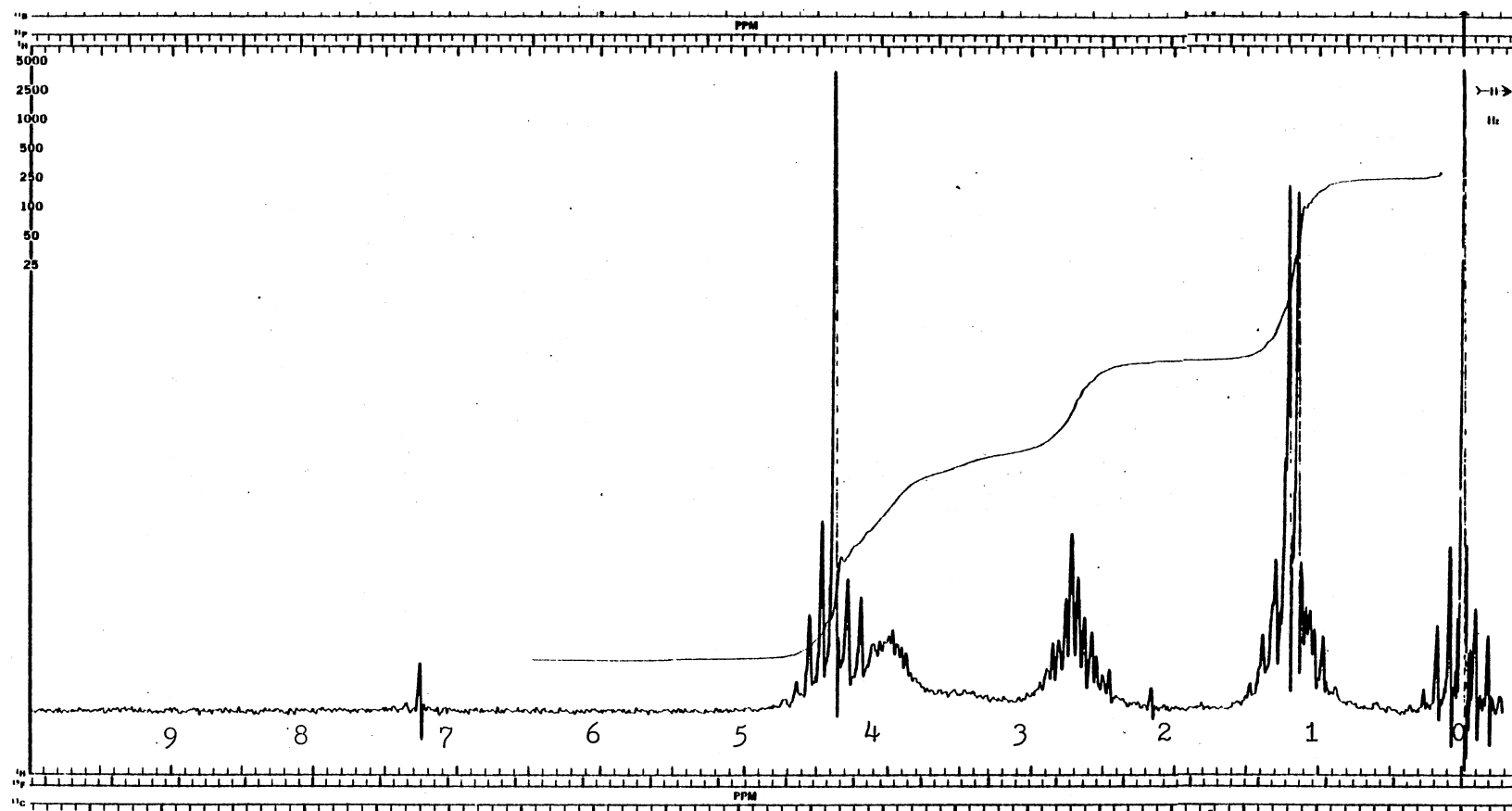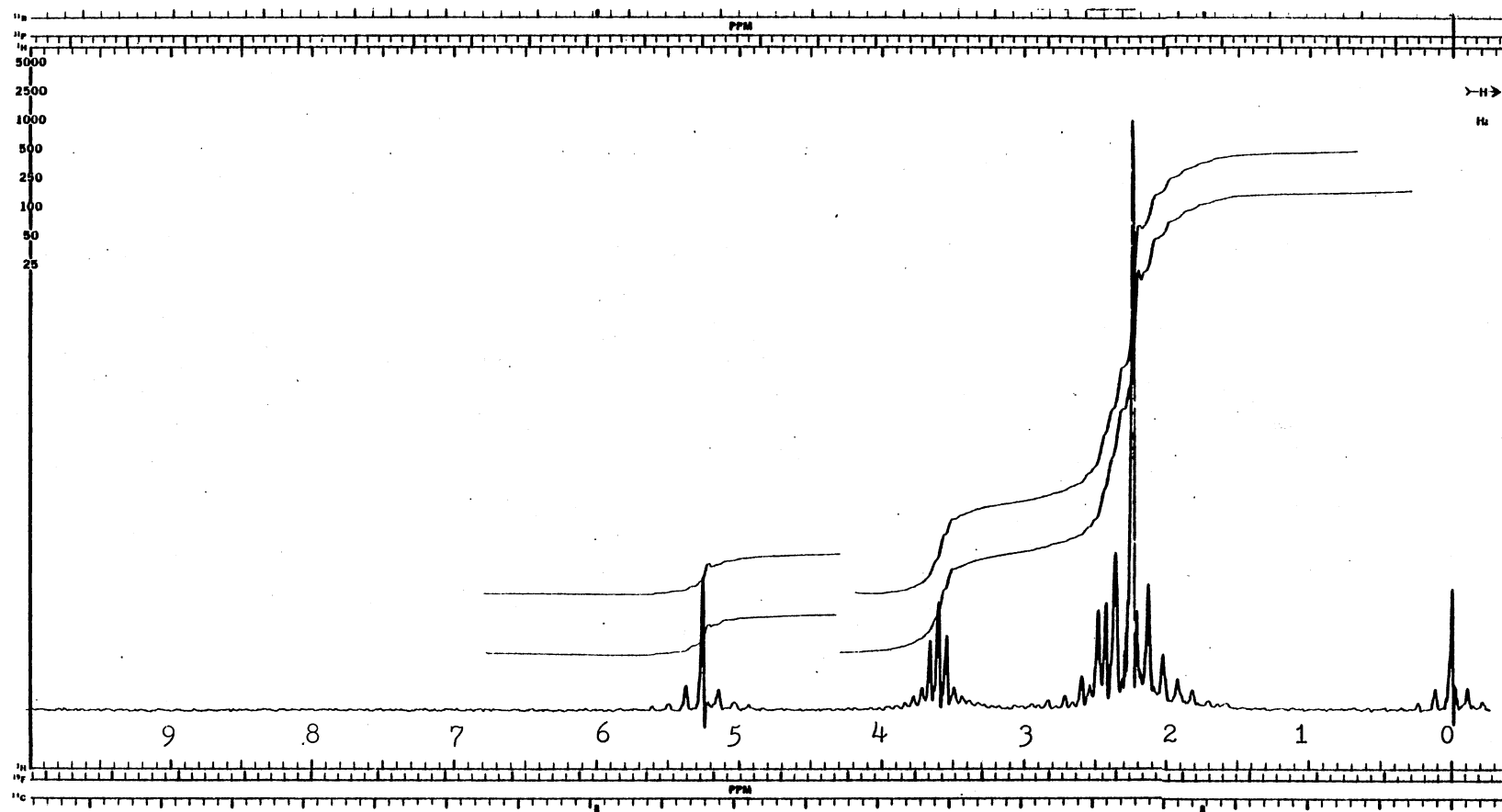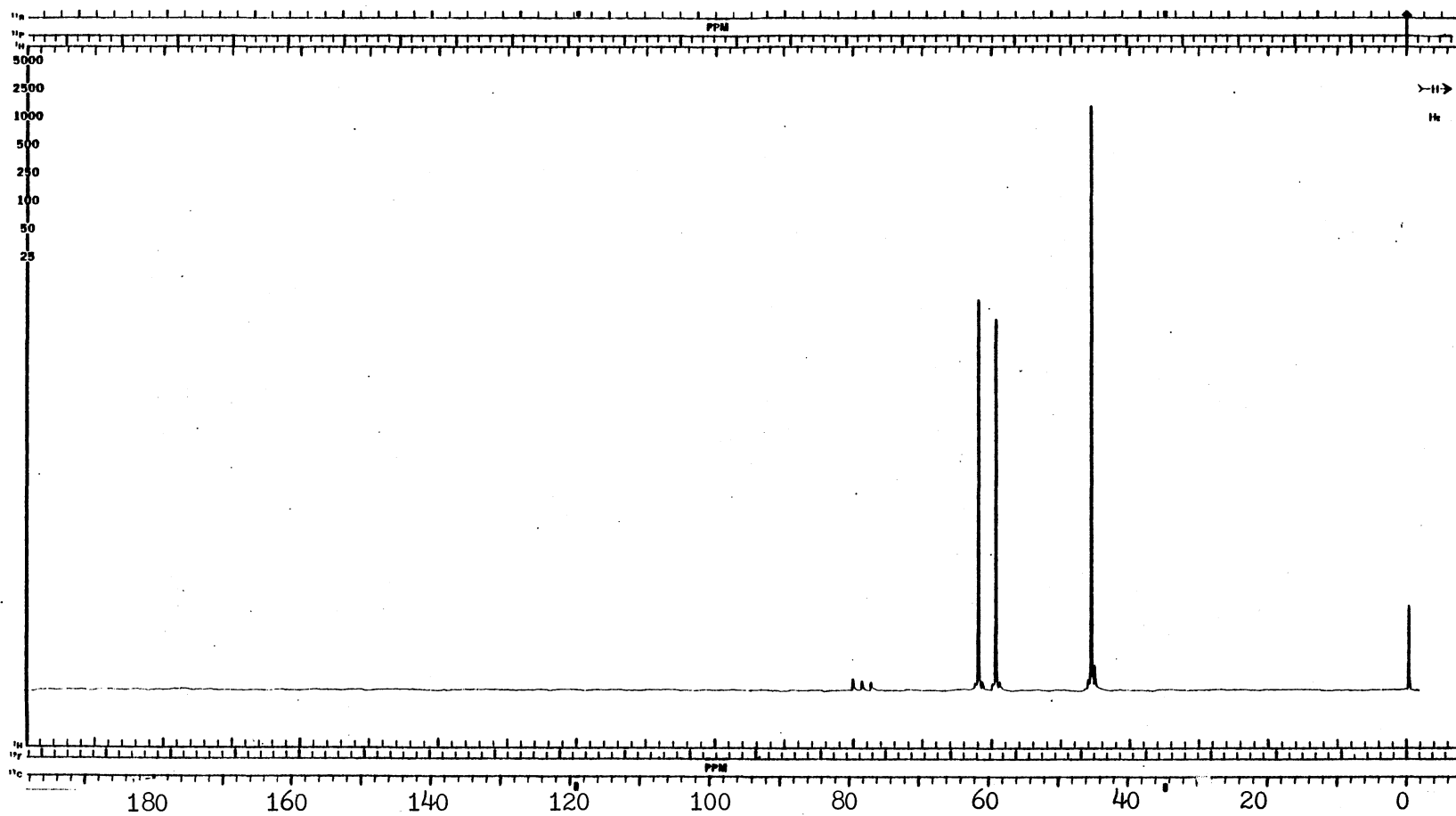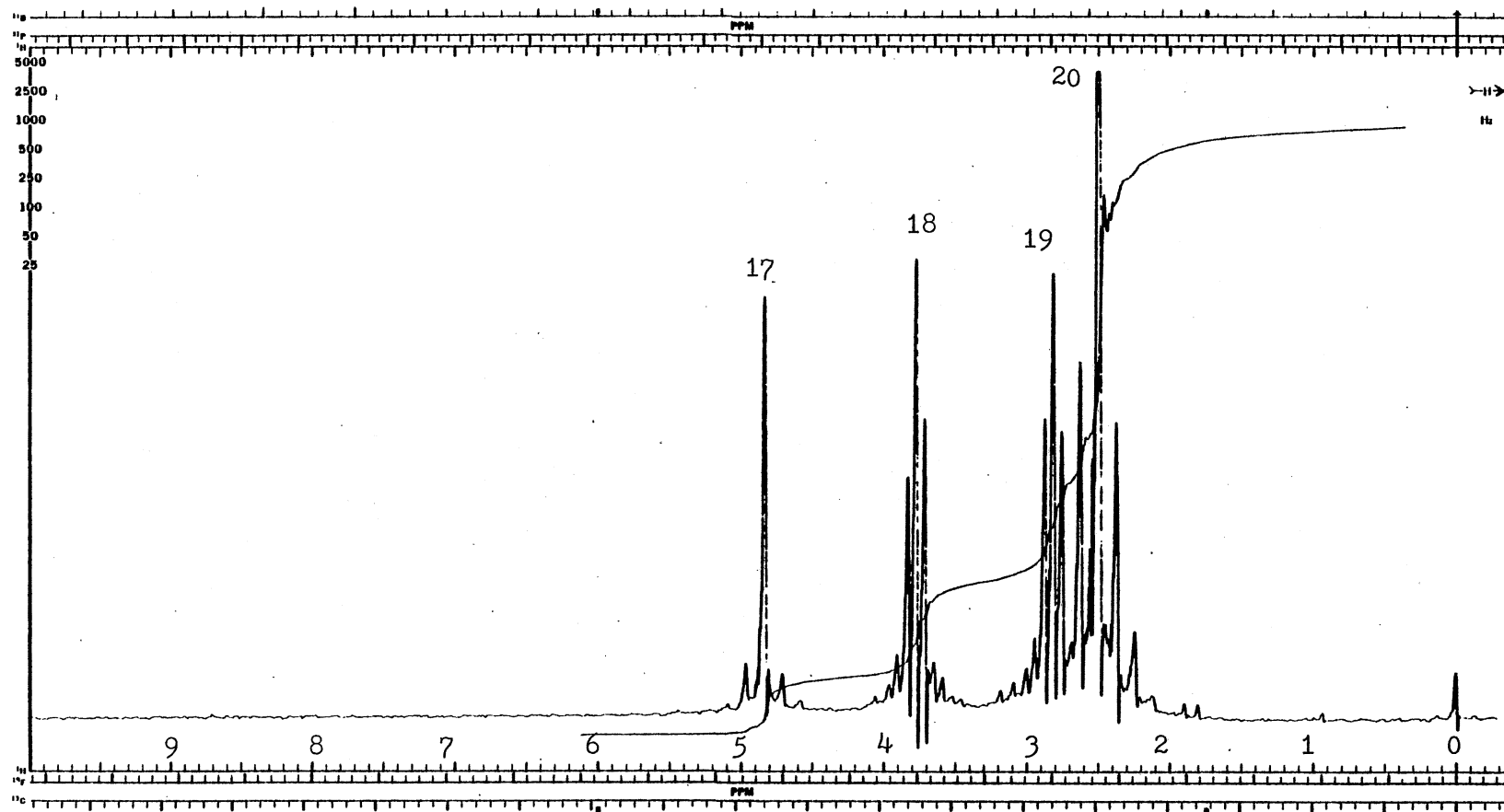
Figure 34. ^{1}H-NMR Spectrum of DIPA-COS Reaction Products in DCCl$_3$ (10 % Sample)
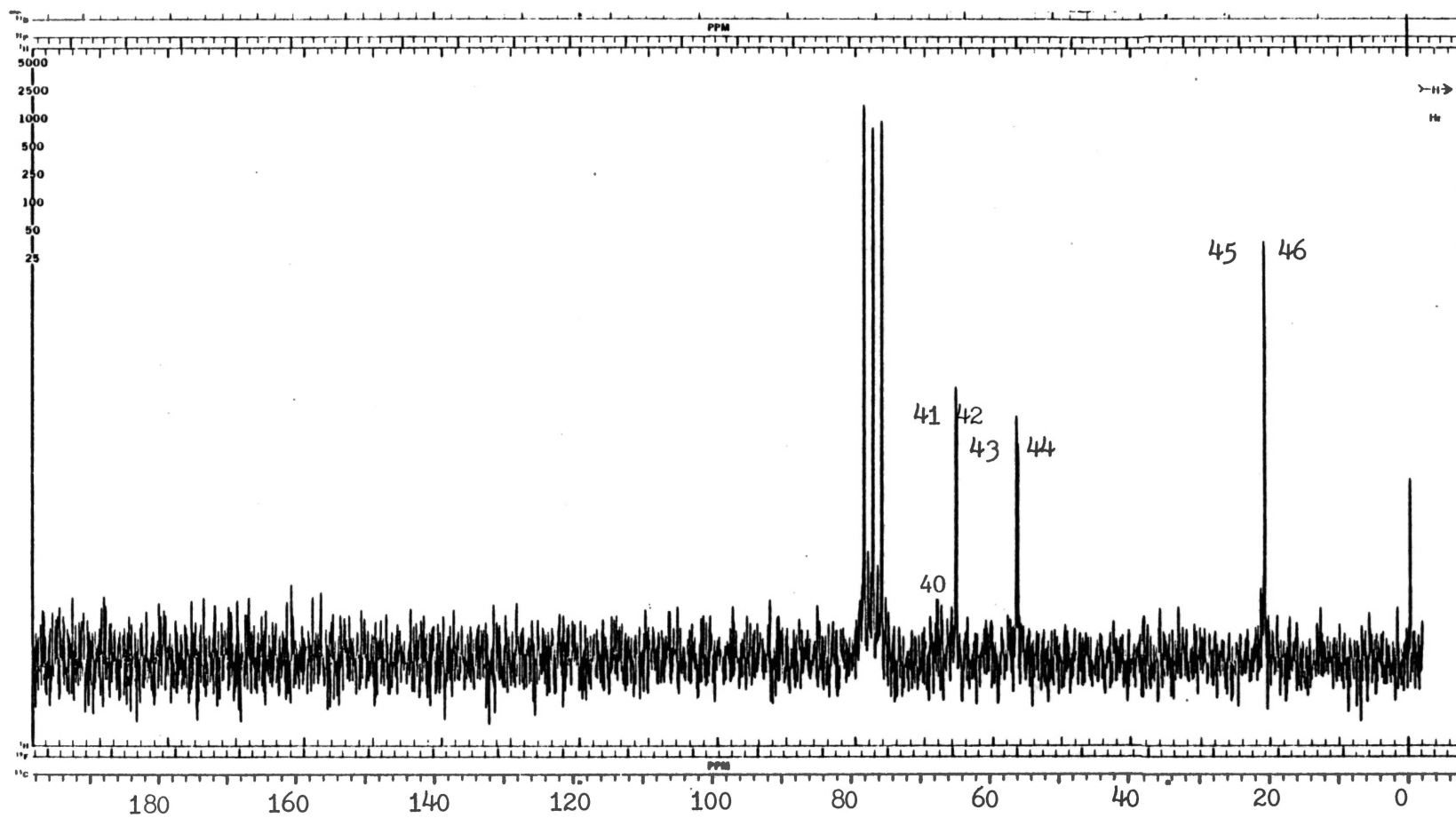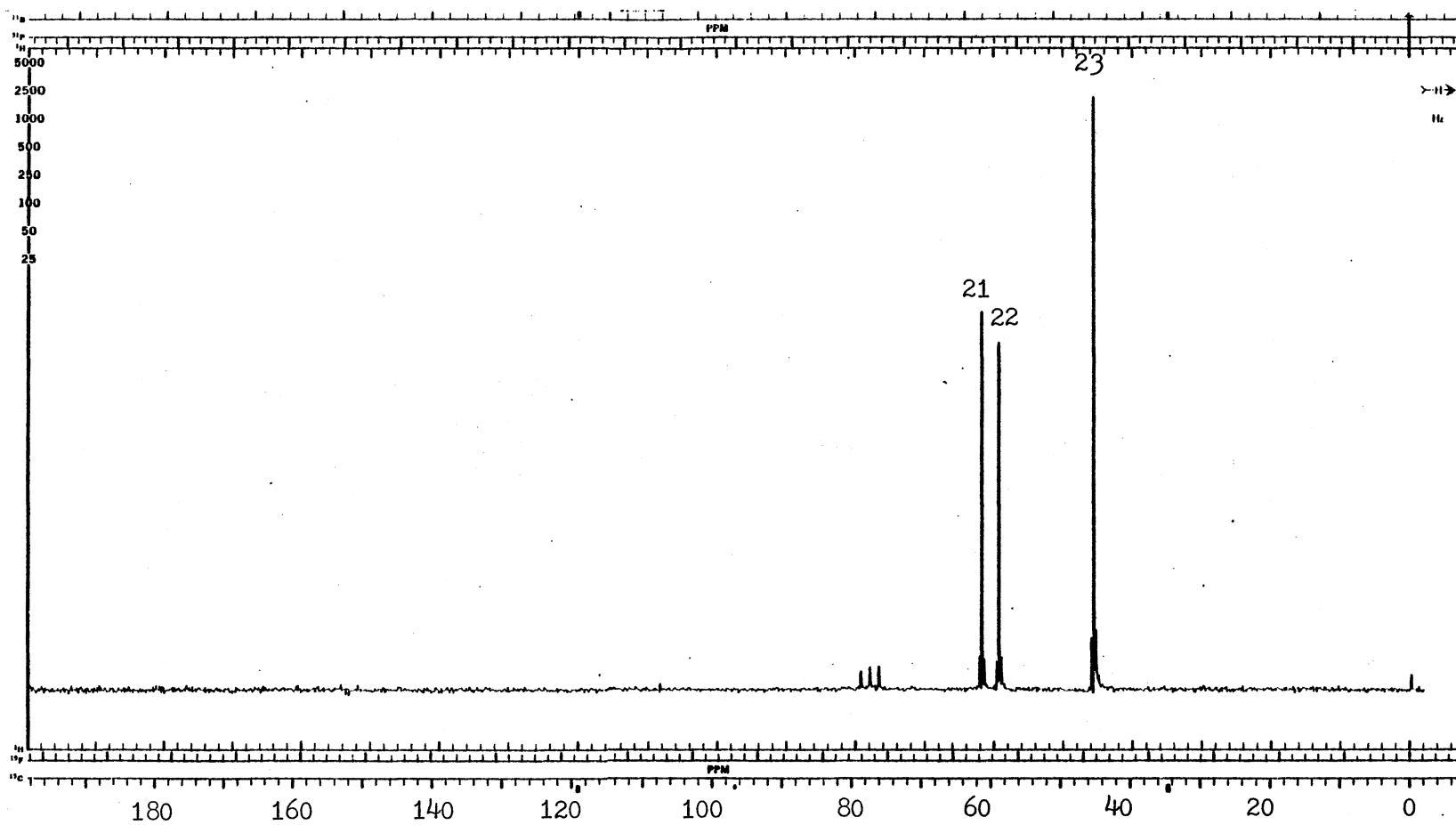
Figure 35. ^{13}C-NMR Spectrum of DIPA-COS Reaction Products in $DCCl_3$ (10 % Sample)
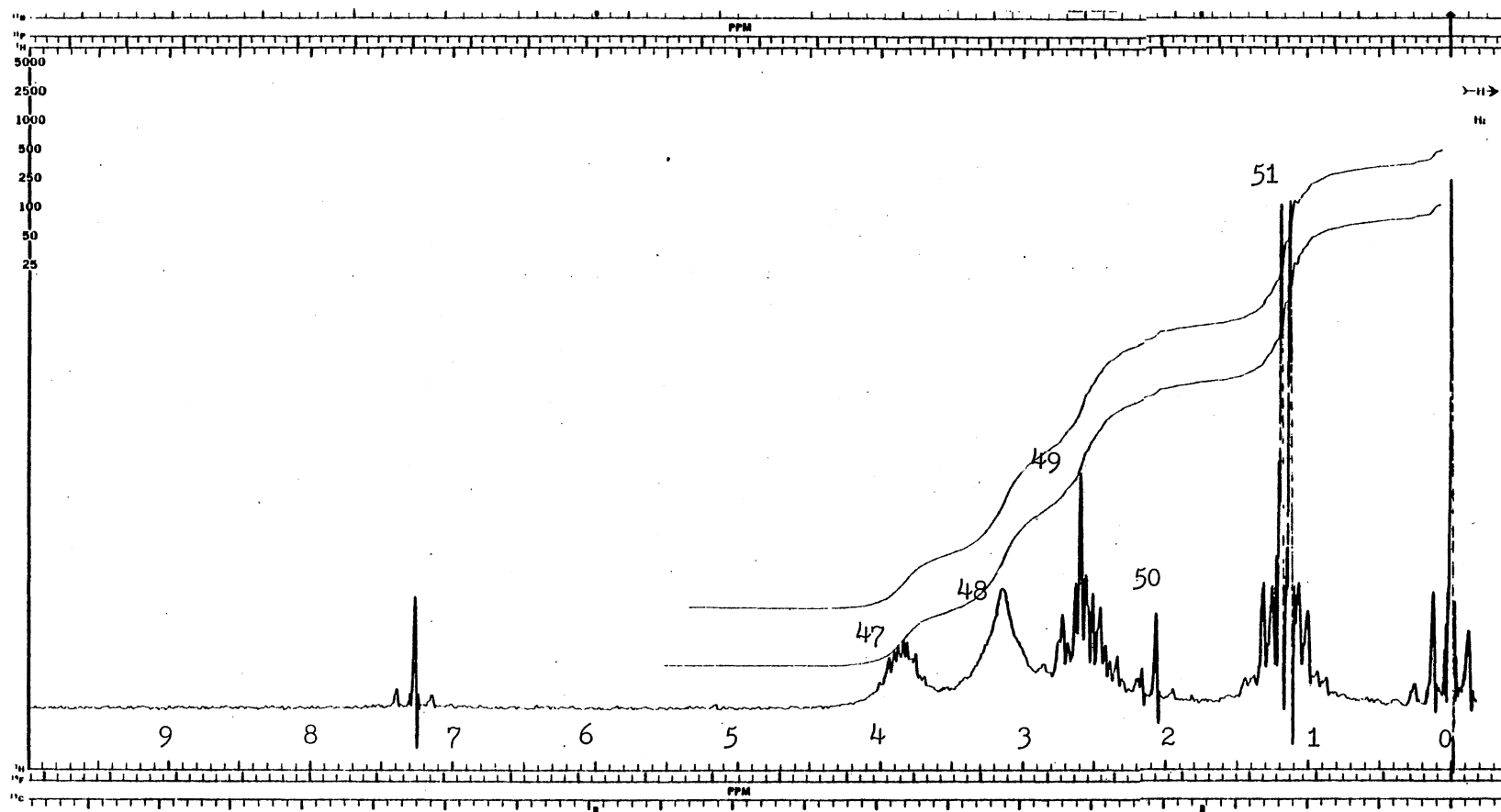
Figure 36. ^{1}H-NMR Spectrum of DIPA-CH$_3$SH Absorption System in DCCl$_3$ (10 % Sample)
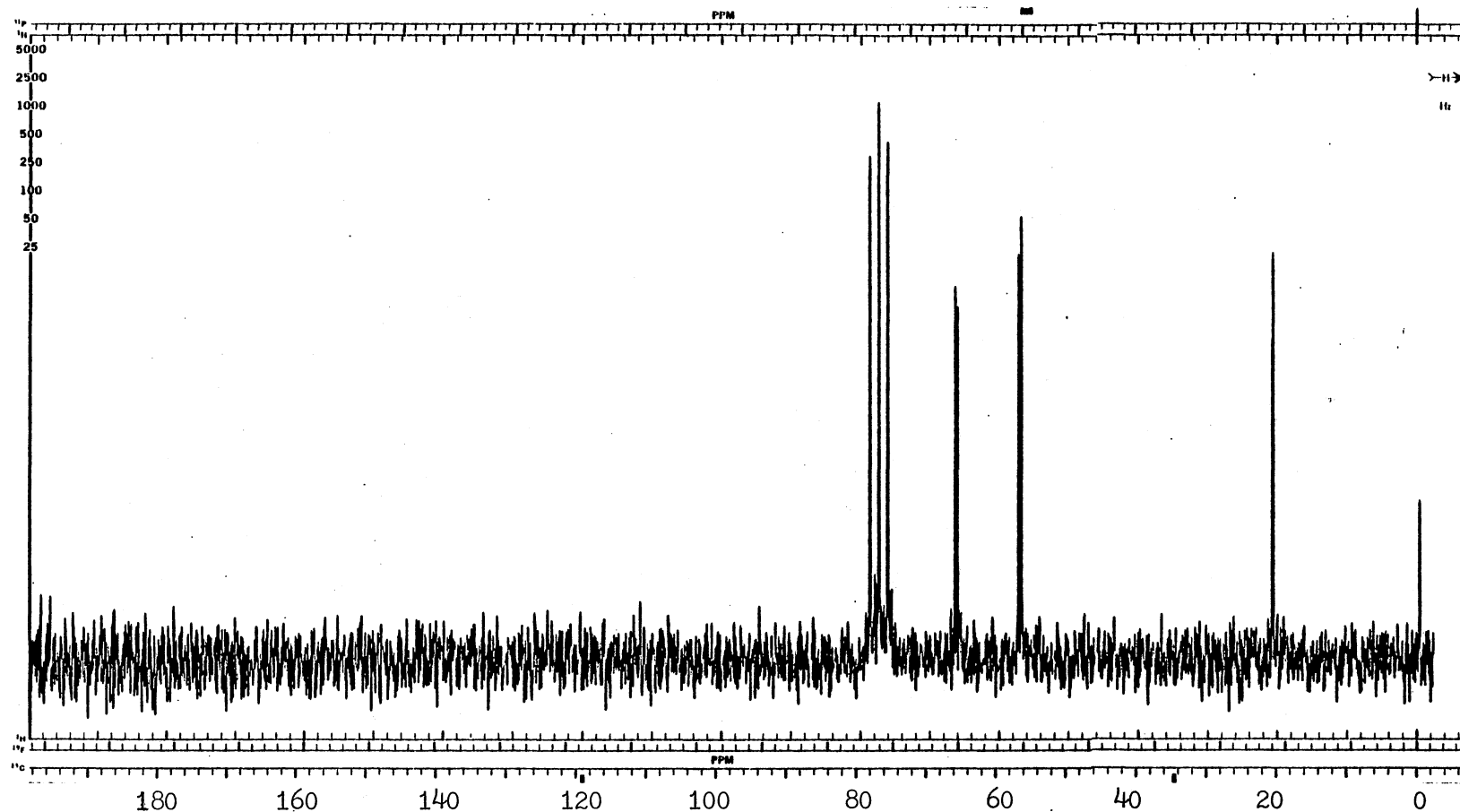
Figure 37. ^{13}C-NMR Spectrum of DIPA-CH$_3$SH Absorption System in DCCl$_3$ (10 % Sample)

Figure 38. ^{1}H-NMR Spectrum of Pure MDEA in $DCCl_3$ (20 % Sample)
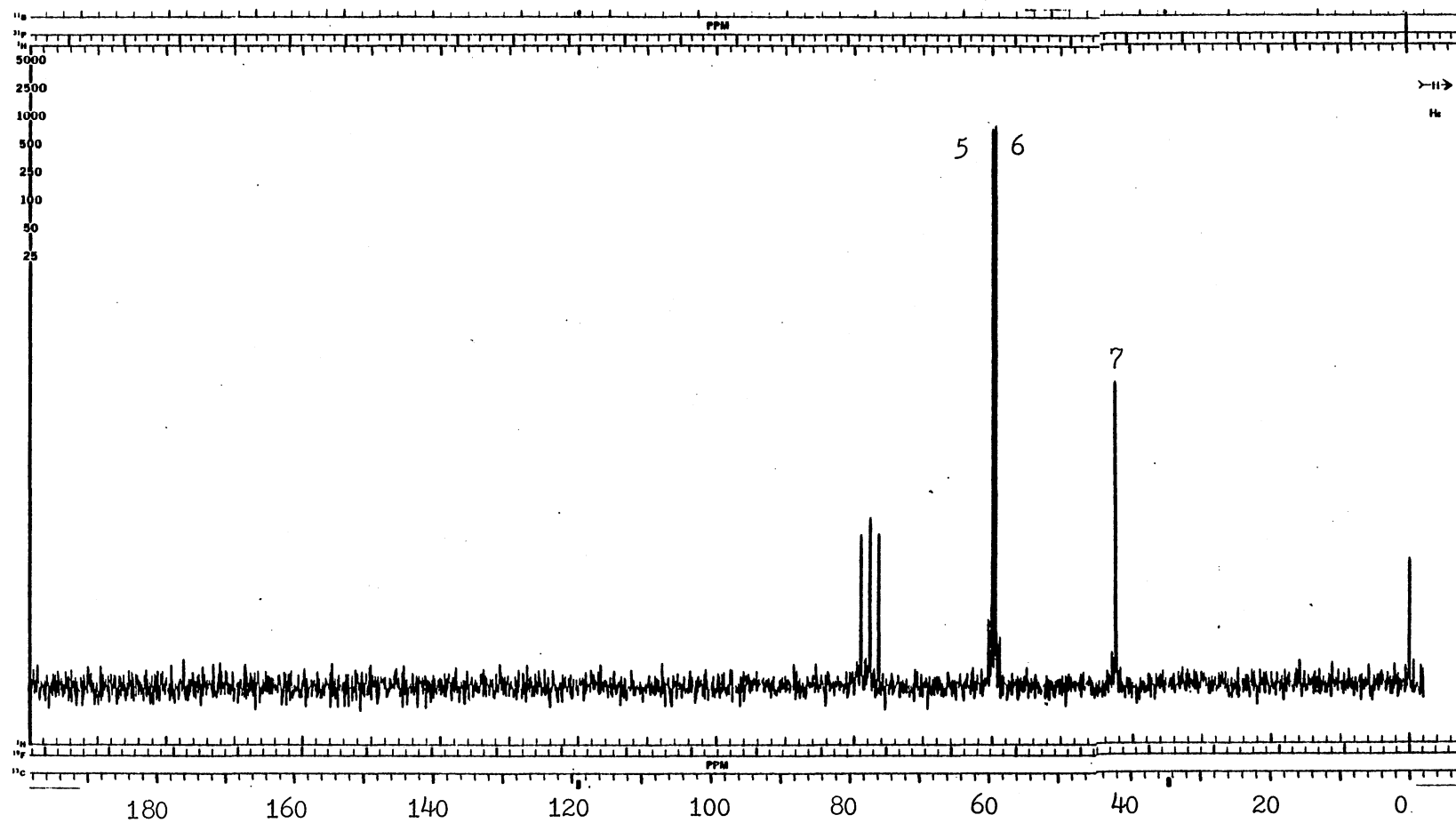
Figure 39. ^{13}C-NMR Spectrum of Pure MDEA in DCCl$_3$ (20 % Sample)

Figure 40. ^{1}H-NMR Spectrum of MDEA-CH$_3$SH Absorption System in DCCl$_3$ (20 % Sample)
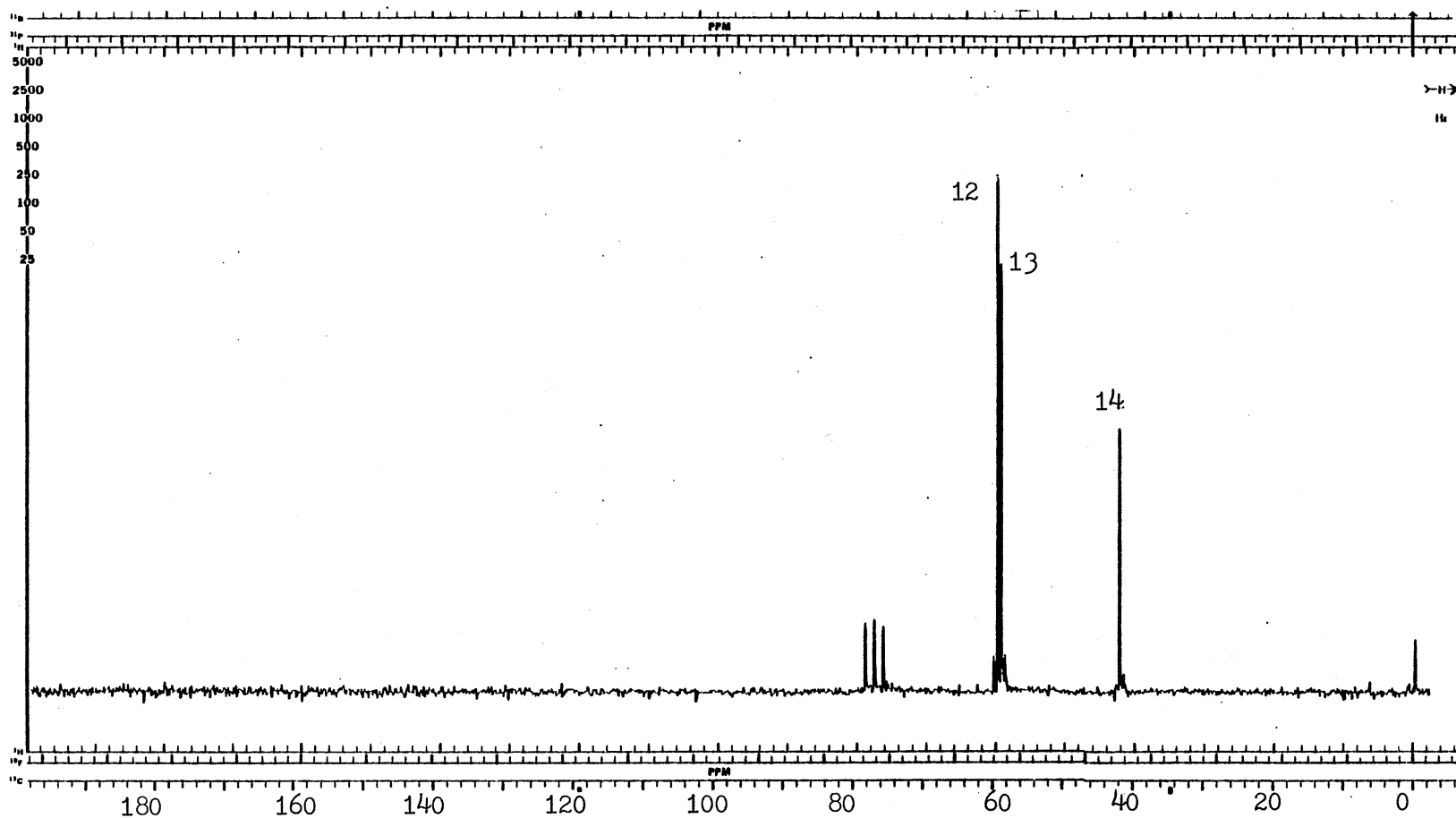
Figure 41. ^{13}C-NMR Spectrum of MDEA-CH$_3$SH Absorption System in DCCl$_3$ (20 % Sample)
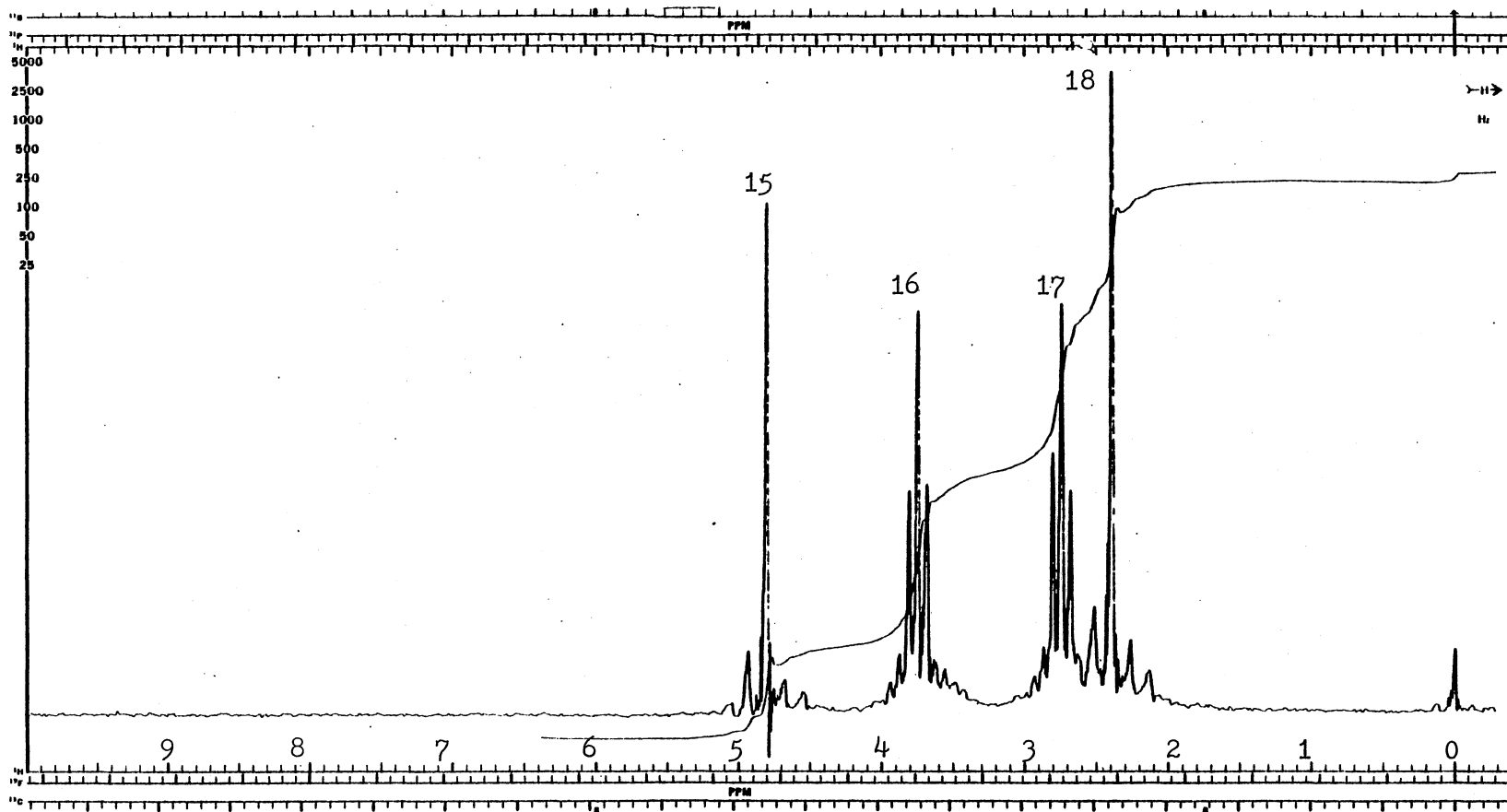
Figure 42. ^{1}H-NMR Spectrum of MDEA-CO$_2$ Reaction Products in D$_2$O (20 % Sample)
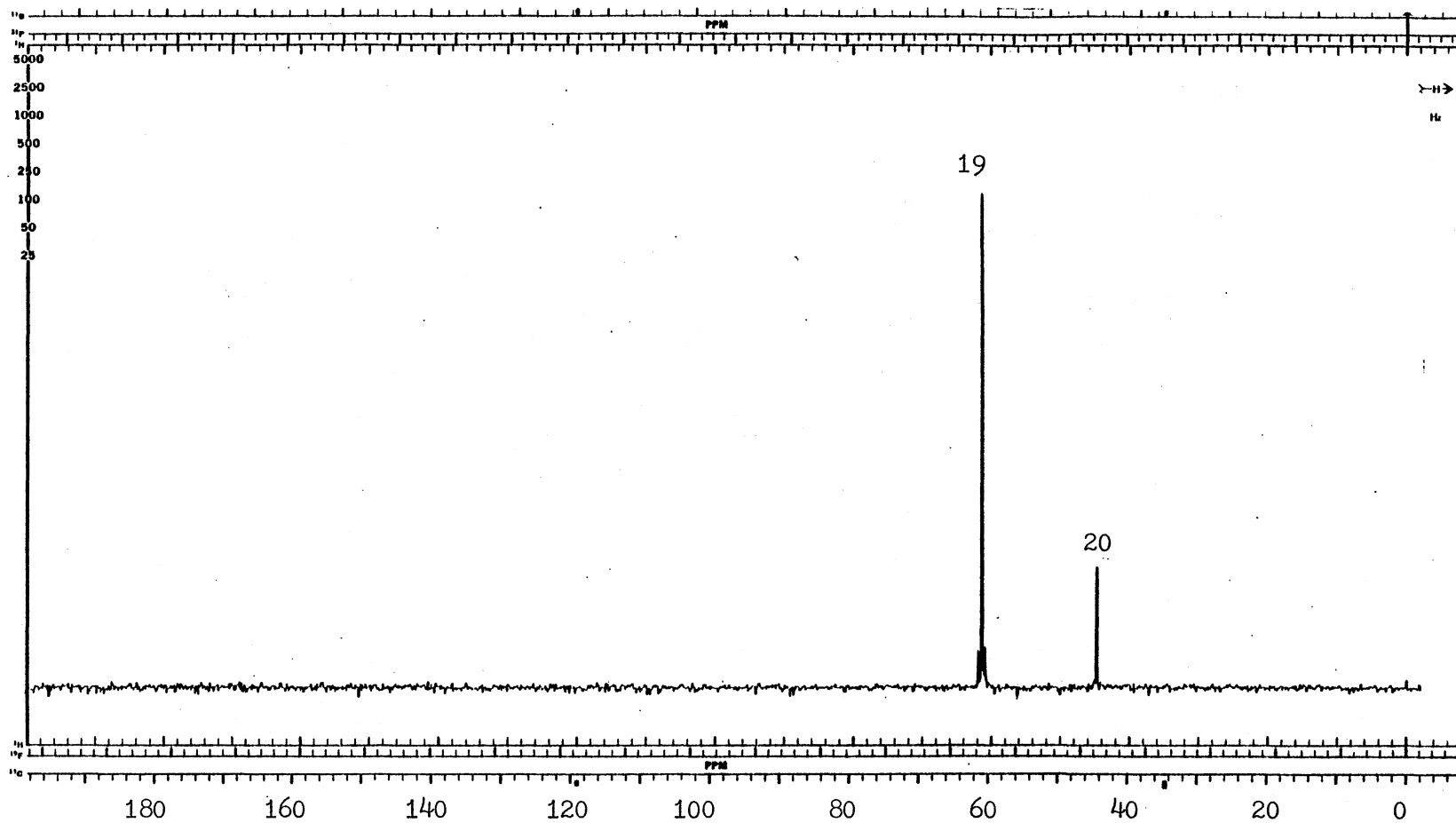
Figure 43. ^{13}C-NMR Spectrum of MDEA-CO_2 Reaction Products in D_2O (20 % Sample)

Figure 44. ^{1}H-NMR Spectrum of MDEA-COS Reaction Products in D_2O (20 % Sample)

Figure 45. ^{13}C-NMR Spectrum of MDEA-COS Reaction Products in D_2O (20 % Sample)
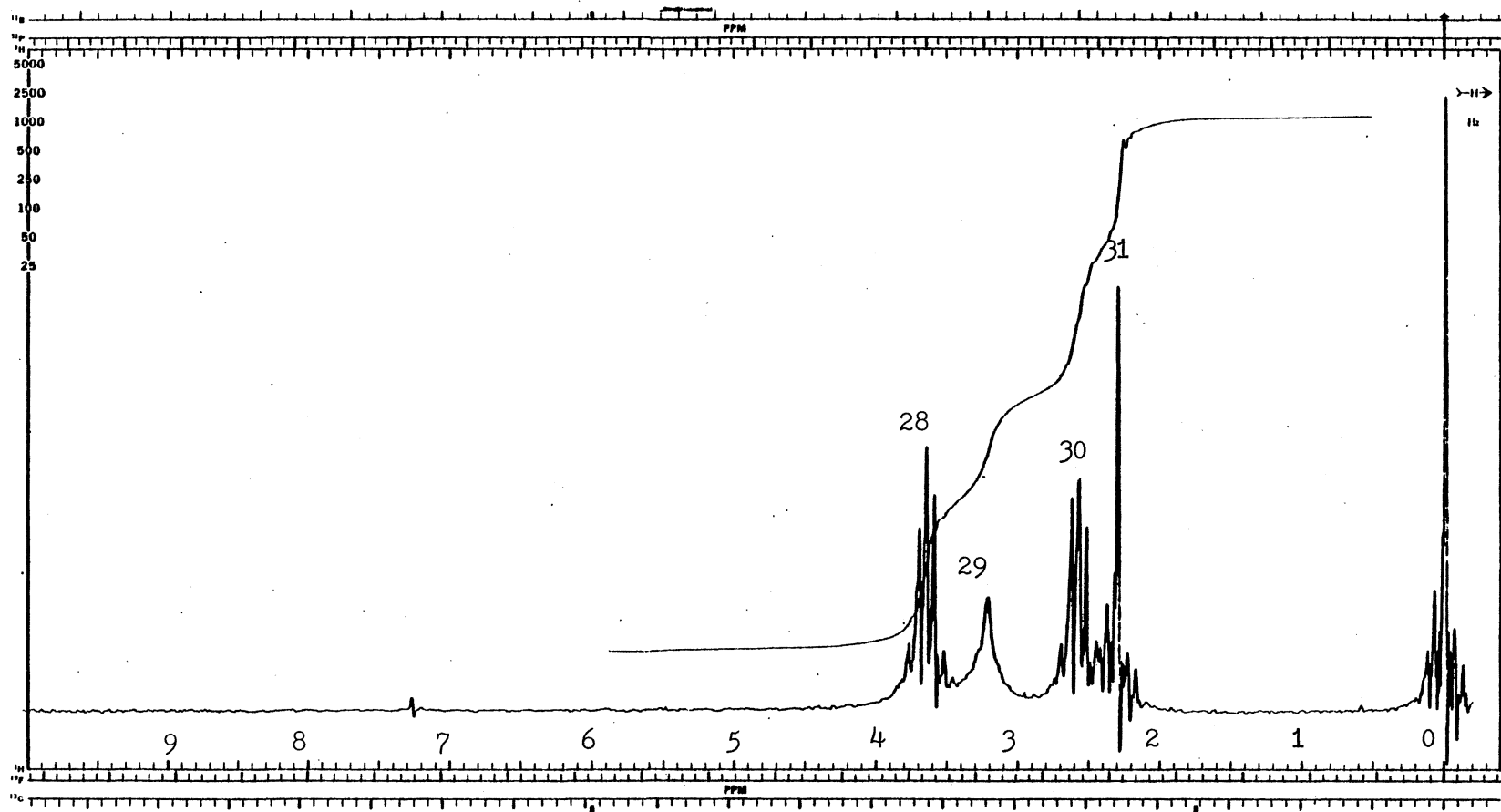
Figure 46. ^{1}H-NMR Spectrum of MDEA-H_2S Reaction Products in DCCl$_3$ (20 % Sample)

Figure 47. ^{1}H-NMR Spectrum of Pure MDEA in D_2O (20 % Sample)

Figure 48. ^{1}H-NMR Spectrum of Pure DMEA in DCCl$_3$ (20 % Sample)

Figure 49. ^{1}H-NMR Spectrum of Pure DMEA in D_2O (20 % Sample)

Figure 50. ^{13}C-NMR Spectrum of Pure DMEA in DCCl$_3$ (20 % Sample)

Figure 51. ^{13}C-NMR Spectrum of Pure DMEA in D_2O (40 % Sample)
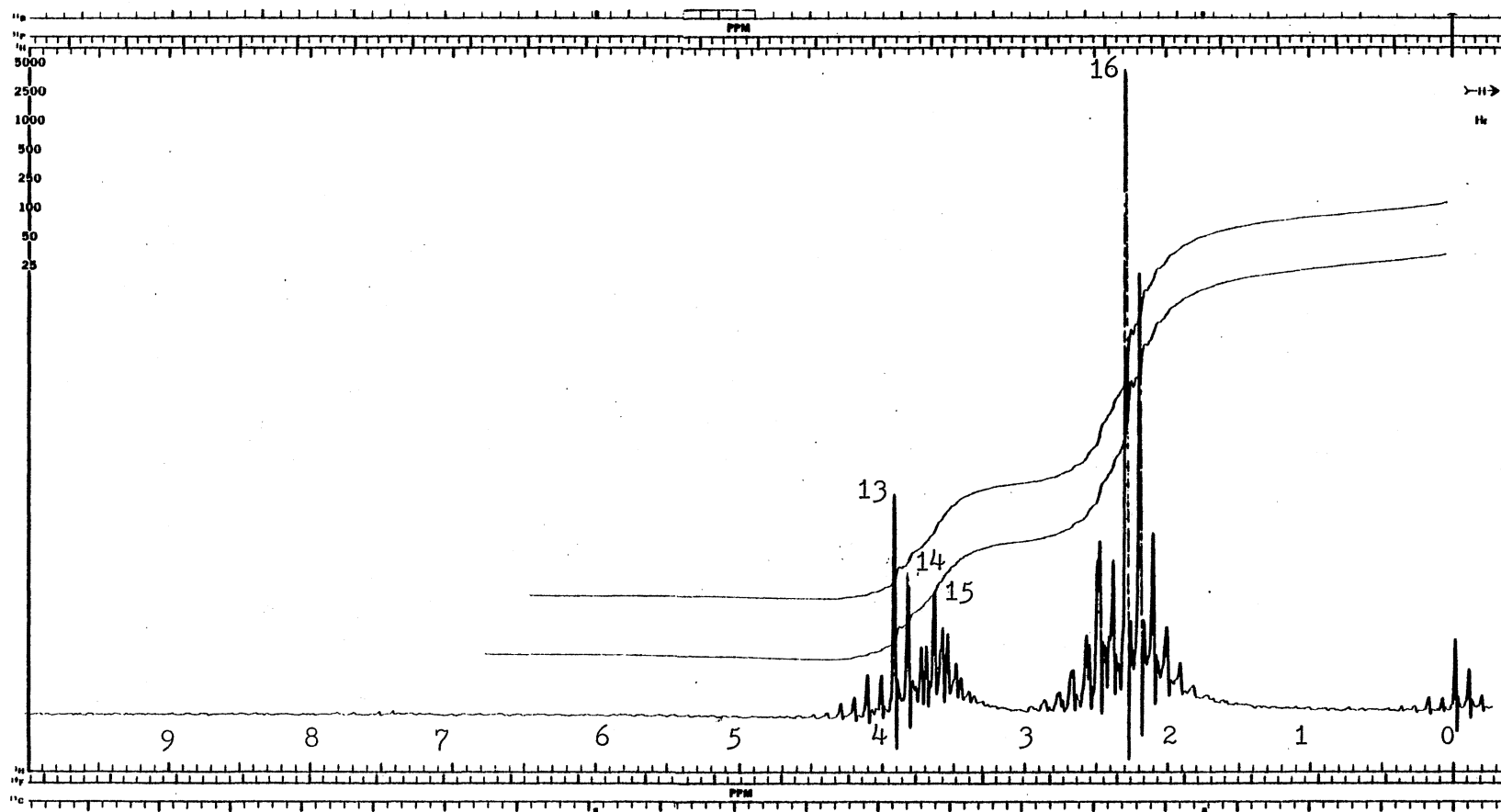
Figure 52. ^{1}H-NMR Spectrum of DMEA-H$_2$S Reaction Products in DCCl$_3$ (20 % Sample)

Figure 53. ^{1}H-NMR Spectrum of DMEA-CO_2 Reaction Products in D_2O (20 % Sample)

Figure 54. ^{13}C-NMR Spectrum of DMEA-CO$_2$ Reaction Products in DCCl$_3$ (20 % Sample)

Figure 55. ^{1}H-NMR Spectrum of DMEA-COS Reaction Products in D_2O (20 % Sample)

Figure 56. ^{13}C-NMR Spectrum of DMEA-COS Reaction Products in DCCl$_3$ (20 % Sample)
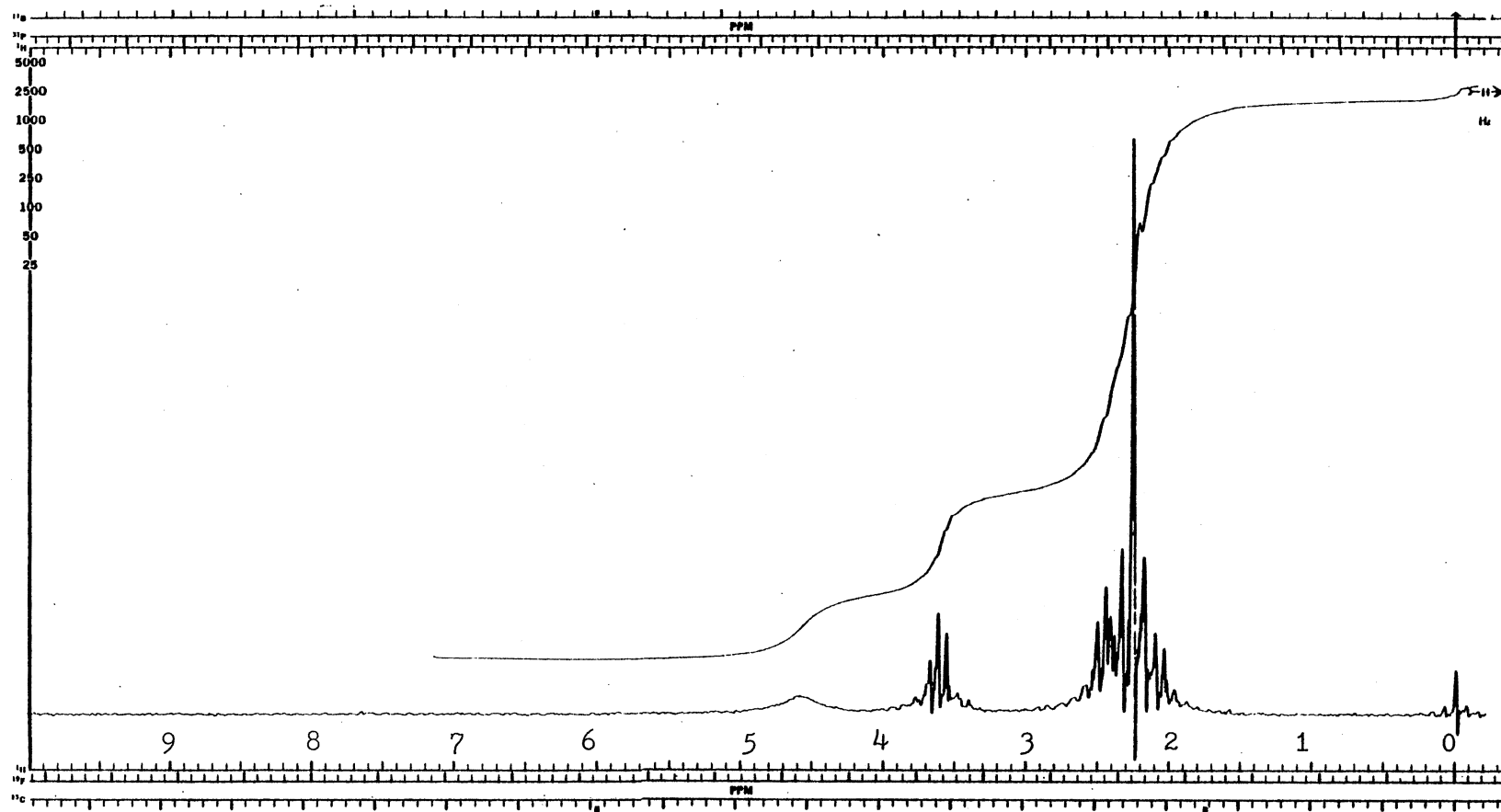
Figure 57. ^{1}H-NMR Spectrum of DMEA-CH$_3$SH Absorption System in DCCl$_3$ (20 % Sample)
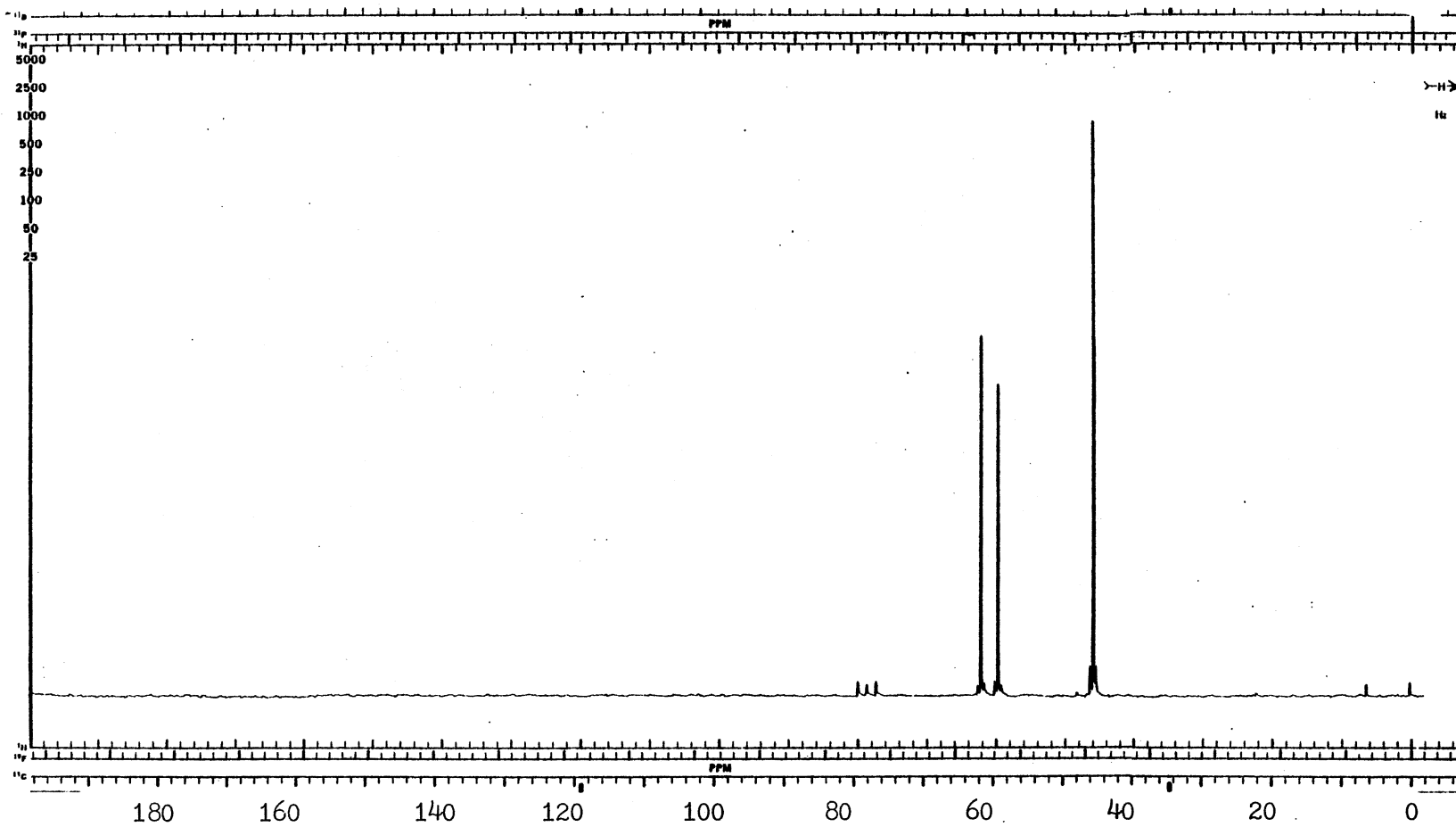
Figure 58. ^{13}C-NMR Spectrum of DMEA-CH$_3$SH Absorption System in DCCl$_3$ (20 % Sample)
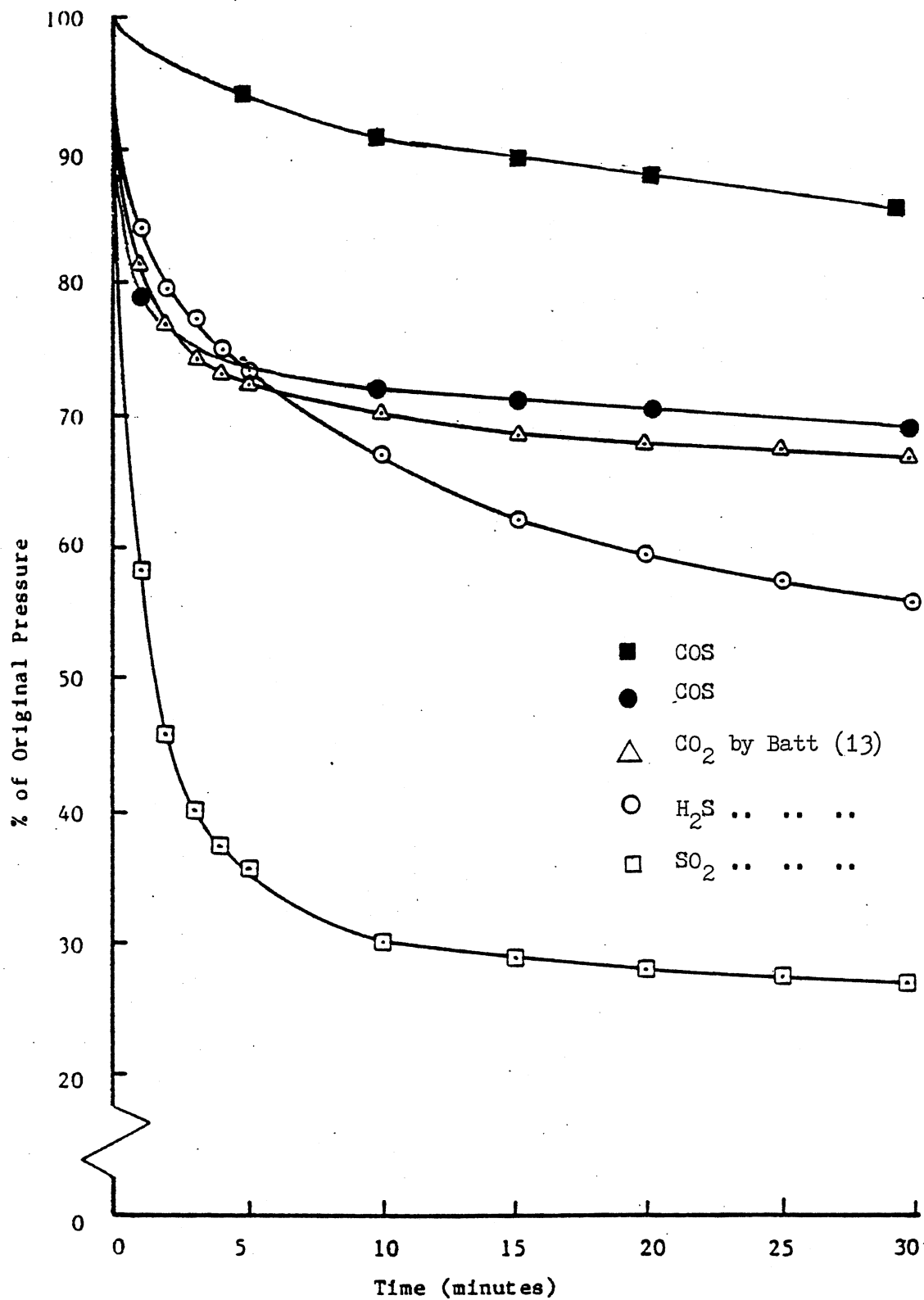
Figure 59. Experimental Results for COS and CH₃SH Reactions With MEA
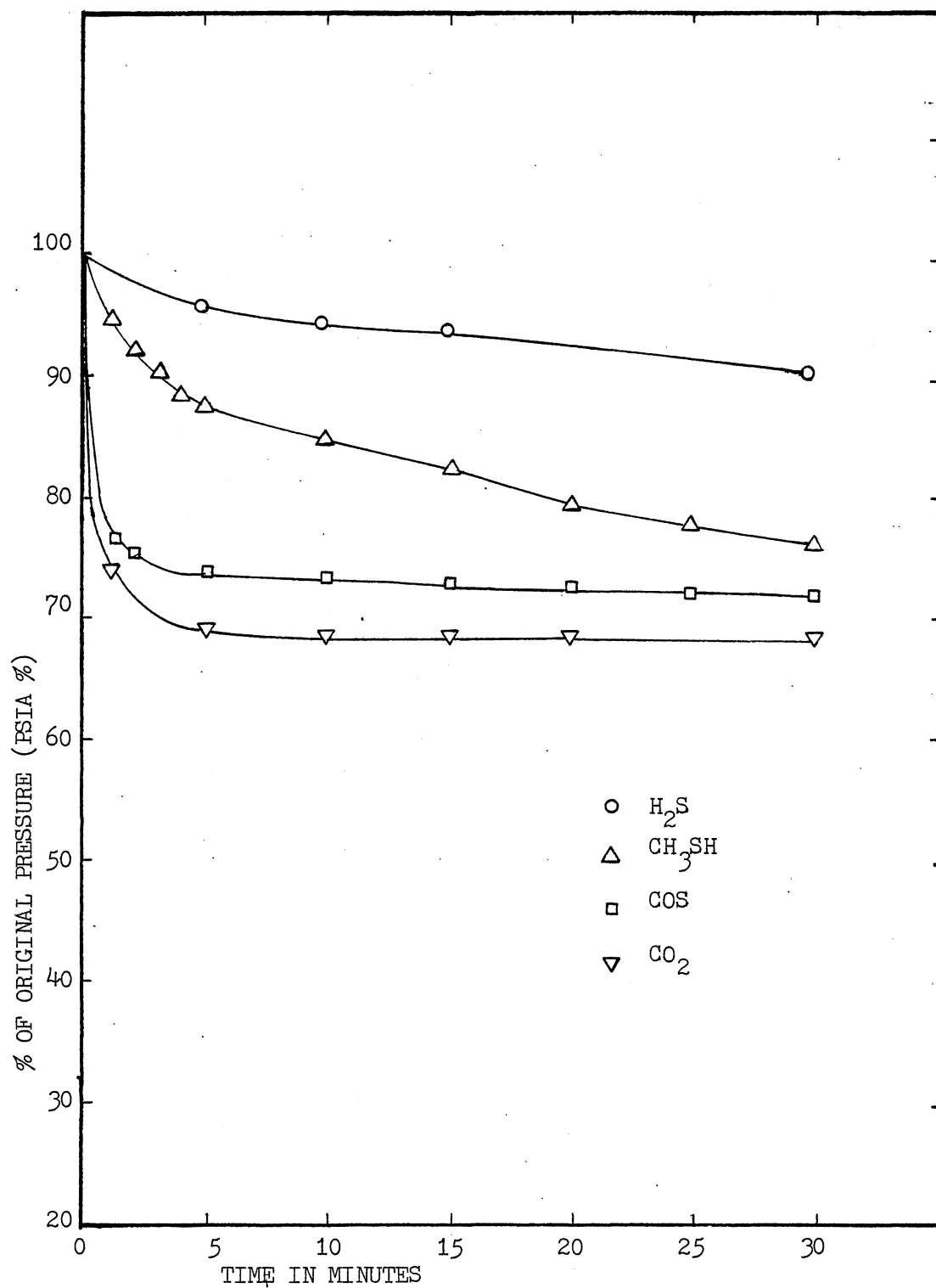
Figure 60. Experimental Results for Acidic Gases Reaction With DGA
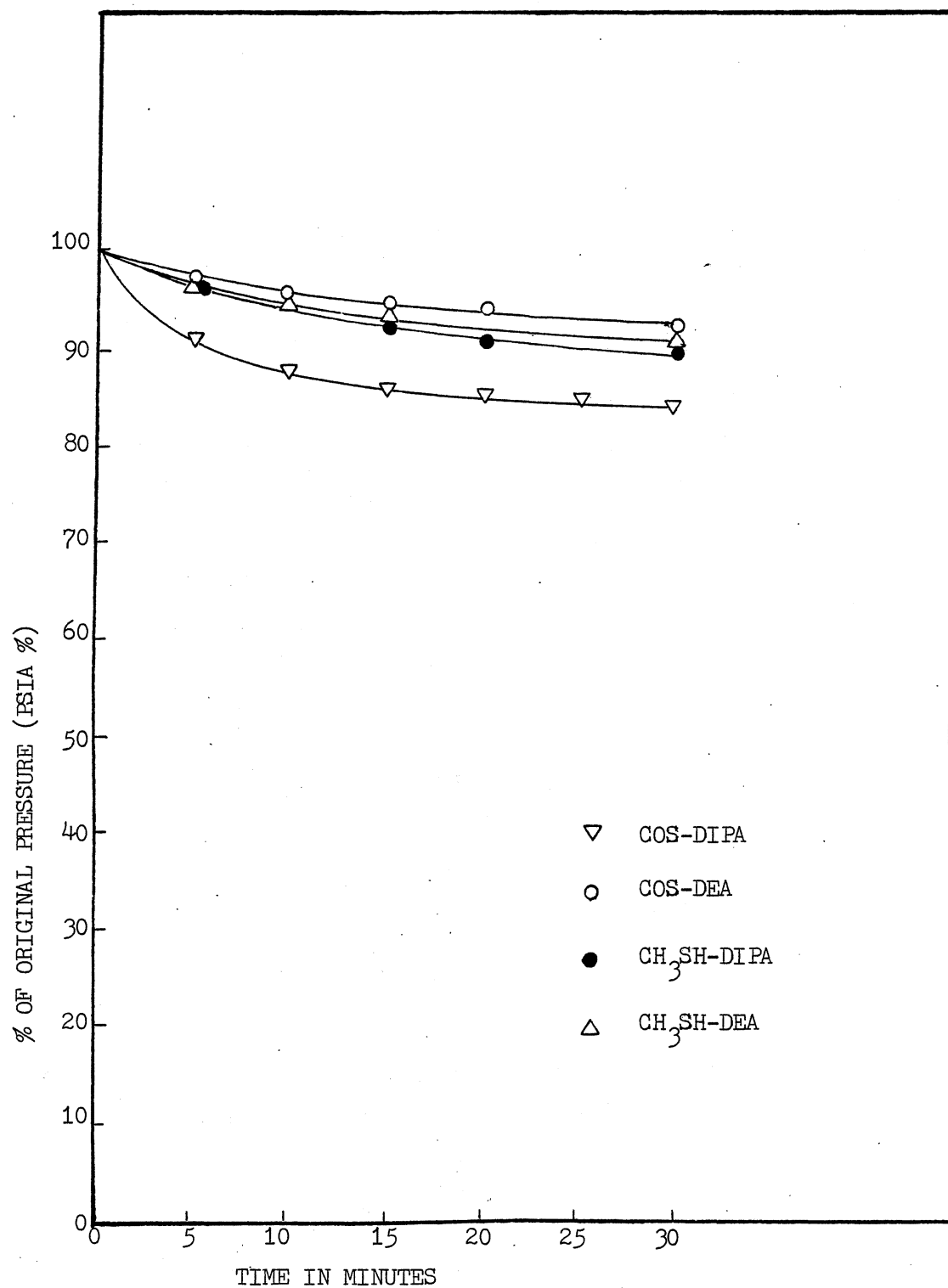
Figure 61. Experimental Results for Acidic Gases Reaction With
Secondary Amines
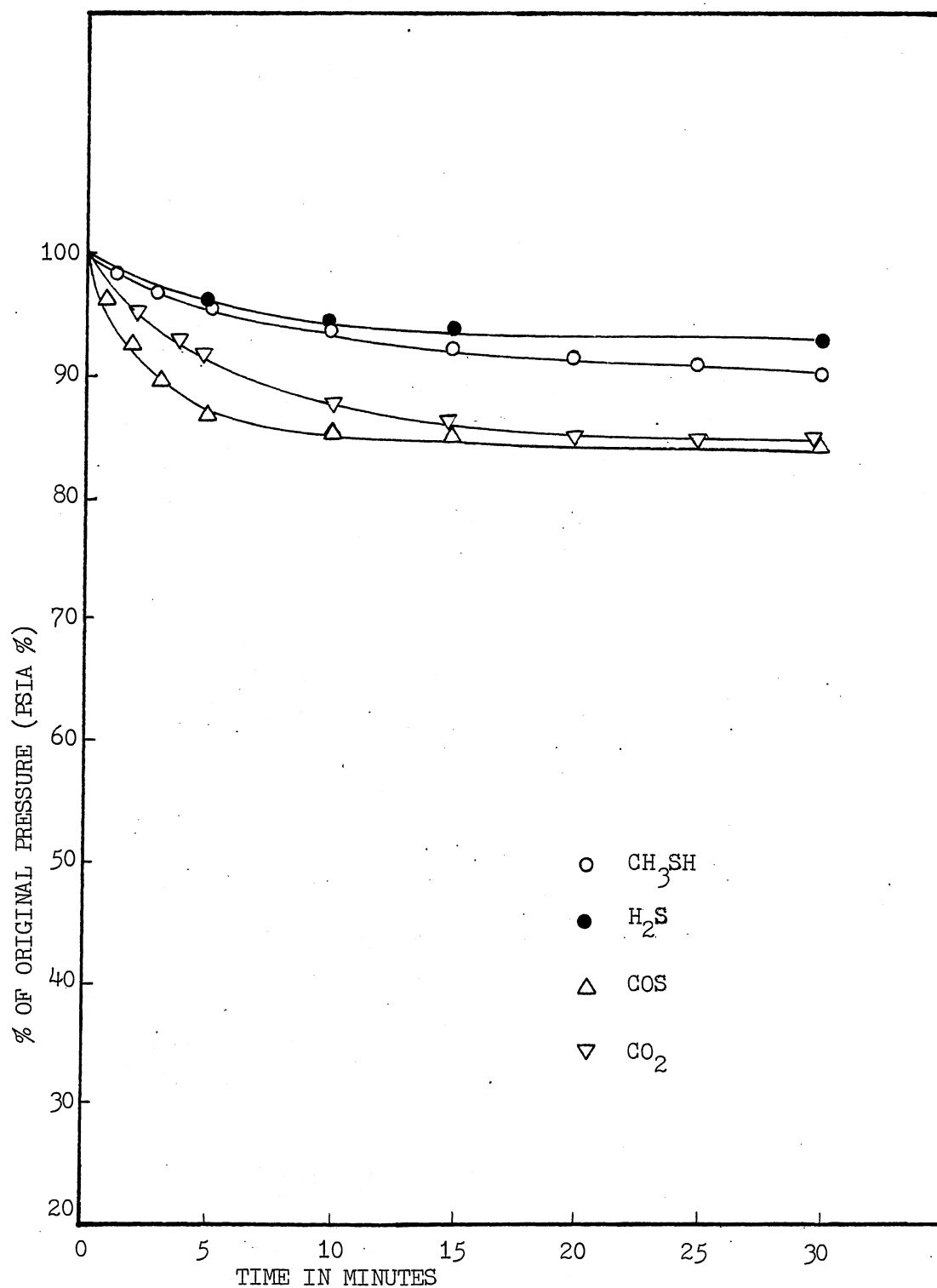
Figure 62. Experimental Results for Acidic Gases Reactions With DIPA
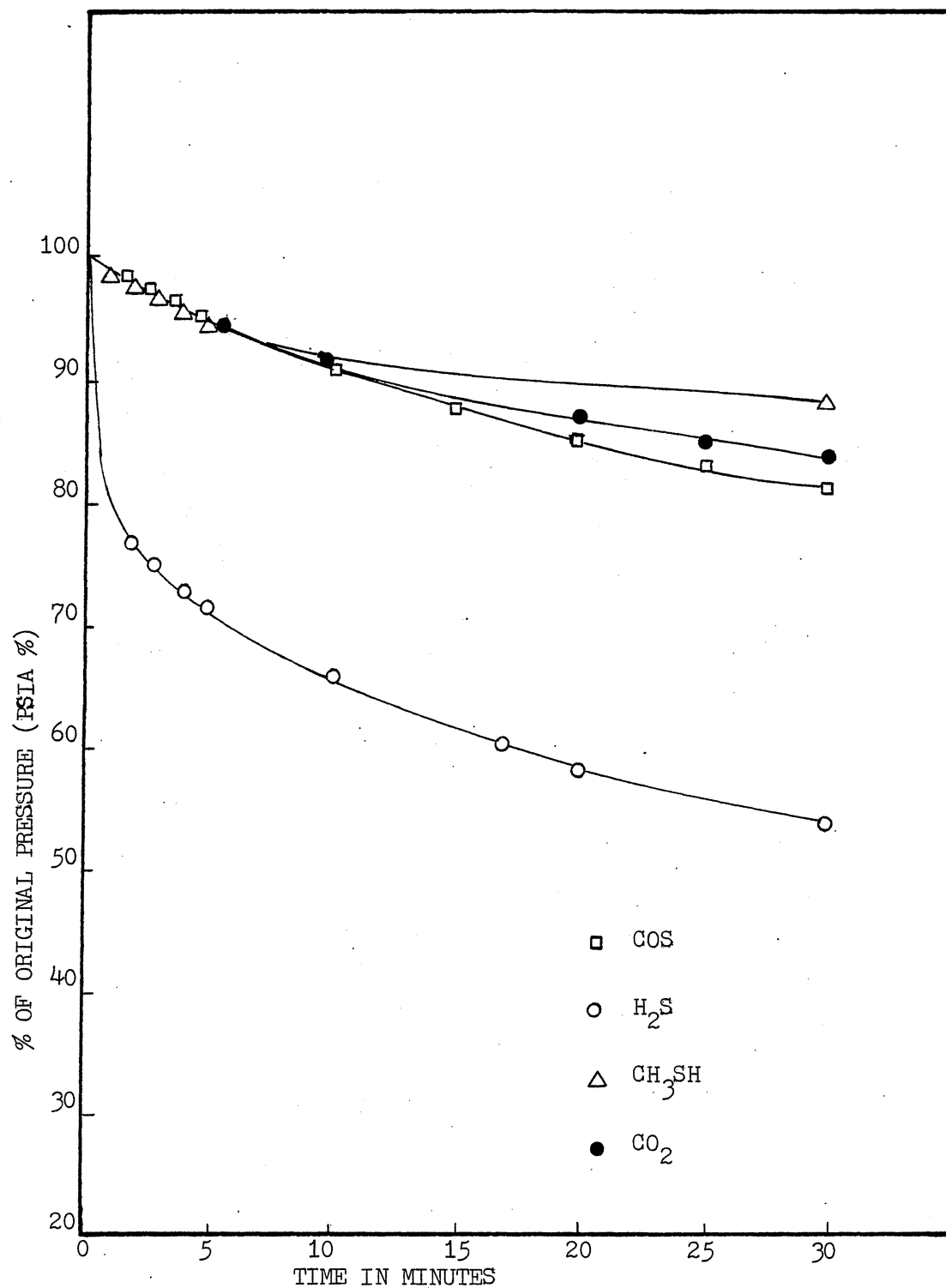
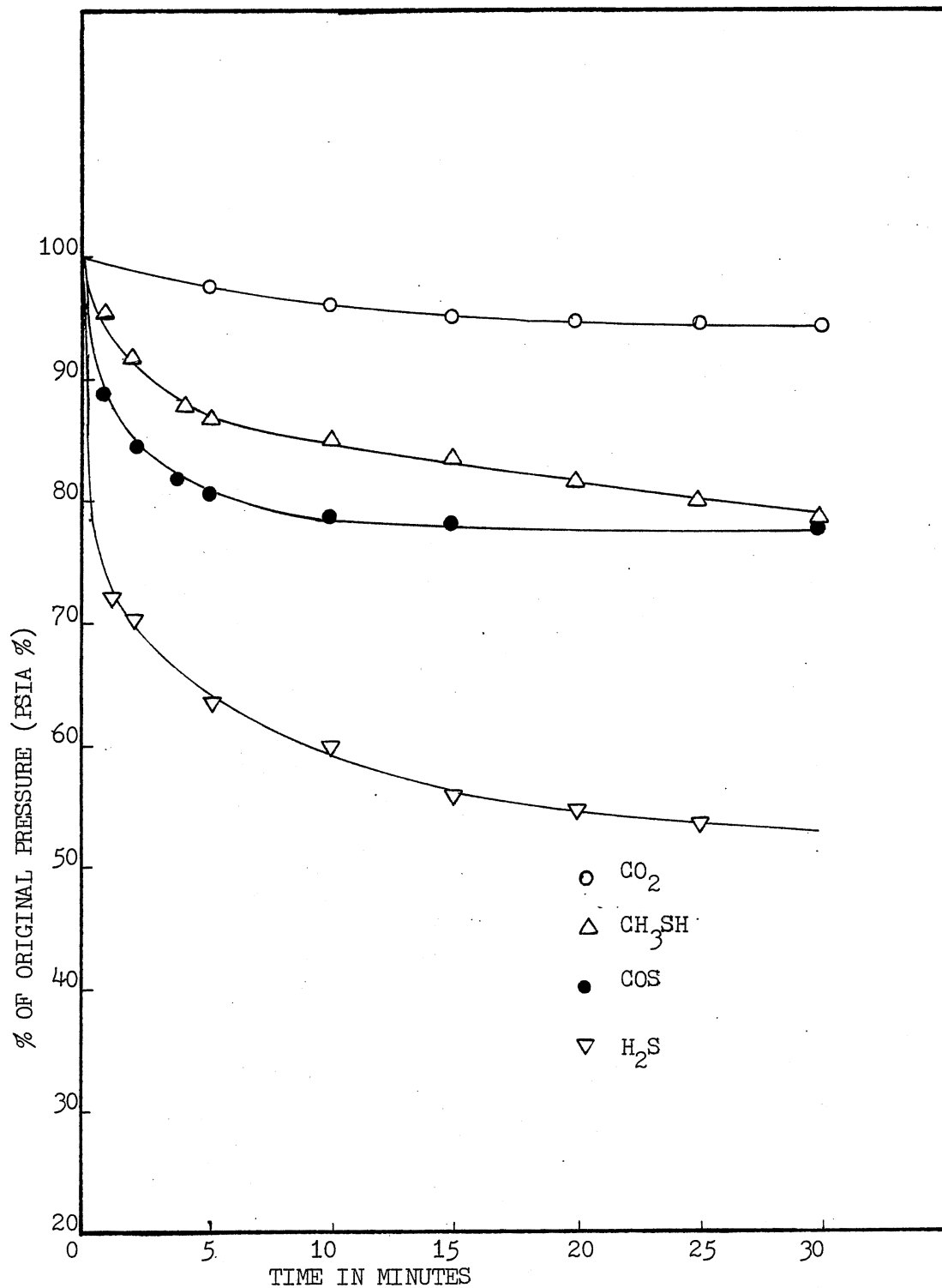Figure 63. Experimental Results for Acidic Gases Reactions With MDEA

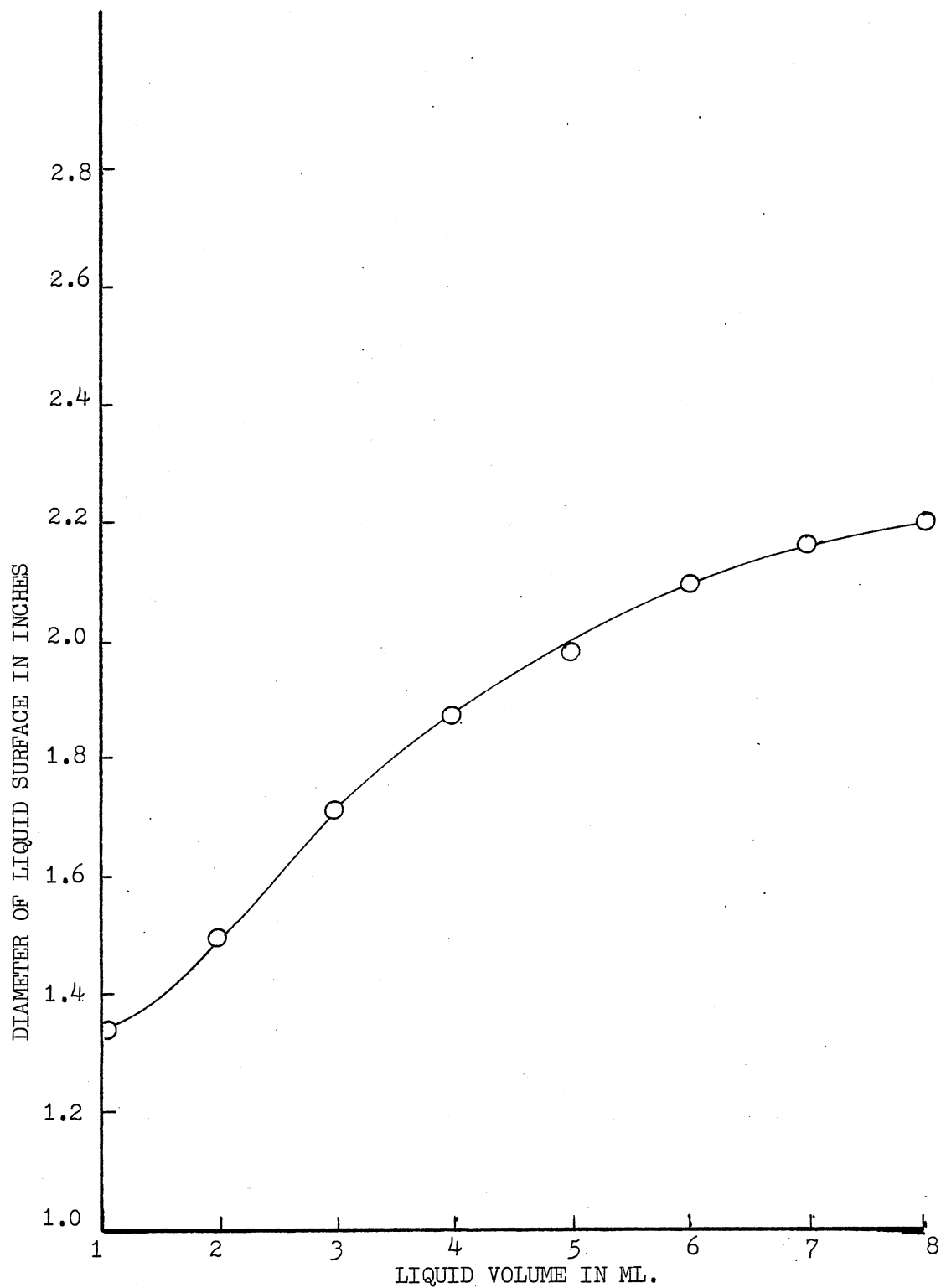Figure 64. Experimental Results for Acidic Gases Reaction With DMEA

Figure 65. Relation of Diameter of Liquid Surface to Liquid Volume

APPENDIX C

SAMPLE CALCULATION

CO2-DMEA System

Moles of CO_2 charged are determined as follows:

$$T_r = \frac{T}{T_c} = \frac{75 + 459.67 \ R}{547.57 \ R} = 0.976$$

$$P_r = \frac{P}{P_c} = \frac{34.696 \ psia}{1071 \ psia} = 0.0324$$

$$Z(T_r, P_r) = 0.985$$

$$n_{CO_2} = P \cdot V / (ZRT)$$

$$= \frac{(34.696 \ psia)(552.5 \ ml)(3.531467 \times 10^{-5} \ ft^3/ml)}{(0.985) \times 10.73 (psia \ ft^3/lb \ mol. \ R)(75 + 459.67 \ R)}$$

$$= 1.1969 \times 10^{-4} \ lb \ mole$$

$$P_{DMEA} = 0.887 \ gm/ml.$$

$$V_{DMEA} = \frac{(1.1969 \times 10^{-4}) \times (89.14) \times (453.59)}{0.887} = 5.46 \ ml.$$

APPENDIX D

REACTION BETWEEN CARBONYL SULFIDE

AND MONOETHANOLAMINE

The reaction between MEA and COS yielded a green colored product. The solid was separated from the liquid mass using a centrifuge. Visible, ultra-violet and infrared spectroscopy was employed to determine the molecular structure of the solid and liquid product mixture.

Deutero-chloroform, deuterium oxide, and deutero-acetone solvents did not dissolve the solid phase significantly; hence they could not be used as internal NMR solvents. The solid product was found to be miscible in carbon tetrachloride (CCl_4) and use of an external D_2O locking arrangement rendered the sample amenable to NMR spectroscopic analysis.

Figure 66 presents a proton scan of spectroscopic grade CCl_4. Peak No. 1 is an impurity proton in CCl_4 solvent. External D_2O locking led to an absorption peak at position No. 2. Figures 67 and 68 are the proton spectra of the solid and the liquid product residue, respectively, dissolved in CCl_4 solvent. Peaks No. 3 and No. 7 are the nitrogen and hydroxyl protons which undergo exchange with D_2O. The two sets of triplets (No. 8 and No. 9) are β and α protons, respectively. Peaks No. 6 and No. 10 are the triplets of the protons bonded to the nitrogen atom.

Carbon-13 spectra of the solid and liquid residue did not reveal any information except for a CCl_4 peak. Apparently the solubility of the solid and the liquid phase in CCl_4 is low, such that the relatively insensitive ^{13}C-NMR spectroscopy does not yield any absorption peak even after 1000 transient scans of the sample.

Infrared spectroscopic analyses were carried out on pure MEA, the solid product phase, and the liquid residue dissolved in CCl_4. They are presented in Figures 69, 70, and 71, respectively. The pure MEA infrared scan (Figure 69) shows the assignment of various groups present in the MEA molecule. Primary amines generally show a broad band of peaks at
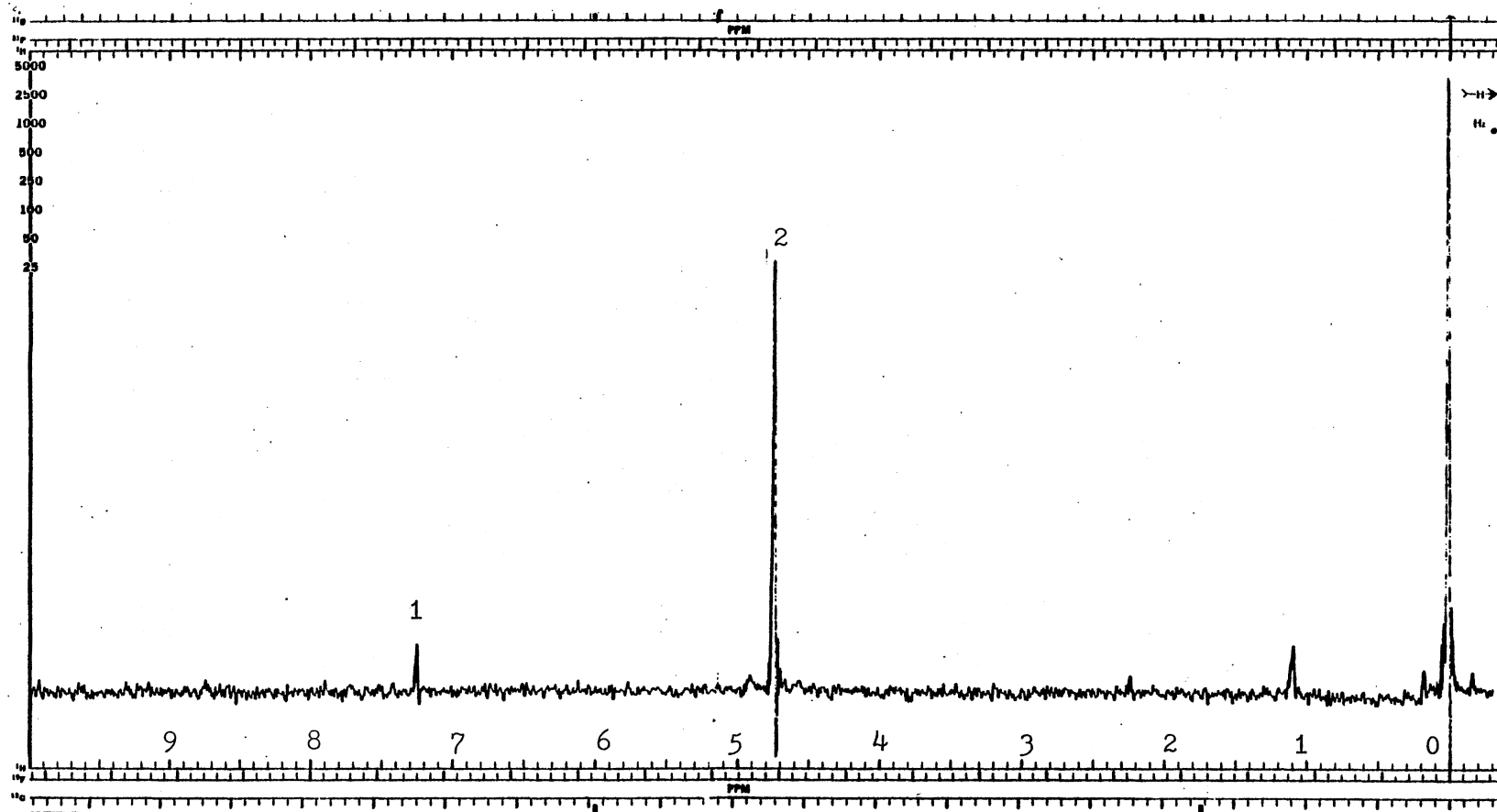
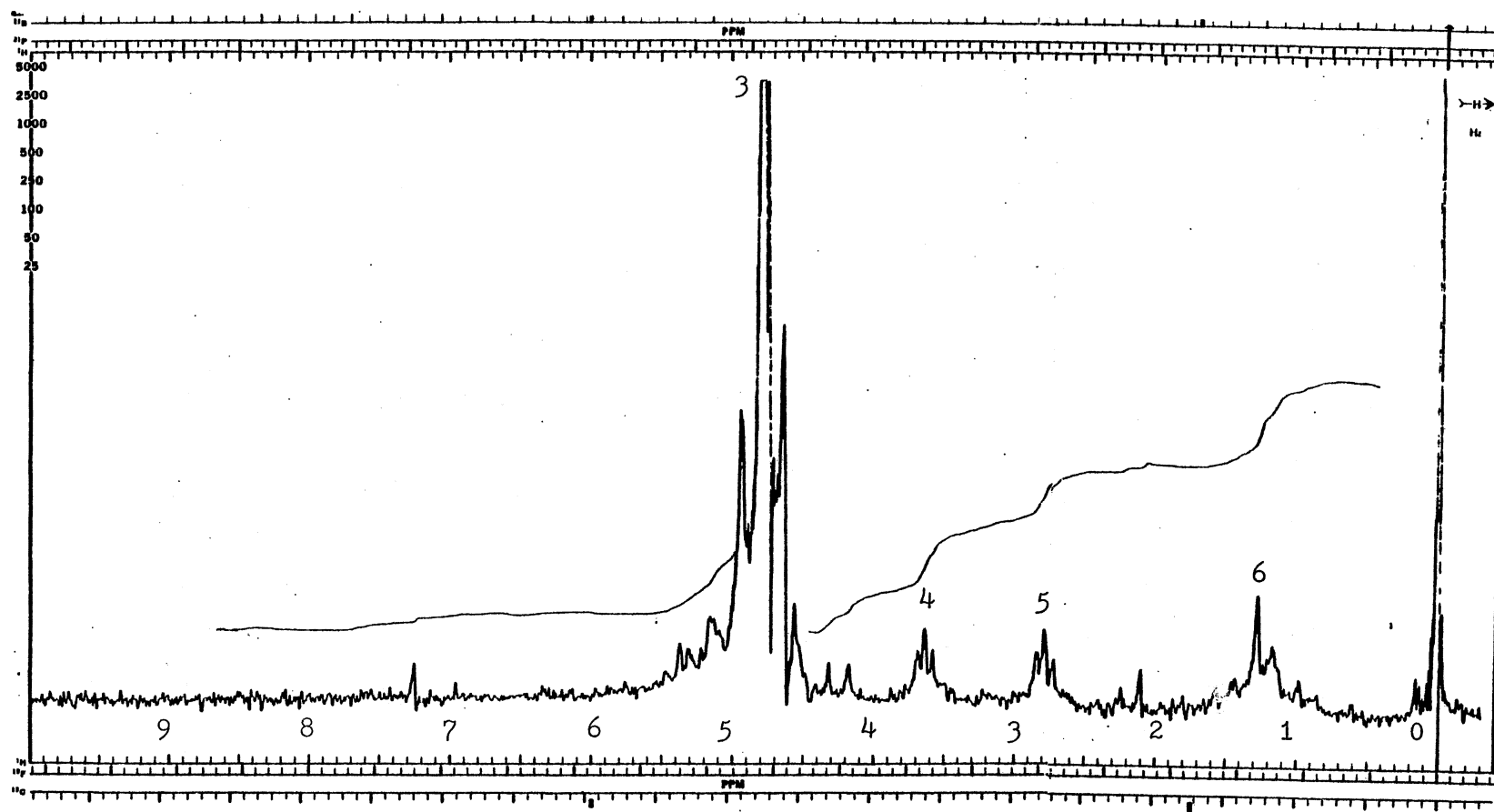Figure 66. ^{1}H-NMR Spectrum of Pure CCL$_4$ (External D$_2$O Lock)

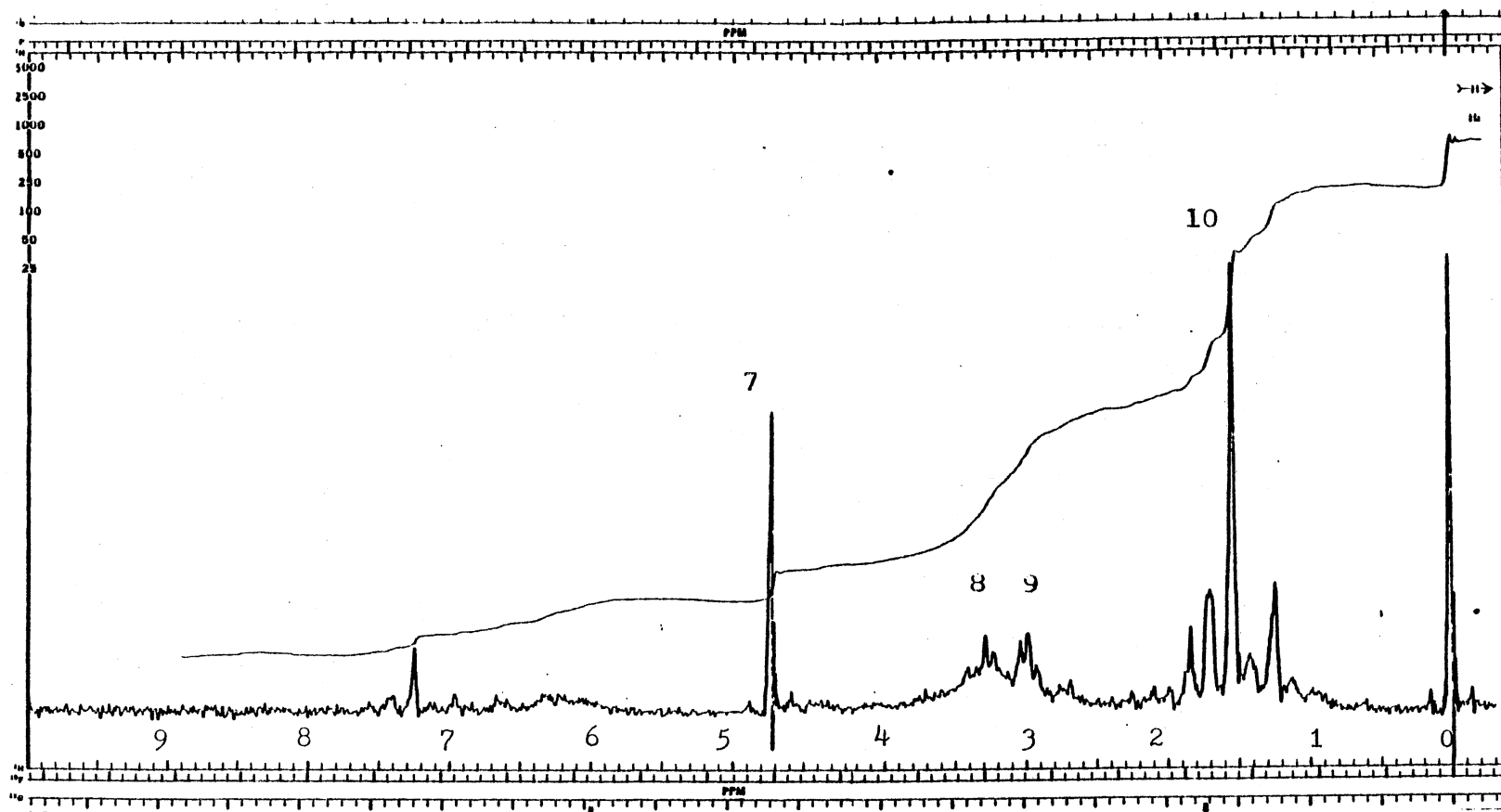Figure 67. ^{1}H-NMR Spectrum of Solid Product in CCl_4 (External D_2O Lock)

Figure 68. ^{1}H-NMR Spectrum of Liquid Residue in CCl_4 (External D_2O Lock)
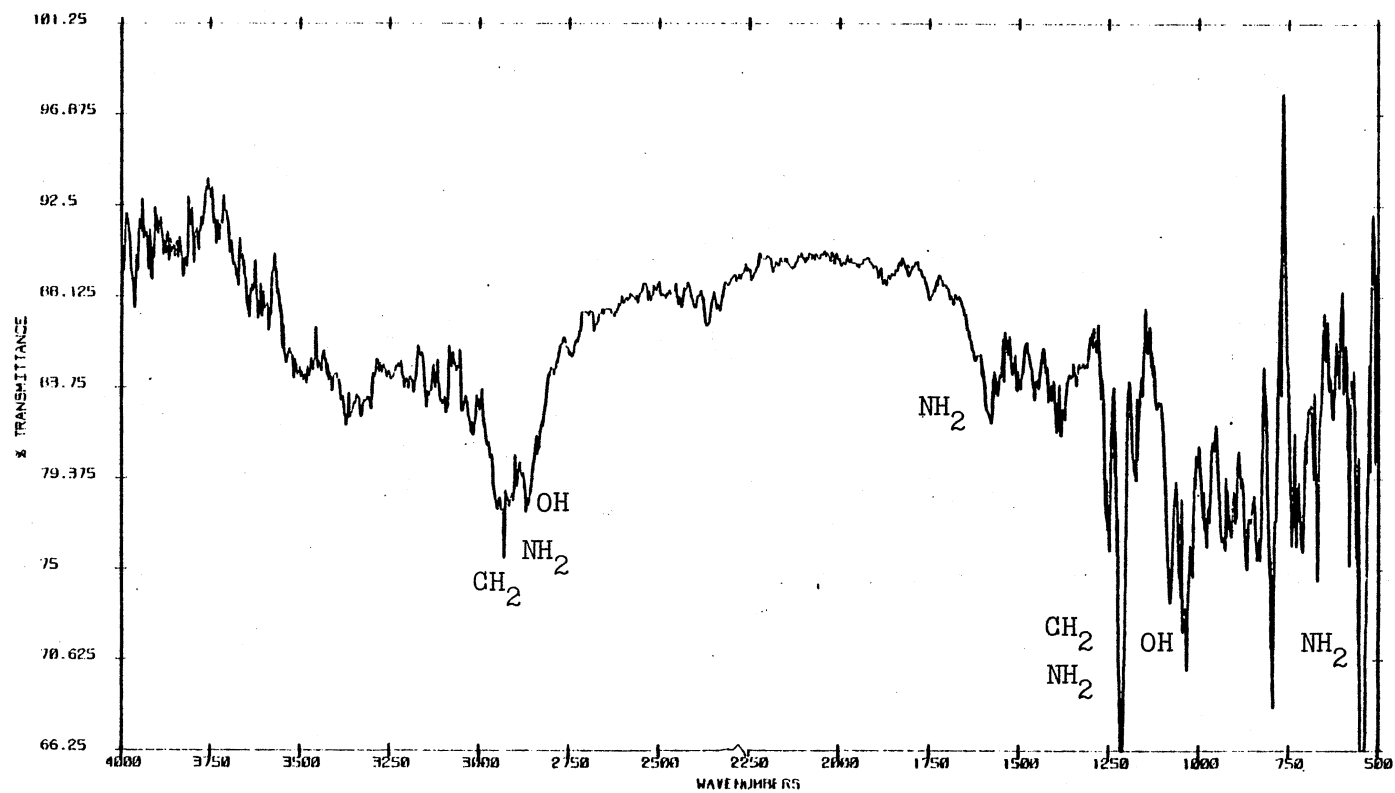
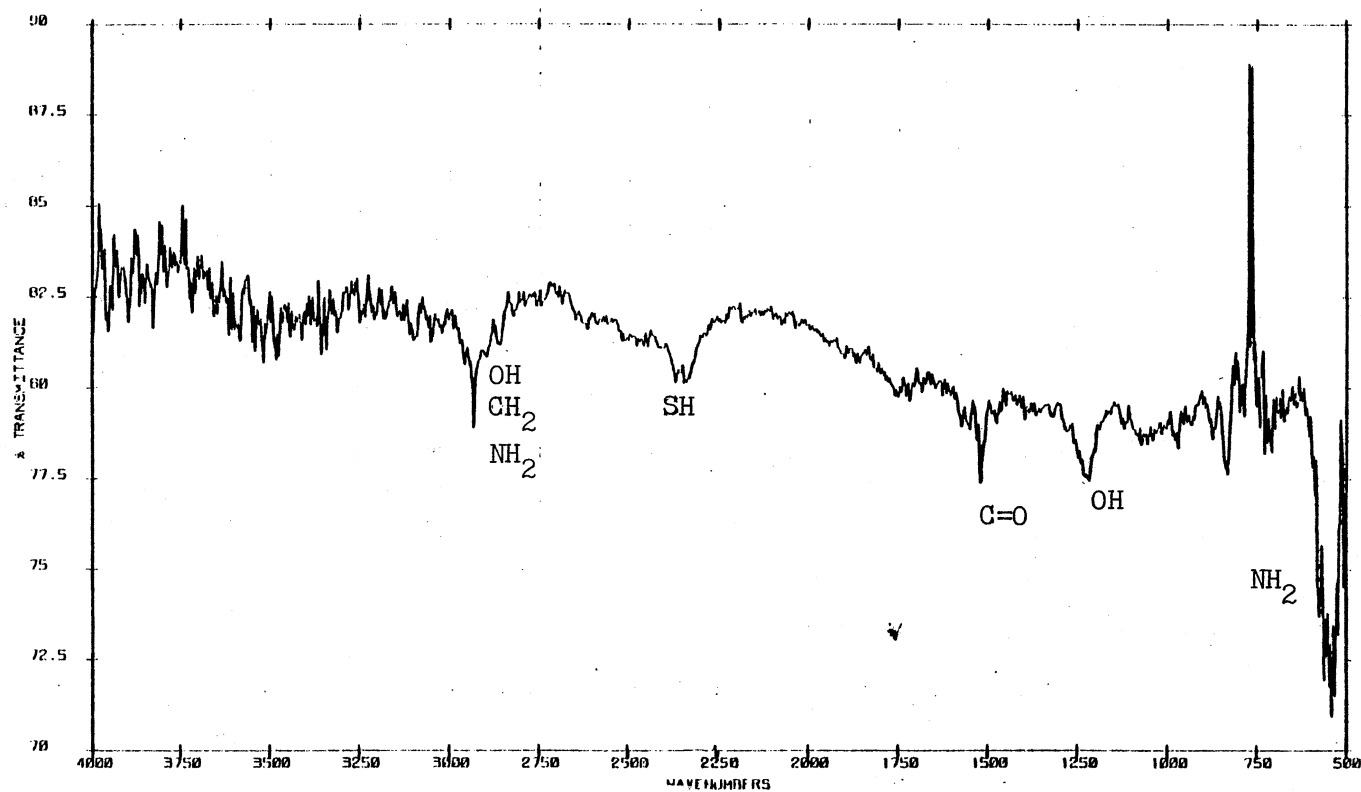Figure 69. Infrared Spectrum of Pure MEA Dissolved in CCl$_4$

Figure 70. Infrared Spectrum of Solid Product Dissolved in CCl_4 (MEA-COS System)

wave numbers less than 1000, which is borne out in Figure 69. Comparison of the pure MEA spectrum with the solid product scan (Figure 70) reveals a new peak of SH centered at 2300 wavenumbers. The thiocarbamate product of MEA has the structure

$$HO \cdot CH_2 \cdot CH_2 \cdot NHC=O$$
$$\mid$$
$$SH$$
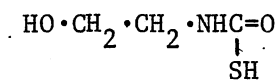
The SH peak was also observed in the liquid residue spectrum (Figure 71). This indicates that some thiocarbamate is retained in the liquid residue. All three spectra indicate strong absorption peaks for wavenumbers less than 800 which signifies appreciable amine group presence in them.
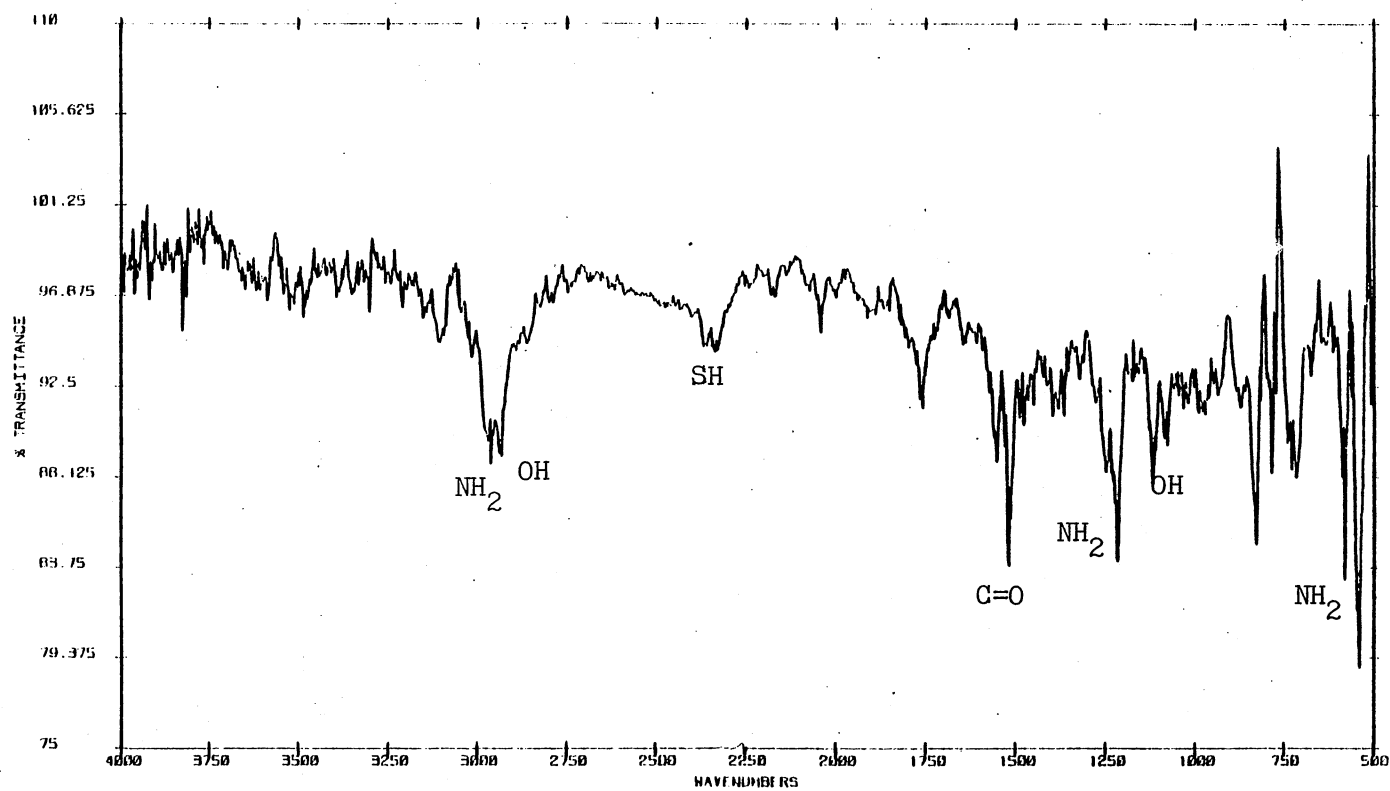
Figure 71. Infrared Spectrum of Liquid Residue Dissolved in CCl_4 (MEA-COS System)

$\mathcal{V}$

VITA

Mahmud Azizur Rahman

Candidate for the Degree of

Doctor of Philosophy

Thesis: STUDY OF REACTIONS OF CARBON DIOXIDE AND SULFUR CONTAINING COM-
POUNDS WITH ETHANOLAMINES

Major Field: Chemical Engineering

Biographical:

Personal Data: Born in Dacca, Bangladesh, February 25, 1954, the
son of Ayesha Rahman and Anisur Rahman.

Education: Graduated with an H.S.C. degree from D. J. Science Col-
lege, Karachi, Pakistan, in June, 1970; received the Bachelor
of Science in Engineering degree from the University of Engi-
neering & Technology, Dacca, Bangladesh, in April, 1976; re-
ceived the Master of Science in Chemical Engineering degree
from Oklahoma State University, Stillwater, Oklahoma, in July,
1978; completed requirements for the Doctor of Philosophy de-
gree at Oklahoma State University, in May, 1984.

Professional Experience: Teaching assistant, School of Chemical
Engineering, Oklahoma State University, 1977-78; research assis-
tant, Fluid Properties Research, Inc., Oklahoma State Univer-
sity, 1978-present.

Membership in Professional Society: American Institute of Chemical
Engineers.